Title

WAVE CHOAS IN THE STADIUM: STATISTICAL PROPERTIES OF SHORT-WAVE SOLUTIONS OF THE HELMHOLTZ EQUATION

Authors

McDonald, S.W.
Kaufman, A.N.

Publication Date

1987-05-01

LBL-19731
Preprint

Lawrence Berkeley Laboratory
UNIVERSITY OF CALIFORNIA

Accelerator & Fusion Research Division

Submitted to Physical Review A

WAVE CHOAS IN THE STADIUM: STATISTICAL PROPERTIES OF SHORT-WAVE SOLUTIONS OF THE HELMHOLTZ EQUATION

S.W. McDonald and A.N. Kaufman

May 1987

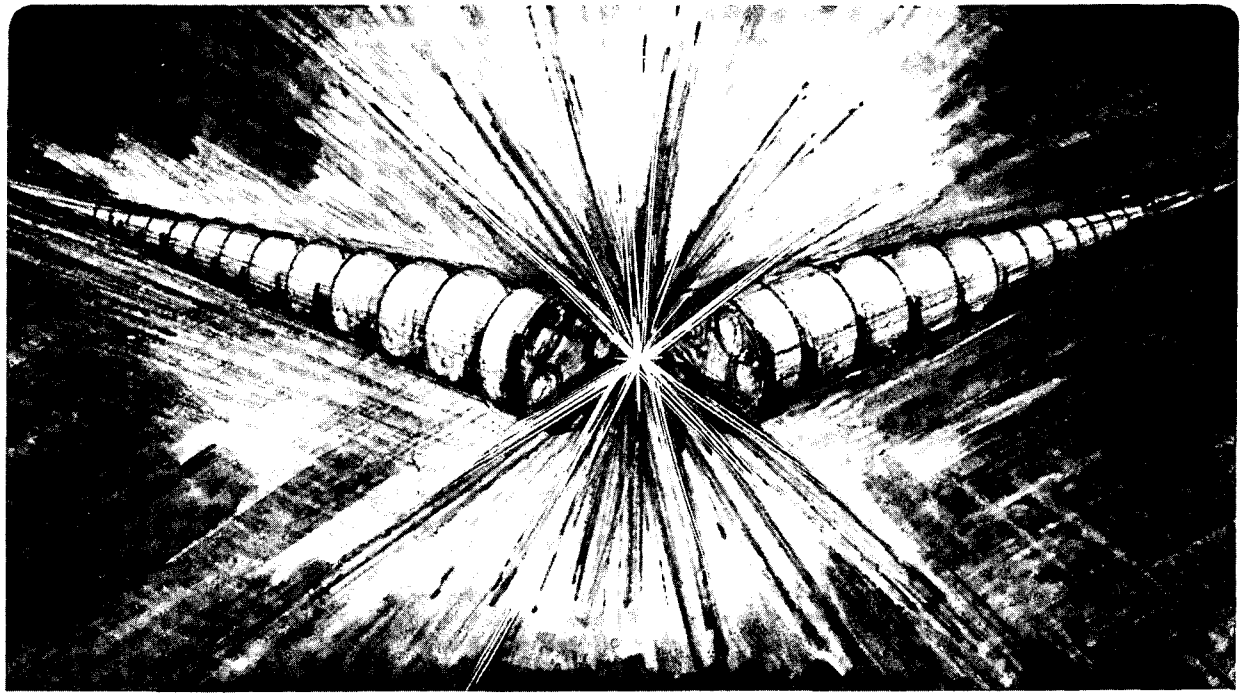

Prepared for the U.S. Department of Energy under Contract DE-AC03-76SF00098

DISCLAIMER

LBL-19731

WAVE CHAOS IN THE STADIUM: STATISTICAL PROPERTIES OF SHORT-WAVE SOLUTIONS OF THE HELMHOLTZ EQUATION*

Steven W. McDonald† and Allan N. Kaufman

Accelerator and Fusion Research Division
Lawrence Berkeley Laboratory
University of California
Berkeley, CA 94720
and
Physics Department
University of California, Berkeley
Berkeley, CA 94720

May 1987

* This work was supported by the Offices of Fusion Energy and of Basic Energy Sciences of the U. S. Department of Energy under Contract No. DE-AC03-76SF00098.

† Present address: Berkeley Scholars, Inc., PO Box 241, Berkeley, CA 94701

LBL-19731

WAVE CHAOS IN THE STADIUM: STATISTICAL PROPERTIES OF SHORT-WAVE SOLUTIONS OF THE HELMHOLTZ EQUATION*

Steven W. McDonald† and Allan N. Kaufman

Physics Department and Lawrence Berkeley Laboratory
University of California, Berkeley, CA 94720

May 1987

ABSTRACT

We numerically investigate statistical properties of short-wavelength normal modes and the spectrum for the Helmholtz equation in a two-dimensional stadium-shaped region. As the geometrical optics rays within this boundary (*billiards*) are nonintegrable, this wave problem serves as a simple model for the study of quantum chaos. The local spatial correlation function $<\psi_n(\underline{x}+\frac{1}{2}\underline{s})\psi_n(\underline{x}-\frac{1}{2}\underline{s})>$ and the probability distribution $P_n(\psi)$ of wave amplitude for normal modes ψ_n are computed and compared with predictions based on semiclassical arguments applied to this nonintegrable Hamiltonian. The spectrum is analyzed in terms of the probability $P(\Delta E)$ of neighboring energy eigenvalue separations, which is shown to be similar to a Wigner distribution for the eigenvalues of a random matrix.

PACS numbers: 03.65.Sq,03.65.Ge,05.40.+j

* This work was supported by the Offices of Fusion Energy and of Basic Energy Sciences of the U. S. Department of Energy under Contract No. DE-AC03-76SF00098.
† Present address: Berkeley Scholars, Inc., PO Box 241, Berkeley, CA 94701

I. Introduction

The growing interest in chaotic Hamiltonian dynamical systems has naturally been accompanied by the search for corresponding attributes of wave systems. The eikonal (WKB or semiclassical) approximation to the solution of a wave problem establishes the connection with an associated dynamical system (the characteristic trajectories of the eikonal equation) and thereby provides a basis for examining the ways in which the structure of the phase space of these trajectories is reflected in the properties of the wave solution. Despite the fact that the applicability of this asymptotic method to a system characterized by nonintegrable trajectories has not been placed on a firm theoretical foundation, it has nonetheless provided the basis for many observations and predictions concerning various aspects of the associated wave problem.

In this paper[1] we expand on the results reported in our previous Letter[2] by investigating statistical properties of a model wave equation for which, depending upon a single parameter, the corresponding dynamical system is either integrable or chaotic. Specifically, for the Helmholtz equation in a two-dimensional stadium-shaped region we examine the spatial structure of eigenfunctions (by means of their spatial correlation and probability distribution of wave amplitude) and the the statistics of the spectrum. In particular, Berry's[3,4] predictions for the spatial properties of individual "chaotic" eigenfunctions (based on the nature of the Wigner function) is discussed in relation to our particular problem in Section II; the results of our numerical tests and the comparison with this theory appear in Section III. In Section IV, we construct the probability distribution of wave amplitude $P(\psi)$ for an individual eigenfunction, as well as for a superposition of neighboring modes. The sensitivity of the eigenvalues and eigenfunctions to variation in parameter (especially near the classical transition from integrability to chaos) is studied in Section V. A statistical description of the spectrum in terms of neighboring level spacings is presented in Section VI. Among the conclusions in Section VII, we suggest that whereas the Liouville density in the phase space of an ergodic Hamiltonian dynamical system eventually spreads uniformly over the energy surface, the expectation of similar behavior of analogous properties of the corresponding wave system may not be realized.

II. Review of Theory

We consider the Helmholtz equation $(\nabla^2 + k_n^2)\psi_n(\underline{x}) = 0$ in the two-dimensional stadium-bounded region (Fig. 1) with $\psi = 0$ on the boundary. [2,5-9] The shape of the boundary is governed by the parameter γ, defined to be the ratio of the half-length a of the straight section to the semicircle radius R. We hold the area constant ($=\pi$) so that the mean density of eigenvalues does not change as this parameter is varied (the equation is solved at fixed γ). This wave problem can be viewed as the time-independent Schrödinger equation for the motion of a particle (mass m, energy $E_n \equiv \hbar\,\omega_n = \hbar^2 k_n^2/2m$ and momentum $\underline{p} = \hbar\,\underline{k}$) in such a two-dimensional region (potential $V(\underline{x}) = 0$ inside, $V(\underline{x}) = \infty$ on the boundary). The wave equation also describes transverse TM modes in a cylindrical electromagnetic cavity (or waveguide) with stadium cross-section (wave frequency $\omega_n = ck_n$ with longitudinal wavenumber $k_z = 0$). It will be helpful to bear these applications in mind as we discuss and interpret our results in the following Sections.

The connection between this wave problem and a classical dynamical system is provided by the *eikonal* approximation. [10] In this method (also known as the WKB or semiclassical approximation) the solution $\psi(\underline{x})$ is assumed to have the form $\psi(\underline{x}) \sim A(\underline{x})\exp[i\,\phi(\underline{x})]$, where the phase $\phi(\underline{x})$ is taken to be much more rapidly varying than the amplitude $A(\underline{x})$. Substituting this form into the wave equation, the magnitudes of the derivatives of the phase and amplitude are ordered as $|\nabla\phi| \gg |A^{-1}\nabla A|$; defining the local wave vector $\underline{k}(\underline{x})$ as the gradient of the phase, this is the statement that a typical wavelength of $\psi(\underline{x})$ is much shorter than the scalelength of variation of its amplitude (here, taken to be the radius R), or $|\underline{k}|R \gg 1$. This assumption leads to the lowest order partial differential equation for the eikonal phase: $[\nabla\phi(\underline{x})]^2 = k_x^2 + k_y^2 = k_n^2$. Since the eigenvalue k_n is related to the wave frequency ω_n in both the Schrödinger and cavity mode equations, we write the *eikonal equation* in the form

$$\Omega(\underline{x},\nabla\phi) = \Omega(\underline{x},\underline{k}) = k_x^2 + k_y^2 = k_n^2 \qquad (1)$$

which defines the *local dispersion relation* $\Omega(\underline{x},\underline{k})$ (*i.e.*, the relationship between the wave

vector $\underline{k}$ and the frequency ω, which may in general depend on position $\underline{x}$). In the case of the Schrödinger equation we have $\Omega = 2mH(\underline{x},\underline{p})/\hbar^2$, where $H(\underline{x},\underline{p})$ is the classical Hamiltonian; here, the value of Ω is proportional to either the classical energy E or the wave function frequency ω. In view of the correspondence with classical mechanics, one may identify the eikonal equation (1) as the Hamilton-Jacobi equation associated with the dynamical system generated by the Hamiltonian (or local dispersion relation) $\Omega(\underline{x},\underline{k})$ (where the phase $\phi(\underline{x})$ plays the role of Hamilton's characteristic action function). The characteristic trajectories, or *rays*, of this dynamical system are governed by Hamilton's equations

$$\frac{d\underline{x}}{dt} = \frac{\partial\Omega}{\partial\underline{k}} \qquad \frac{d\underline{k}}{dt} = -\frac{\partial\Omega}{\partial\underline{x}} \tag{2}$$

For this system, the rays in $\underline{x}$-space are simply straight lines with specular reflection from the boundary.

In the case of a circular boundary ($\gamma = 0$), a typical single ray trajectory is confined to an annulus (Fig. 2) depending on initial conditions. This is due to the rotational symmetry which makes the angular momentum a constant of the motion in addition to the value of Ω (the "energy"). The presence of two constants of the motion in a system with two degrees of freedom implies[11] that a trajectory in the four-dimensional $(\underline{x},\underline{k})$ phase space lies on a two-dimensional surface which is a torus. This is an example of an *integrable* dynamical system. In the noncircular stadium geometry ($\gamma > 0$), however, the presence of the short straight section (of any length) breaks the circular symmetry and thus destroys the conservation of angular momentum. As shown in Fig. 3, a single typical trajectory appears to cover the entire interior of the stadium. Indeed, it has been shown [12,13] that almost all ray trajectories ergodically cover the three-dimensional surface of constant $\Omega = \omega$ (the only integral of the motion) in phase space; furthermore, Bunimovich[12] has shown that this billiard system is mixing. There are, however, special trajectories which are not chaotic: these are the periodic orbits such as the ones which bounce vertically between the straight sections, or horizontally on the midline of the stadium. The initial conditions which generate these orbits constitute only a set of measure zero in phase space and the trajectories are unstable to perturbations in initial conditions.

The generalization of the traditional asymptotic semiclassical quantization methods for one-dimensional systems (*e.g.*, the Bohr-Sommerfeld rules) to systems with more than one degree of freedom is the Einstein-Brillouin-Keller (EBK) method. [14-16] This method (for a good discussion, see Percival [17]) can be applied only to integrable Hamiltonian ray systems because it is based on the quantization of the action variables. As such, the procedure requires the transformation of the Hamiltonian $\Omega(\underline{x},\underline{k})$ to a new Hamiltonian $\hat{\Omega}(\underline{I})$ which is a function of the action variables $\underline{I}$ alone. For integrable systems with N degrees of freedom, the N actions are defined as[11]

$$\underline{I} \equiv \frac{1}{2\pi} \oint_{\Sigma} \underline{k} \cdot d\underline{x} \tag{3}$$

where the N paths $\{\Sigma\}$ are N irreducible and independent circuits around the N-torus in phase space on which the trajectories lie. Each of these actions is then quantized as

$$\underline{I} \rightarrow \underline{I}_{\underline{m}} \equiv \underline{m} + \tfrac{1}{4}\underline{\alpha} \tag{4}$$

where the $\underline{m}$ are integers ($\underline{m}$ = 0,1,2,...) and the numbers $\underline{\alpha}$ are *Maslov indices* [10] which are related to the topological structure of the torus in phase space. These conditions discretize the set of classical tori and implicitly determine the eigenvalues $\omega_{\underline{m}} = k_{\underline{m}}$ in the wave spectrum by setting $\omega_{\underline{m}} = \hat{\Omega}(\underline{I}_{\underline{m}})$. The interpretation of this quantization procedure is that a short wavelength normal mode of an N-dimensional wave system labelled by N integers corresponds roughly to the family of trajectories of the associated *integrable* dynamical system which lie on the phase space N-torus labelled by the corresponding values of the N actions (given by quantization conditions (4)).

As our model system of rays bouncing inside a circular boundary is integrable, the EBK quantization procedure can be carried out as follows. The two irreducible paths $\{\Sigma\}$ required for the action integrals (3) can be visualized by "inflating" the picture of the trajectory in Fig. 2 into a torus: from the inner radius of the orbit, the ray moves outward over the top of the torus, reflects at the outer boundary and then continues back toward the inner minimum radius along

the bottom of the torus. The two irreducible paths are then the long way around the torus (the angular direction) and the short way around the torus (the radial direction); *i.e.*, $\{\Sigma\} = (\theta, r)$. In this case, these two paths can be separated by expressing the Hamiltonian Ω in canonical polar variables,

$$\omega = k_n^2 = \tilde{\Omega}(r, k_r, k_\theta) = k_r^2 + \frac{k_\theta^2}{r^2} \tag{5}$$

In this form, it is evident that k_θ is a constant of the motion and is in fact the angular momentum L, or angular action I_θ defined by (3). The radial action I_r is given by the integral around the radial direction (from the inner radius $a_{\omega L} = L/\sqrt{\omega}$ to the perimeter and back)

$$\begin{aligned} I_r &\equiv \frac{1}{2\pi} \oint k_r(r; L, \omega)\, dr \\ &= \frac{1}{\pi} \left\{ \left[k_n^2 R^2 - L^2 \right]^{1/2} - L \cos^{-1} \frac{L}{k_n R} \right\} \end{aligned} \tag{6}$$

where $k_n^2 = \omega$ is the value of $\tilde{\Omega}$. This relation $I_r(L, \omega)$ now implicitly defines a new Hamiltonian $\hat{\Omega}(L, I_r)$ in action-angle variables (by replacing k_n^2 with $\hat{\Omega}$ in (6)), as well as the transformation $I_r(r, k_r, k_\theta)$ from the canonical set of polar variables to action-angle variables by using (5) to express k_n^2 in terms of r, k_r and k_θ in (6).

The quantization of the actions by (4) can be shown[16] to be

$$L = m \qquad I_r \rightarrow I_n = n + \tfrac{3}{4} \qquad m, n = 0, 1, 2, \ldots \tag{7}$$

The term 3/4 in the definiton of I_n is the Maslov index for the projection of the radial motion in phase space onto $\underline{x}$-space (which accounts for the focusing of the rays along the inside of the annulus and their reflection from the boundary). The substitution of these conditions into (6) discretizes the set of classical tori and implicitly determines the eigenvalues in the wave spectrum, $\omega_{m,n} = \hat{\Omega}(m, I_n)$. These expressions were first derived by Keller and Rubinow[16] and yield eigenvalues which are in very good agreement with the exact spectrum (the zeros of Bessel functions).

If the ray system is not integrable (as in our case of rays bouncing inside a stadium boundary) then the EBK quantization procedure fails (the set of N actions does not exist). It is not known in this case what the correspondence is between normal modes of the wave system and objects in the ray phase space (such as the tori for integrable systems), if indeed there is any correspondence at all. It is one of the goals of this paper to examine the solutions of the wave equation in the stadium geometry in an attempt to discover and elucidate such a connection. This investigation will be carried out in the light of Berry's[3,4] conjectures on the statistical properties of eigenfunctions of the Schrödinger equation based on the phase space structure of classical ray systems which are chaotic.

As the description of the ergodic properties of a Hamiltonian ray system is most natural in the $(\underline{x},\underline{k})$ phase space, it is advantageous to explore the implications of such behavior for the corresponding normal modes in terms of a phase space representation of the waves. An example of such a quantity is the Wigner function,[18] which may be defined in terms of the $\underline{x}$-space representation of a wave $\psi(\underline{x})$ in N dimensions as

$$W(\underline{x},\underline{k}) \equiv \int_{-\infty}^{\infty} \psi(\underline{x} + \tfrac{1}{2}\underline{s})\psi^*(\underline{x} - \tfrac{1}{2}\underline{s})\, e^{-i\,\underline{k}\cdot\underline{s}}\, d^N s \tag{8}$$

The properties and applications of this function have been discussed by many authors.[3,4,19] It is of interest because it is often regarded as a candidate for a wave analogy of the classical Liouville density of the associated ray system. The transform in (8) is invertible and yields the product

$$\psi(\underline{x})\psi^*(\underline{x}') = \int_{-\infty}^{\infty} W(\underline{k}, \tfrac{1}{2}(\underline{x} + \underline{x}'))\, e^{i\,\underline{k}\cdot(\underline{x} - \underline{x}')}\, \frac{d^N k}{(2\pi)^N} \tag{9}$$

while the projection onto $\underline{x}$-space is

$$|\psi(\underline{x})|^2 = \int_{-\infty}^{\infty} W(\underline{x},\underline{k})\, \frac{d^N k}{(2\pi)^N} \tag{10}$$

For a wave which is rapidly oscillating on $\underline{x}$-space (such as in the eikonal approximation) the Wigner function is in general a rapidly varying function on phase space. Berry[3] has introduced the local spatial average of the Wigner function

$$<W(\underline{x},\underline{k})> \equiv \frac{1}{\Delta^N} \int_{-1/2\underline{\Delta}}^{1/2\underline{\Delta}} W(\underline{x}+\underline{s},\underline{k})\, d^N s \tag{11}$$

with

$$\lim_{\lambda \to 0} \Delta = 0 \qquad \text{but} \qquad \lim_{\lambda \to 0} \frac{\lambda}{\Delta} = 0$$

where λ is a typical wavelength of $\psi(\underline{x})$ and Δ is the smoothing length. (Thus we consider local averages over many wavelengths of increasingly shorter wavelength modes, $\lambda/\Delta \to 0$). This averaging process eliminates some of the oscillatory nature of the Wigner function (typical of quantum or physical optics effects) and, together with the tendency to shorter wavelength, allows one to make predictions for $<W>$ based on its interpretation in terms of classical mechanics or geometrical optics.

For time-independent *integrable* ray systems with N degrees of freedom, Berry[4] has taken the crudest approximation

$$<W_{\underline{m}}(\underline{x},\underline{k})> \approx \delta^N(\underline{I}(\underline{x},\underline{k}) - \underline{I}_{\underline{m}}) \tag{12}$$

where $\underline{I}(\underline{x},\underline{k})$ is the set of N actions expressed in terms of $\underline{x}$ and $\underline{k}$, and the $\underline{I}_{\underline{m}}$ are their corresponding quantized values in the EBK analysis. This expression was obtained[4] by using an eikonal representation for $\psi(\underline{x})$ in (8) and performing the integral in the stationary phase approximation. Although Balasz[20] has shown that the Wigner function can be a δ-function only on linear subspaces of phase space, this approximation conforms to the expectation based on the correspondence between the classical phase space tori and stationary states of the wave system.

As we have noted, the correspondence between normal modes and objects in the classical phase space of *nonintegrable* ray systems is unknown. However, the analogy between the

Wigner function and the classical Liouville density has led Berry and Voros[21] to take as a crude approximation for time-independent ergodic ray systems

$$<W_n(\underline{x},\underline{k})> \approx \frac{1}{\Gamma_n}\delta(\Omega(\underline{x},\underline{k}) - \omega_n) \tag{13}$$

which is a one-dimensional δ-function selecting the $2N-1$ dimensional surface (with volume Γ_n) corresponding to the eigenfrequency ω_n. Although Voros[21] has to some extent justified this approximation, its status is more that of a conjecture and indeed a proposal for the definition of chaos in stationary states of wave systems.

The verification of these hypotheses (particularly (13)) is an important step in determining the criteria for and the nature of what has become known as *quantum chaos* and its relation to corresponding classical concepts. The Wigner function, however, is a difficult quantity to construct and study numerically for systems with more than one degree of freedom, due to its definition in terms of a multiple Fourier integral (8) over wave functions which themselves must be computed numerically in nonseparable geometry. Instead of investigating the Wigner function associated with a normal mode directly, one can gain some insight by studying the eigenfunction itself. This is because, as Berry[3] points out, the approximations (12) and (13) when substituted into (10) and (9) have implications for statistical properties of the individual eigenfunctions $\psi(\underline{x})$. In this way, predictions for the local average intensity

$$\Pi(\underline{x}) \equiv <|\psi(\underline{x})|^2> \tag{14}$$

and the spatial correlation function

$$C(\underline{x},\underline{s}) \equiv \frac{1}{\Pi(\underline{x})}<\psi(\underline{x} + \tfrac{1}{2}\underline{s})\psi^*(\underline{x} - \tfrac{1}{2}\underline{s})> \tag{15}$$

may be computed for either the integrable or chaotic case. Here the local average $< >$ is defined as in (11). We note that this definition of the spatial correlation differs from that used recently by Shapiro and Goelman;[6] we believe that (15) is a more natural definition in that it does not rely on the prescription of some "self-avoiding space-filling path in coordinate space."

Furthermore, the present definition coincides with the standard correlation function studied in wave propagation and turbulence theory when the local spatial average $< >$ is interpreted as an ensemble average; in that case, the averaged Wigner function can be properly interpreted as the local spectral function of the wave.

We have attempted to test the accuracy of these asymptotic forms of the Wigner function by numerically investigating $\Pi(\underline{x})$ and $C(\underline{x},\underline{s})$ for individual eigenfunctions of the Helmholtz equation in both the circular ($\gamma = 0$) and stadium ($\gamma > 0$) geometry. In the integrable circular case, we have from (12)

$$<W_{m,n}(r,k_r,k_\theta)> = \delta(k_\theta - m)\delta(I_r(r,k_r,k_\theta) - I_n) \tag{16}$$

where we have used $I_\theta = L = k_\theta$ for the angular action. For the radial action function $I_r(\underline{x},\underline{k}) = I_r(r,k_r,k_\theta)$ we substitute $\omega = \tilde{\Omega}(r,k_r,k_\theta)$ from (5) into (6) to obtain

$$I_r(r,k_r,k_\theta) = \frac{1}{\pi}\left\{\frac{R}{r}\left[k_r^2 r^2 + k_\theta^2\left(1 - \frac{r^2}{R^2}\right)\right]^{1/2} - k_\theta \cos^{-1}\frac{k_\theta r}{R\sqrt{k_r^2 r^2 + k_\theta^2}}\right\} \tag{17}$$

The quantization rules (7) have been used in (16) for the $\underline{I_m}$. When (16) is inserted into (10), one finds the local average intensity

$$\Pi_{m,n}(r) = \frac{1}{2\pi}\frac{k_{m,n}^2}{\sqrt{k_{m,n}^2 R^2 - m^2}\sqrt{k_{m,n}^2 r^2 - m^2}} \qquad (r \le R) \tag{18}$$

for a short wavelength eigenmode of the circle with semiclassical eigenvalue $k_{m,n}$. We observe that $\Pi_{m,n}(r)$ is just the classical density of rays with the quantized values of the actions $\underline{I}$. This expression is correctly normalized on the annular region between the boundary of the circle and the radial turning point $a_{\omega,m} \equiv m/k_{m,n}$ (where it becomes infinite), and is proportional to $k_r^{-1}(r)$ in that annulus. The singularity at $a_{\omega,m}$ is of course "softened" when wave effects are considered; this is an example of the caustic phenomenon observed in regions of $\underline{x}$-space where rays focus.

The spatial correlation function is obtained by inserting (16) into (9) and dividing by $\Pi_{m,n}(r)$

$$C_{m,n}(r,\theta;s,\phi) = \exp\left[im\frac{s}{r}\sin(\phi-\theta)\right]\cos\left[\frac{s}{r}\sqrt{k_{m,n}^2 r^2 - m^2}\cos(\phi-\theta)\right] \tag{19}$$

where (r,θ) are the coordinates of a point $\underline{x}$ inside the circle, s is the distance measured from $\underline{x}$, and ϕ is the angle of $\underline{s}$ (relative to the positive x-axis). Again, this expression is valid only in the classically allowed annulus. Note the definite anisotropy in the angle ϕ at a fixed point (r,θ) due to the contribution to $\psi(\underline{x})$ of only two (ingoing and outgoing) local wave vectors, $\underline{k}_{\pm}(r) = (k_\theta, \pm k_r(r))$. Thus, for $\underline{s}$ along the radial direction ($\phi = \theta$) the correlation function has the spatial dependence of the local radial wavenumber $C = \cos k_r(r)s$ while for $\underline{s}$ in the angular direction ($\phi = \theta \pm \pi/2$) the variation is that of the angular wavenumber $C = \exp \pm ims/r$ (for small s, $s/r \simeq$ the angular deviation from the point $\underline{x}$). We also note that for $r \simeq a_{\omega,m}$, C is approximately constant in the radial direction indicative of the transverse correlation in the caustic region due to the focusing of rays.

These expressions for Π and C are in agreement with the more general formulas derived by Berry in Ref.[3] (when made specific to the present problem). In that work, he also discusses the general presence in integrable systems of caustic singularities in Π and the anisotropy in C due to only a finite number of local wave vectors contributing to ψ at each point $\underline{x}$. He also predicts the form of Π and C for a relatively general ergodic system (of which the stadium with $\gamma > 0$ is a simple example), based on the assumption (13). Thus we have upon substitution of (13) into (10) the local intensity for a wave in the (ergodic) stadium geometry

$$\Pi_n(\underline{x}) = \frac{\int \delta(k^2 - \omega_n)\, d^2k}{\int_A d^2x \int \delta(k^2 - \omega_n)\, d^2k} = A^{-1} \tag{20}$$

where A is the area of the stadium ($= \pi$). This uniform intensity conforms to expectation based on the ergodic nature of the rays which densely cover the interior of the stadium. It should be remembered that this is the average local intensity; *i.e.*, the short wavelength oscillations of

the mode have been averaged out, so that it is a prediction of uniform average intensity. The correlation function is computed with (13) in (9):

$$C_n(\underline{x},\underline{s}) = \frac{1}{\Pi_n(\underline{x})\Gamma_n}\int e^{i\,\underline{k}\cdot\underline{s}}\,\delta(k^2-\omega_n)\,\frac{d^2k}{(2\pi)^2} = J_0(k_n s) \tag{21}$$

Here $k_n^2 \equiv \omega_n$, and the integral has been computed using polar variables and Bessel's identity.

Following Berry,[3] we observe that expressions (20) and (21) for the ergodic stadium are strikingly different from the corresponding formulas (18) and (19) for the integrable circle in two important respects: (*i*) The local average intensity in the circle is dominated by the caustic singularity while no caustics are expected to exist in the stadium, and (*ii*) the correlation function in the circle is nonuniform in $\underline{x}$ and anisotropic in $\underline{s}$ (being influenced by a finite number of local wave vectors), whereas in the stadium it is expected to be uniform and isotropic. This isotropy of C seems reasonable based on the ergodicity of the underlying rays: almost every point $\underline{x}$ in the interior of the stadium will be "visited" (approached arbitrarily closely) by any ergodic trajectory infinitely many times as $t \to \infty$ (and the angle of $\underline{k}$ will take on almost all values in this neighborhood of $\underline{x}$). Thus, if a normal mode of the stadium in some sense corresponds to an infinite-time ergodic trajectory, it could be thought of as being composed of an infinite number of local eikonal contributions with an almost continuous local wave vector spectrum.

III. Numerical Results

We have numerically solved the boundary value wave problem discussed in the previous Section using a boundary integral technique developed by Riddell. [22] This method permits the independent investigation of any region of the spectrum (*i.e.*, without computing all lower eigenvalues) as well as the capability of constructing the values of any particular eigenfunction over an arbitrary domain within the bounded region (even at just one point). These are important

properties because in order to test the predictions of Section II one must examine short wavelength eigenmodes for comparison with semiclassical theories. The geometry of Fig. 1 admits reflection symmetries across the axes, which give rise to four independent parities of solutions; we have restricted our study to the odd-odd class (nodal lines on axes). In a compromise between large eigenvalues and numerical accuracy, we have concentrated on a small part of the spectrum near $k_n \approx 65$, which is approximately 200 levels above the ground state in this parity class; in this regime there are typically 15-20 wavelengths across the interior. We have tested the precision of our numerical technique in the case of the circle against the exact analytical solutions $J_m(k_{m,n}r)\sin m\theta$ (m even, for odd-odd modes). In the range $50 < k < 100$, 97% of our numerically obtained eigenvalues have ± 0.001 absolute error, while 90% have error less than ± 0.0005. Furthermore, numerically constructed eigenfunctions were found to have relative error of about 10^{-4}. We assume that these error estimates carry over to the case of the stadium.

A perspective view of a typical circular ($\gamma = 0$) eigenfunction is shown in Fig. 4, where $|\psi|^2$ is plotted in the positive quadrant for $k_{40,5} = 65.012$ (angular quantum number $m = 40$, radial index $n = 5$). The visual comparison of $|\psi|^2$ with the classical probability density is apparent: (*i*) in the classically disallowed region ($r < a_{\omega,m}$) the amplitude is vanishingly small; (*ii*) the caustic region formed by the first and largest peak of $J_{40,5}(k_{40,5}r)$ corresponds to the focusing of the geometrical optics rays along the inside rim of the annulus; and (*iii*) the radial decay of amplitude (smoothing over the rapid wave oscillations) within the annulus appears to verify Eq.(18).

In Fig. 5, we plot the local correlation function $C(\underline{x},\underline{s})$ for this mode. As a typical example we have chosen the point $\underline{x} = (r,\theta) = (0.866,0.867)$ and have computed the correlation as a function of $|\underline{s}|$ at three angles $\phi = 0, \pi/4, \pi/2$. The crosses denote the numerical data and are compared to the solid curve representing the theoretical prediction based on the real part of Eq.(19). It should be noted that the local average indicated in (15) was in practice carried out for this case over an area encompassing only about two wavelengths as opposed to the limiting process stated in (11); numerically we may examine eigenmodes with large (but finite)

wavenumber, but due to (15) we must smooth only over regions where the local average intensity Π remains somewhat uniform. Nevertheless, we may conclude two things on the basis of these results: (*i*) The Wigner function for eigenstates of systems which are classically integrable appears to be concentrated on the torus in phase space corresponding to the semiclassically quantized values of the actions (because expression (19) was derived from the approximation (12)), and (*ii*) the part of the spectrum we are examining is probably "asymptotic" enough to test predictions based on semiclassical arguments.

In Fig. 6 we display a perspective view of $|\psi|^2$ in the positive quadrant for a typical eigenfunction in the stadium geometry ($\gamma = 1$). The eigenvalue $k = 65.326$ is again approximately 200 levels above the ground state of the odd-odd parity class (since, although we have stretched the circle into a stadium, we have kept the area constant). The irregular distribution of $|\psi|^2$ over the stadium is in striking contrast to that in the circle, and the connection of such a "random-looking" eigenfunction with an underlying ergodic classical system seems at first appealing. On the basis of the ergodic nature of almost all trajectories in the stadium however, one would expect a more uniform distribution of amplitude than that which is observed in Fig. 6*a*; in fact, the semiclassical prediction of (20) seems not to be borne out in this case. Instead, we would characterize the appearance of this mode as consisting of many small localized regions (of several wavelengths) with relatively high intensity somewhat randomly interspersed among larger areas of much lower intensity. As previously noted,[2,23] the nodal curves as in Fig. 6*b* appear to wander randomly through the domain. Although this behavior is frequently mentioned as a symptom of wave chaos, we feel this feature should only be emphasized to the extent that it facilitates the visualization of the local wave vector spectrum: the random weaving of these contours tends to indicate an isotropic distribution of local wave vectors as predicted by Eqs.(13) and (21).

The numerical computation of the correlation function $C(\underline{x},\underline{s})$ for this mode is presented in Fig. 7 (again denoted with crosses) and compared to the prediction (21) at three angles of $\underline{s}$. The agreement with theory here is not as definite as in the circular case and the expected isotropy is not fully realized. These results were obtained by replacing the local average in (15) by an

average over the entire stadium (even though the local intensity $|\psi|^2$ is evidently not uniform) since any local average performed as in the case of the circle for finite wavenumber would produce anisotropy in the correlation. Similar (and in fact worse) agreement[1] with theory has been found for other randomly selected modes, including ones near $k \approx 100$ (nearly 600 levels above the ground state). If we assume that stadium modes in this part of the spectrum can be considered to be "asymptotic" in the same sense as circular modes in the same range, then we must conclude that the prediction (13) is not substantiated. In other words, these results seem to indicate that the Wigner function corresponding to these modes exhibits more structure on the energy surface than does the classical invariant Liouville density for an ergodic trajectory. Thus, both the distribution of intensity and the behavior of the spatial correlation suggest that an individual eigenmode of the stadium does not correspond to an ergodic family of orbits (but possibly, to only a finite-time subset of ergodic orbits).

We have constructed[1] a number of eigenfunctions in this region of the spectrum ($k \approx 65$), as well as several in the regime $k \approx 100$; six consecutive modes in each range are shown in Fig. 8. Most of the modes (approximately 80%) are similar to the one pictured in Fig. 6 in that they share the property of random intensity distribution and anisotropic correlation. A small number of modes (about 10%), however, were observed to have a more uniform intensity distribution. In contrast, the remaining 10% of the eigenfunctions we constructed were surprising because they appeared to correspond to periodic ray trajectories. Examples of this are the modes shown in Figs. 8d and 8i; these "bouncing ball" modes seem to be associated with ray trajectories which bounce between the straight sides of the stadium (although the waves do exhibit a finite value of k_x). In later work, Taylor and Brumer[7] and Heller[8] have also observed this type of mode. Although "bouncing ball" modes were predicted by Keller and Rubinow[16] to exist for arbitrarily shaped two-dimensional regions, their arguments assume that the boundary was everywhere focusing and that the ray system was integrable. Although there is no firm theoretical foundation for quantizing ergodic ray systems and constructing normal modes in terms of periodic orbits (which are in general isolated and unstable to perturbation), Heller[8] has recently given arguments for the existence of such periodic orbit modes in the spectrum of a general

ergodic ray/wave system. Bai, Hose, Stefanski and Taylor[9] have also offered an explanation of bouncing ball modes based on an adiabatic quantization procedure. Another class of mode we observed is represented by those in Fig. 8f,g; this "whispering gallery" type of mode was also predicted by Keller and Rubinow, although again the arguments were based on the existence of a torus corresponding to an integrable family of orbits which skips around the boundary.

Percival[17] has introduced the term *irregular* to describe modes corresponding to classically nonintegrable Hamiltonians (whereas integrable ray systems would possess *regular* modes). In view of the different types of modes found in the spectrum of the stadium, some of which appear more similar to the regular modes of the circle than to the majority of stadium modes, we propose to further differentiate the types of irregular modes. Thus, we refer to the majority of stadium modes (as in Fig. 6) as *chaotic waves*, and term the more regular-looking modes (as in Figs. 8d,i,f,g) *localized waves*. Here this is suggested as a primarily subjective visual distinction, but in the next Section we shall consider a quantitative measure of the difference between these classes of modes.

IV. Amplitude Distribution: P(ψ)

Berry[3] has proposed a simple quantitative measure for distinguishing between regular and irregular waves, loosely based on the concepts of eikonal theory. If one assumes that the wave ψ at a point $\underline{x}$ in the stadium can be written as a sum of eikonal "wavelets", each contribution arising from successive passes through an arbitrarily small neighborhood of $\underline{x}$ along a single chaotic trajectory, then $\psi(\underline{x})$ would have the form

$$\psi(\underline{x}) \sim \sum_{j=0}^{\infty} A_j e^{i\,|\underline{k}|L_j} \tag{22}$$

Since in this model the rays propagate freely between reflections from the boundary, the phase of

the jth contribution to ψ is simply proportional to the total pathlength L_j between the $(j-1)$ and jth arrival "near" $\underline{x}$: $\phi_j(\underline{x}) = \int \underline{k} \cdot d\underline{x} = |\underline{k}| L_j$. Now, as this system is mixing, the L_j's may be considered to be independent random variables. With these assumptions, one concludes on the basis of the central limit theorem that $\psi(\underline{x})$ is a *gaussian random variable* for all $\underline{x}$. Thus, the probability of finding the value ψ at any point inside the stadium, without knowledge of the surrounding values, is distributed as a gaussian, $P(\psi) \sim e^{-\beta\psi^2}$.

Naturally, this should be viewed as only a qualitative argument (indeed, this is probably not even a correct interpretation of a stadium mode at all). Other amplitude and phase contributions (such as those due to boundary reflections and possible focusing) have been ignored, and nothing has been said about quantization. It does, however, serve to convey this general idea: if an irregular wave supported by chaotic rays may be represented by a superposition of a large (possibly infinite) number of eikonal wavelets, then the chaotic paths of the rays could produce a phase decorrelation of the individual contributions, yielding a gaussian random variable at each point.

This is a simple statistical test to perform. Evaluating a single normalized eigenfunction ψ at approximately 5000 points in the interior of the quadrant, the probability distribution $P(\psi)$ is constructed as a normalized histogram with 100 bins. For eigenfunctions normalized to unity in the quadrant of area $\pi/4$, the width of the numerical distribution $P(\psi)$ is $\sqrt{4/\pi}$:

$$\psi_{\text{rms}}^2 \equiv \int \psi^2 P(\psi)\, d\psi = A^{-1} \int \psi^2\, d^2x = A^{-1} = 4/\pi \tag{23}$$

This is true for all modes at all values of γ. Therefore, each numerical $P(\psi)$ at any value of γ may be compared with the same standard normalized gaussian prediction

$$P_0(\psi) \equiv 2^{-3/2} \exp(-\pi\psi^2/8) \tag{24}$$

The result for the stadium mode of Fig. 6 at $k = 65.326$ is displayed in Fig. 9. Despite the rough form of the numerical data, it seems that the general shape of the probability distribution is fairly well described by the gaussian prediction. Actually, the jagged peaks are due to the finite wavelength of the mode, as each peak in the distribution represents a local minimum or

maximum in the wave (a wave peak). When the wavelength is shortened (larger eigenvalue) each mode contains more waves and the peaks in $P(\psi)$ tend to coalesce. Figure 9 is typical of the general agreement with this theory found for all of the chaotic type of $\gamma = 1$ stadium modes examined. Similar results have been reported by Shapiro and Goelman,[6] although their experimental histogram for $P(\psi)$ is not compared with a standard gaussian curve, and these authors seem to be unaware of Berry's prediction.

In contrast, the bouncing ball modes possess a somewhat different characteristic probability distribution as shown in Fig. 10. While the "wings" of the numerical $P(\psi)$ seem to fit the gaussian prediction, there is a definite disagreement near $\psi = 0$. Of course, this central peak is readily explained in view of the localized bouncing ball mode structure shown in Fig. 8d: it reflects the large semicircular ends of the stadium where these modes are evanescent. In fact, the distribution for bouncing ball modes is similar to those found for circular modes.

Figure 11 shows $P(\psi)$ for the circular mode shown in Fig. 4. Here, the effect of an evanescent region is overwhelming: this is due to the large interior disk where the high angular momentum mode has very low amplitude. Furthermore, the probability of finding large values of ψ is greater for the circular mode than for the chaotic stadium mode: this reflects the existence of the caustic region in Fig. 4. We conclude that a regular mode is characterized by a non-gaussian probability distribution; in this case, $P(\psi)$ displays a balance between the extremes of high and low amplitude regions (since the width of $P(\psi)$ is constant) and in this way it describes the dominant features of this type of mode. By this measurement, localized stadium modes (such as bouncing ball modes) are similar to regular modes, even though the nature of the ray-wave correspondence which this association entails remains unexplained.

In order to quantify these observations, for each mode studied we have measured the fit to the proposed gaussian (24) by computing the residual defined by

$$\rho^2 \equiv \frac{1}{n} \sum_{i=1}^{n} \left[P(\psi_i) - P_0(\psi_i) \right]^2 \tag{25}$$

Here, n is the number of bins in the histogram $P(\psi)$ (we have used $n = 100$). This quantity

was evaluated for sample eigenfunctions with $60 \leq k \leq 70$ at both $\gamma = 0$ and $\gamma = 1$; in addition, we have also investigated the trend in ρ as γ takes on intermediate values. The results are shown in the graph of ρ *vs.* γ in Fig. 12.

At $\gamma = 0$, the residual ρ varies over a wide range from the worst fit (large ρ) for high angular momentum modes to the best for low angular momentum modes (small m). Almost all modes examined for $\gamma \geq 0.25$ exhibit a uniformly better fit to the predicted gaussian by an average factor of about four. The obvious exceptions to this general behavior (denoted by the squares) are the bouncing ball modes, which have values of ρ typical of low angular momentum circular modes; this again is consistent with earlier remarks. The intermediate value of $\gamma = 0.125$ represents the case where the wavelength of the modes in this range of the spectrum is comparable to the irregularity in the boundary (the length of the straight section) and appears to mark a transition between systems with regular and irregular modes (at least as far as this measurement is concerned). If this transition is truly a wave effect (the mode "sensing" the irregularity) then the threshold should decrease to lower values of γ as the wavelength is shortened as in the ray limit (where rays are ergodic for all $\gamma > 0$). In the next Section, however, we present an observation which would seem to contradict this idea of a "wave threshold".

We have also considered the statistics of a linear superposition of two neighboring levels ψ_1 and ψ_2

$$\psi_\alpha \equiv \psi_1 + \psi_2 \cos\alpha \tag{26}$$

where α is a relative phase and ψ_α is properly normalized. The average probability distribution

$$\bar{P}(\psi) \equiv \frac{1}{\pi}\int_0^\pi P(\psi_\alpha)\, d\alpha \tag{27}$$

is then computed by constructing the histogram $P(\psi_\alpha)$ at 13 values of α for $0 \leq \alpha \leq \pi$ and averaging.

In the circular case, the levels chosen were the high angular momentum mode of Fig. 4 and a neighboring low angular momentum mode with $k_{4,19} = 65.067$ for which $\Delta k = 0.055$. An

example of the superposed mode structure at a single value of α is shown in Fig. 13; although the nodal and intensity patterns for this combination appears somewhat "irregular", they are not quite as random as those found for chaotic stadium modes. The average $\bar{P}(\psi)$ is displayed in Fig. 14 and the residual ρ of the fit to the standard gaussian is plotted in Fig. 12 as the cross at $\gamma = 0$. The fit is now better than for any pure state, including that for chaotic stadium modes, despite the fairly ordinary appearance of the wave function. One reason for this is the smoothing out of the "wings" of the probability distribution due to the better statistics involved in the averaging: the jagged peaks have coalesced with the varying amplitude of the wave peaks at different values of α. Note that the central peak of $\bar{P}(\psi)$ near $\psi = 0$ persists.

For the $\gamma = 1$ stadium, we have studied the superposition of $k_1 = 65.326$ and $k_2 = 65.412$ ($\Delta k = 0.086$). The averaged distribution $\bar{P}(\psi)$ shown in Fig. 15 is now an extremely good fit due to the averaging process; this is confirmed by its value of ρ in Fig. 12 (the cross at $\gamma = 1$). It seems that the net effect of averaging over the relative phase of two superposed modes is about a factor of three in the value of ρ gauging the fit to the standard gaussian. The superposition of many modes and subsequent averaging may produce better gaussian statistics even for the circular case.

We have also studied the statistics of the normal derivative $\psi_\eta \equiv \partial\psi/\partial\eta$ evaluated on the boundary for regular and irregular modes. As a comparison, both Berry[24] and Ott and Manheimer[25] have suggested that the mean square value of the normal derivative of an irregular mode should satisfy

$$\langle\psi_\eta^2\rangle_B = k^2\langle\psi^2\rangle_A = 4k^2/\pi \tag{28}$$

where the average on the left is over the boundary and that on the right is over the interior (*i.e.*, by (23) it is equal to the width $\psi_{rms}^2 = 4/\pi$). We have tested this hypothesis and have examined the distribution $P(\psi_\eta)$. Numerically, we could sample the normal derivative at only 50-100 points along the one-dimensional boundary, as opposed to the approximately 5000 interior sample points available for constructing $P(\psi)$. In order to increase the statistics, we considered the superposition

$$\psi[\underline{\theta}] \equiv \psi_1 \cos\theta_1 + \psi_2 \cos\theta_2 \tag{29}$$

and have allowed θ_1 and θ_2 to vary independently in $0 \leq \theta \leq \pi$ (keeping $\psi[\underline{\theta}]$ properly normalized). The averaged distribution of normal derivative is thus constructed in analogy with (27)

$$\bar{P}(\psi_\eta) \equiv \frac{1}{\pi^2}\int_0^\pi P(\psi_\eta[\underline{\theta}])\, d\theta_1 d\theta_2 \tag{30}$$

For the case of regular modes at $\gamma = 0$, we again examined the combination of the low and high angular momentum modes previously introduced. The distribution $\bar{P}(\psi_\eta)$ shown in Fig. 16 has a root mean square of 61.87, which is to be compared with the value $k \approx 65.0$ (for both modes) to be used in (28). The distribution for the superposition of the two irregular modes at $\gamma = 1$ ($k_1 = 65.326, k_2 = 65.412$) is shown in Fig. 17, where the width is 61.07. In both cases the root mean square is near the predicted value (although (28) does not apply to regular modes) and, perhaps surprisingly, $\bar{P}(\psi_\eta)$ for the superposition of two irregular modes is fairly well-approximated by a gaussian.

These results tend to substantiate the prediction that chaotic irregular modes can be characterized as gaussian random functions. They also point out that in terms of $P(\psi)$ as a criterion, the classification of regular and irregular waves based on corresponding ray properties may need refinement (at least for this system) in order to account for the anomalous properties of bouncing ball modes. Moreover, while most stadium modes are chaotic by this standard, they do not manifest the uniform intensity expected from a primitive concept of ray-wave correspondence. As previously argued, these are also aspects of higher eigenvalue ranges so that they do not appear to be finite wavelength effects.

V. Variation of Modes with γ

We have observed another peculiar qualitative aspect of the contrast between stadium and circular eigenfunctions in terms of the differing properties of the corresponding rays. As previously stated, almost all orbits in the stadium are ergodic for all values of $\gamma > 0$, whereas the graph of ρ *vs.* γ in Fig. 12 seems to indicate that in order for wave functions to become chaotic, γ has to be large enough for the wavelength to "sense" the straight section a in the boundary. Thus, even though the modes in the range of the spectrum near $k = 65$ meet the eikonal condition for $\gamma \approx 0$ ($kR(\gamma) \approx 65$, $\lambda/R \approx 0.1$), the values of $ka = k\gamma R$ or $a/\lambda = \gamma R/\lambda$ are a factor of γ smaller. (Recall that a, the half-length of the straight section, and R, the radius of the semicircle, are both γ-dependent since the area is held constant: $R(\gamma) = [1 + (4\gamma/\pi)]^{-1/2}$). For these modes, the threshold γ for irregularity should be such that,

$$1 \approx \frac{a(\gamma)}{\lambda} = \gamma\frac{R(\gamma)}{\lambda} = \frac{\gamma}{\lambda}\left[1 + \frac{4\gamma}{\pi}\right]^{-1/2} \tag{31}$$

which for $k \approx 65$ gives $\gamma \approx 0.1$ as observed in Fig. 12.

In an attempt to observe this wave transition, we have followed the evolution of several eigenvalues and eigenfunctions as γ is increased slightly above zero. Figure 18 is a graph of the trajectories of six eigenvalues as a function of γ, for $0 \leq \gamma \leq 0.07$. The parenthetical number labelling each curve refers to the value of m (angular momentum) of that mode at $\gamma = 0$. Immediately obvious is the quite disparate behavior of the high and low angular momentum modes, the latter displaying much greater sensitivity to the change in boundary shape even at very small γ. A similar sensitivity of low angular momentum modes to perturbation has been noticed by Tabor[26] in a different problem, but here these modes seem to be "feeling" the straight section in a regime much lower than the threshold (31).

Equally striking is the evolution of the eigenfunctions of the low angular momentum modes. The pictures in Fig. 19 depict the changes in $J_2(k_{2,20}r)\sin 2\theta$ at 0.01 intervals for $0 \leq \gamma \leq 0.07$. Particularly interesting are the mode structures at $\gamma = 0.02$ and $\gamma = 0.05$.

Further analysis shows that near $\gamma = 0.05$, the eigenvalue of this mode is very near another eigenvalue (although not shown in Fig. 18) so that this fairly chaotic pattern may be due to the mixing of nearly degenerate modes. This effect of the collision of eigenvalue trajectories will be discussed below.

The structure of the mode in Fig. 19*c* is very reminiscent of that found in stadium bouncing ball modes. In the interval $0 \leq \gamma \leq 0.02$, the nodal line which at $\gamma = 0$ was the positive x-axis has swung radially leaving behind a large section of the quadrant with very small amplitude. This could be interpreted as an effect of spontaneous circular symmetry breaking compatible with the ray picture: the low angular momentum mode represents almost diametrically oscillating rays (with $a_{\omega,m} \simeq 0.03$), so that as γ is increased slightly the most stable family of rays (*i.e.*, the ones bouncing between the straight sections) with nearly this property are "favored" to represent the mode. Although there is no rigorous theory for this correspondence (since even the low angular momentum ray torus in phase space is destroyed when γ differs from zero), it would be interesting to determine if the bouncing ball modes observed at $\gamma = 1$ do indeed originate from small m modes at $\gamma = 0$.

The rather insensitive behavior of the high angular momentum eigenvalues in Fig. 18 is accompanied by only a slight change in the eigenfunctions. Figure 20 shows that the rapidly oscillating angular structure of an $m = 48$ mode is modulated so that the amplitude is diminished near $\theta = \pi/4$ (although the caustic peak seems unaffected). These whispering gallery type modes may persist and evolve into similar structures such as the mode shown in Fig. f, but this connection has not been investigated.

In the next Section, the spectrum of eigenvalues will be analyzed statistically at different γ in terms of the probability distribution of neighboring energy level spacings $P(\Delta E)$, for $E \equiv k^2$. The graph of eigenvalue evolution in Fig. 18 has a bearing in this regard as it reveals several instances of apparent eigenvalue trajectory crossings. Such an intersection implies a degeneracy of modes at that value of γ, and as such is an important contribution to $P(\Delta E)$ at $\Delta E = 0$. It is common lore that eigenvalues generically do not cross under perturbation and that such a degeneracy marks a symmetry of the system. Although there has been much discussion[27-29] of this

phenomenon and its relation to the integrability of the corresponding ray system, we shall not address the general question of eigenvalue crossings for the present system, except in the light of Fig. 18 and the computation of $P(\Delta E)$. It is important to remember that the two-fold degeneracy of modes in the circle ($\sin m\theta$ and $\cos m\theta$, due to the continuous angular symmetry) is removed when the modes are separated into reflection parity classes. Therefore, crossings or near degeneracies due to this effect do not appear in Fig. 18 or in $P(\Delta E)$.

Considering the wide range of eigenvalue sensitivity to boundary perturbation exhibited in Fig. 18, it is natural to expect the several crossings indicated. However, it is difficult to determine numerically whether these trajectories actually intersect or narrowly avoid each other as schematically illustrated in the inset; the numerical error in the eigenvalue produces an uncertainty in both trajectories in a small neighborhood of the apparent crossing. Even the computation of the eigenfunctions of the two modes involved at values of γ before and after the intersection is not necessarily a good test because in the vicinity of the near degeneracy there is considerable mixing and the identity of the eigenvalue-eigenfunction association is lost.

The behavior of the eigenvalues as a function of γ near $\gamma = 1$ is similar to that found for small γ; that is, most modes are fairly insensitive to changes in the boundary, but there are exceptions. The eigenvalues of bouncing ball modes in this regime follow trajectories which can be understood in terms of the fact that they are quite accurately given by a rectangular quantization formula

$$\begin{aligned} k^2 &= \pi^2\left[\frac{m^2}{a^2}+\frac{n^2}{R^2}\right] = \frac{\pi^2}{\gamma^2}\left[1+\frac{4\gamma}{\pi}\right](m^2+\gamma^2 n^2) \\ \frac{dk}{d\gamma} &= \frac{2k}{4\gamma+\pi} - \frac{k}{\gamma}\left[\frac{(m/\gamma n)^2}{1+(m/\gamma n)^2}\right] \\ &\approx \frac{2k}{4\gamma+\pi} \end{aligned} \tag{32}$$

where the approximation $n \gg m$ has been made corresponding to these modes with large k_y. From this it is clear that both the first and second derivatives are of the order of k. Other authors [29,30] have used the second derivatives (or second differences) of eigenvalue trajectories to

classify the regular and irregular spectrum, noting that irregular modes are generally more sensitive to perturbation. This result is contradictory in that respect; bouncing ball modes (which seem to share more of the properties of regular modes) are very sensitive, whereas the chaotic irregular stadium modes are stable and insensitive to perturbation.

Whispering gallery modes on the other hand are much less sensitive. Considering an approximate one-dimensional perimeter quantization rule, one has

$$k = \frac{2\pi n}{4a + 2\pi R} = \frac{n[1 + (4\gamma/\pi)]^{1/2}}{1 + (2\gamma/\pi)}$$
$$\frac{dk}{d\gamma} = \frac{2k}{\pi}\left[\left[1 + \frac{4\gamma}{\pi}\right]^{-1/2} - \left[1 + \frac{2\gamma}{\pi}\right]\right] \tag{33}$$

At $\gamma = 1$, the numerical factor in brackets is about 0.052 which greatly diminishes the dependence on k. In fact, for very small γ,

$$\frac{dk}{d\gamma} \approx \frac{4k\gamma^2}{\pi^3}$$

which explains the insensitivity of high angular momentum modes near $\gamma = 0$.

VI. Statistics of the Spectrum

In addition to the striking qualitative and quantitative differences between circular and stadium eigenfunctions presented in the previous Sections, we have also statistically compared the eigenvalue spectra of the circular and stadium cases. Many authors[27-36] have considered different properties of the spectrum in order to characterize the nature of quantum chaos and its relation to the ergodic properties of the corresponding classical system. A statistical description of the spectrum in terms of the probability distribution of neighboring level separations has received particular attention, and in a previous Letter[2] we first reported numerical results on this

measurement for the present problem. In more recent work, Bohigas, Giannoni and Schmit,[33] Casati, Chirikov and Guarneri,[34] Seligman, Verbaarschot and Zirnbauer,[35] and others[36] have attempted to relate this and other statistics (for the spectra of other Hamiltonians) to similar statistics found for ensembles of random matrices. Here, we analyze our results for the stadium in the light of recent theoretical investigations which describe the tendency of levels to "cluster" or "repel" depending on the nature of the underlying ray phase space.

As stated in the numerical analysis of Section III, we have considered eigenvalues of only one parity (odd-odd), and due to computational restrictions we have limited our investigation to the region of the spectrum $50 < k < 100$. In two dimensions, the mean asymptotic density of eigenvalues is

$$n(k)\,dk = 2\pi\frac{A}{(2\pi)^2}k\,dk = \frac{1}{2}k\,dk \tag{34}$$

(since the area A = const. = π). Using this, the number of eigenvalues (of a single parity) expected in this range is approximately 450, with $k = 50$ about 150 levels above the ground state. We shall be interested in theoretical results concerning the statistics of the energy eigenvalue $E \equiv k^2$, which in two dimensions is more appropriate as the density $n(E)$ is constant due to (34). Thus for a single parity p, we expect the density and average separation to be

$$\begin{aligned} n(E) = n(k)\frac{dk}{dE} &= \frac{1}{2}k\frac{1}{2k} \\ n_p(E) &= \frac{1}{4}n(E) = \frac{1}{16} \\ \overline{\Delta E} &= n_p^{-1}(E) = 16 \end{aligned} \tag{35}$$

In the circular ($\gamma = 0$) case, we numerically computed 451 odd-odd parity eigenvalues in this range of the spectrum. As a check, these results may be compared with the exact number of 454 obtained using standard Bessel function routines. The discrepency in number is due to our numerical procedure which missed 16 eigenvalues while determining 13 "spurious" ones. Comparing individual eigenvalues, we determined our reliable error in k to be ± 0.001; this is an error in E of about ± 0.2 (for k near 100). We assume this estimate to be valid even when $\gamma > 0$.

From the eigenvalue data for the circle, we compute the level spacings and construct a histogram for the probability distribution $P(\Delta E)$ with bin size $\Delta_B E = 2$. In Fig. 21*a* we present the results obtained from the numerical eigenvalues, and in Fig. 21*b* is the distribution using the exact eigenvalues. The numerical omission of some eigenvalues and inclusion of several spurious ones is largely responsible for the disagreement between these two histograms although the general structure is the same for both. The feature to be emphasized is the fact that the distribution is peaked at $\Delta E = 0$, signifying that the spectrum is clustered; this is countered by the existence of a rather long tail (values of ΔE up to 71 were observed) in order to maintain the average value given by (35) (numerically $\overline{\Delta E} = 16.654$, exactly $\overline{\Delta E} = 16.544$ due to the absence of the $m = 0$ modes for odd-odd parity). Berry and Tabor[37] have shown that for a generic integrable Hamiltonian, the distribution $P(\Delta E)$ is of exponential form (Poisson statistics) when effects of the average eigenvalue density dependence on E are subtracted (these do not appear in two dimensions).

The distribution in Fig. 21 has the appearance of an exponential, but in order to test this hypothesis we have instead studied the cumulative probability

$$N(\Delta E) \equiv \int_0^{\Delta E} P(s)\, ds \tag{36}$$

of level separations less than ΔE. With our statistics, this is a smoother function of ΔE and does not depend on the choice of a bin size as does the histogram. Thus, if the normalized probability distribution has the form

$$P(\Delta E) = \alpha e^{-\alpha \Delta E} \tag{37}$$

then

$$N(\Delta E) = 1 - e^{-\alpha \Delta E} \tag{38}$$

The experimental $N(\Delta E)$ from our numerical data and the best one-parameter fit of the form (38) (demanding normalization) are displayed in Fig. 22; this fit was obtained for the value of

$\alpha = 1/20.77$. Since for a normalized distribution of this form $\alpha^{-1} = \overline{\Delta E}$, this result for the mean level separation is in disagreement with numerical evidence and the asymptotic theory of (35). We therefore conclude that, although the probability distribution of level spacings $P(\Delta E)$ for the circular (integrable) case exhibits the characteristics of the prediction (37) indicating level clustering, it must not be of this simple form. There are two possible explanations: (*i*) the circular case is too special (*i.e.*, it does not meet the genericity requirements of Ref.[37]), or (*ii*) we have not investigated a large enough region of the spectrum to include more "asymptotic" eigenvalues.

For the nonintegrable stadium ($\gamma = 1$), we have numerically computed 445 eigenvalues in the same range of the spectrum. The histogram representing the spacing distribution $P(\Delta E)$ is shown in Fig. 23, again with bin size $\Delta_B E = 2$. By comparison with the circular case, this distribution indicates a more uniform arrangement of the eigenvalues; very few small or large spacings were detected while the distribution is peaked near the average value (35). Zaslavskii[32] has attempted to explain this tendency of the levels to "repel" (the behavior of $P(\Delta E)$ as $\Delta E \rightarrow 0$) in terms of the Kolmogorov entropy of the associated dynamical system. The authors in Refs.[33-36] have tried to relate this feature to the similar behavior exhibited by the eigenvalues of random matrices as studied by Wigner, Dyson, Mehta and others[38] In these theories, it is found that $P(\Delta E)$ has the form

$$P(\Delta E) = a(\Delta E)^{\alpha} e^{-\beta(\Delta E)^2} \tag{39}$$

so that the repulsion is modelled by

$$P(\Delta E) \simeq a(\Delta E)^{\alpha}; \qquad \text{for } (\Delta E/\overline{\Delta E}) \ll 1 \tag{40}$$

Again, we test this prediction by attempting to fit the integral of (39) to the smoother numerical $N(\Delta E)$ shown in Fig. 24. The best two-parameter fit (demanding normalization) yields the values $\alpha = 0.71, \beta = 0.0025$. The average value $\overline{\Delta E}$ of the normalized theoretical curve with these parameters is 16.1, as compared with the data average of 16.4.

Zaslavskii has related the exponent α to the K-entropy K by

$$\alpha = C/\ln K \tag{41}$$

where C is some constant that depends on the system. Using extremely simplified formulas given in Ref.[32], we find for the stadium that $K \approx 2\gamma = 2$ so that the constant C in (41) is 0.49; this is in remarkable agreement with the value of about 1/2 calculated by Zaslavskii and Filonenko[39] for skipping electrons. Actually, one should measure the dependence of α on K (or γ) in order to test the validity of the prediction (41).

VII. Conclusion

We have numerically examined the statistical properties of short wavelength eigenfunctions and eigenvalue spectrum of the solutions of the Helmholtz equation in a stadium-shaped two-dimensional region. These results were analyzed with a view towards understanding the features of the waves and spectrum in terms of the properties of the corresponding geometrical optics rays, which for the stadium are ergodic. We also compared our numerical findings with theoretical predictions based on semiclassical arguments applied to bound nonintegrable Hamiltonian systems. Our results can be summarized as follows:

(1) Most eigenfunctions for the stadium appear to be composed of small regions (of several wavelengths) with relatively high intensity randomly interspersed among larger areas of low amplitude. This *chaotic* wave structure differs considerably from the uniform intensity distribution over the interior of the stadium which would be expected on the basis of the ergodic nature of the rays.

(2) Many eigenfunctions are quite regular in appearance and share many of the features of circular modes. Moreover, most of these *localized* modes display an obvious relationship with underlying periodic ray trajectories. This is especially so for the largest class of this type which

correspond to the family of bouncing ball orbits. Also in this category are the whispering gallery modes which appear to have been identified.

These qualitative remarks contrasting the wide variety of eigenmode structures found in the stadium with the comparatively ordinary circular modes have been substantiated to a degree with a statistical analysis. The construction of the probability distribution $P(\psi)$ has provided one method for distinguishing between the circular and the localized stadium modes on the one hand and the chaotic stadium modes on the other. The principal conclusion is

(3) Chaotic eigenfunctions may be described by gaussian statistics (*i.e.*, $P(\psi)$ and $P(\partial\psi/\partial\eta)$ are well-approximated by a gaussian distribution). This result supports the idea that a wave constructed from many contributions at a point due to the multiple random passages of mixing ray trajectories is phase decorrelated. In this respect, the chaotic nature of most stadium modes seems to be related to the similar behavior of the corresponding rays despite the fact that the eigenfunctions do not exhibit uniform intensity over the interior. Like circular modes, the localized stadium eigenfunctions (such as bouncing ball modes) exhibit extremely non-gaussian distributions.

Considering the apparent contradiction noted in (1) above between the ergodic nature of the rays and the nonuniform intensity distribution observed in chaotic stadium modes, we have attempted to illuminate the correspondence between these normal modes and some object in the ray phase space. Therefore, we have numerically computed the local spatial correlation for several regular and chaotic modes, and have compared our results with theoretical predictions derived from rather crude assumptions for the locally averaged Wigner function. The numerical evidence seems to infer the following conclusions:

(4) The locally averaged Wigner function associated with a short wavelength regular mode of an N-dimensional integrable ray system can be fairly well-approximated by an N-dimensional delta function in phase space which is nonzero only on the torus which corresponds to the mode in the eikonal (EBK) theory.

This conclusion was inferred from the extremely accurate matching of the numerical correlation function of sample circular modes with the prediction based on this singular behavior of

the locally smoothed Wigner function. In this way, the Wigner function provides a realization of the correspondence between regular modes and integrable rays.

(5) The locally averaged Wigner function constructed from asymptotic irregular modes is probably not described as simply by a one dimensional delta function on the frequency surface corresponding to the frequency eigenvalue. It may have more complicated structure either within this surface or in the transverse direction off the manifold. This is to some extent corroborated by the uneven intensity distribution observed in chaotic stadium modes.

Again, this is a judgement inferred from the comparison of the numerical correlation data with theory based on just such a delta function assumption; here the agreement was not as clear as in the circular case. Since the Wigner function itself was not explicitly constructed, the correspondence between chaotic modes and chaotic rays (if indeed one exists) remains uncertain.

(6) Finally, the spectrum of the stadium geometry can be characterized by a distribution of neighboring level spacings which is similar to the Wigner distribution found for ensembles of random matrices.

Acknowledgements

We have benefited greatly from discussions with Michael Berry, Giulio Casati, Wallace Manheimer and Robert Riddell. This work was supported by the Offices of Fusion Energy and of Basic Energy Sciences of the U.S.Department of Energy under Contract No.DE-AC03-76SF00098.

References

1. Based on the Ph.D: thesis submitted by S. W. McDonald, University of California, Lawrence Berkeley Laboratory, Report #LBL-14837, 1983 (unpublished), University Microfilms #8413506.
2. S. W. McDonald and A. N. Kaufman, *Phys. Rev. Lett.* **42**, 1189 (1979).
3. M. V. Berry, *J. Phys. A* **10**, 2083 (1977).
4. M. V. Berry, *Phil. Trans. Roy. Soc. A* **287**, 237 (1977).
5. G. Casati, F. Valz-Gris and I. Guarneri, *Lett. Nuov. Cim.* **28**, 279 (1980).
6. M. Shapiro and G. Goelman, *Phys. Rev. Lett.* **53**, 1714 (1984).
7. R. D. Taylor and P. Brumer, *Faraday Discuss. Chem. Soc.* **75**, 110, 117 (1983); M. Shapiro, R. D. Taylor and P. Brumer, *Chem. Phys. Lett.* **106**, 325 (1984); P. Brumer and M. Shapiro, *Chem. Phys. Lett.* **72**, 528 (1980); K. Christoffel and P. Brumer, *Phys. Rev A* **31**, 3466 (1985) and **33**, 1309 (1986).
8. E. J. Heller, *Phys. Rev. Lett.* **53**, 1515 (1984).
9. Y. Y. Bai, G. Hose, K. Stefanski and H. S. Taylor, *Phys. Rev. A* **31**, 2821 (1985).
10. V. P. Maslov and M. V. Fedoriuk, *Semi-Classical Approximation in Quantum Mechanics* (Reidel, 1981).
11. V. I. Arnold, *Mathematical Methods of Classical Mechanics* (Springer-Verlag, New York, 1978).
12. L. A. Bunimovich, *Funct. Anal. Appl.* **19**, 254 (1974).
13. G. Bennettin and J.-M. Strelcyn, *Phys. Rev. A* **17**, 773 (1978).
14. A. Einstein, *Verhand. Phys. Deut. Ges.* **19**, 82 (1917).
15. L. Brillouin, *J. Phys. Radium* **7**, 353 (1926).
16. J. B. Keller, *Ann. Phys. (N.Y.)* **4**, 180 (1958); J. B. Keller and S. I. Rubinow, *Ann. Phys.* **9**, 24 (1960).
17. I. C. Percival, *Adv. Chem. Phys.* **36**, 1 (1077).

18. E. P. Wigner, *Phys. Rev.* **40**, 749 (1932).

19. J. E. Moyal, *Proc. Camb. Phil. Soc. Math. Phys. Sci* **45**, 99 (1947); R. Kubo, *J. Phys. Soc. Jap.* **19**, 2127 (1964); B. Leaf, *J. Math. Phys.* **9**, 65, 769 (1968); E. J. Heller, *J. Chem. Phys.* **65**, 1289 (1976), **67**, 3339 (1977); H. Bremmer, *Radio Science* **8**, 511 (1973); W. Siegel, *Acta Phys. Pol.* **B7**, 29 (1976); M. J. Bastiaans, *Opt. Comm.* **25**, 26 (1978), **30**, 321 (1979), *Opt. Acta* **26**, 1265, 1333 (1979), *J. Opt. Soc. Am.* **69**, 1710 (1979); R. F. O'Connell and E. P. Wigner, *Phys. Lett.* **83A**, 145 (1981).

20. N. L. Balasz, *Physica* **102A**, 236 (1980).

21. A. Voros, *Ann. Inst. H. Poincaré* **24A**, 31 (1976) and also in *Stochastic Behavior in Classical and Quantum Hamiltonian Systems*, Eds. G. Casati and J. Ford, *Lecture Notes in Physics* **93** (Springer-Verlag, Berlin and New York, 1979).

22. R. J. Riddell, Jr., *J. Comp. Phys.* **31**, 21 (1979).

23. R. M. Stratt, N. C. Handy and W. H. Miller, *J. Chem. Phys.* **71**, 3311 (1979).

24. M. V. Berry, private communication.

25. E. Ott and W. M. Manheimer, *Phys. Rev. A* **25**, 1808 (1982).

26. M. Tabor, *Adv. Chem. Phys.* **46**, 73 (1981).

27. M. V. Berry, *Ann. Phys.* **131**, 163 (1981).

28. T. P. Valkering and W. J. Caspers, *Physica* **63**, 113 (1973); J. von Neumann and E. P. Wigner, *Physik Z.* **30**, 467 (1929); R. Ramaswamy and R. A. Marcus, *J. Chem. Phys.* **74**, 1379, 1385 (1981); R. Ramaswamy, *J. Chem. Phys.* **76**, 15 (1982).

29. D. W. Noid, M. L. Koszykowski, M. Tabor and R. A. Marcus, *J. Chem. Phys.* **72**, 6169 (1980).

30. I. C. Percival, *J. Phys. B* **6**, 559 (1973); N. Pomphrey, *J. Phys. B* **7**, 1909 (1974).

31. E. Haller, H. Köppel and L. S. Cederbaum, *Phys. Rev. Lett.* **52**, 1665 (1984); T. Ishikawa and T. Yukawa, *Phys. Rev. Lett.* **54**, 1617 (1985); T. Yukawa, *Phys. Rev. Lett.* **54**, 1883 (1985); K. Nakamura, Y. Nakahara and A. R. Bishop, *Phys. Rev. Lett.* **54**, 861 (1985).

32. G. M. Zaslavskii, *Sov. Phys. Usp.* **22(10)**, 788 (1979); *Phys. Rep.* **80**, 157 (1981).

33. O. Bohigas, M. J. Giannoni and C. Schmit, *Phys. Rev. Lett.* **52**, 1 (1984).

34. G. Casati, B. V. Chirikov and I. Guarneri, *Phys. Rev. Lett.* **54**, 1350 (1985).

35. T. H. Seligman, J. J. M. Verbaarschot and M. R. Zirnbauer, *Phys. Rev. Lett.* **53**, 215 (1984).

36. P. Pechukas, *Phys. Rev. Lett.* **51**, 943 (1983); G. Casati, I. Guarneri and F. Valz-Gris, *Phys. Rev. A* **30**, 1586 (1984); M. Kús, *Phys. Rev. Lett.* **54**, 1343 (1985); O. Bohigas, R. U. Haq and A. Pandey, *Phys. Rev. Lett.* **54**, 1645 (1985); T. Terasaka and T. Matsushita, *Phys. Rev. A* **32**, 538 (1985).

37. M. V. Berry and M. Tabor, *Proc. Roy. Soc.* **A356**, 375 (1977).

38. E. P. Wigner, *Math. Ann.* **67**, 325 (1958), and in *Symmetries and Reflections*, edited by E. P. Wigner (Ox Bow, Woodbridge, Connecticut, 1979), p. 203; *Statistical Theories of Spectra: Fluctuations*, edited by C. E. Porter (Academic, New York, 1965); F. J. Dyson, *J. Math. Phys.* **3**, 40, 157, 166 (1962); M. L. Mehta, *Nucl. Phys.* **18**, 395 (1960) and *Random Matrices and the Statistical Theory of Energy Levels* (Academic, New York, 1967); T. A. Brody, J. Flores, J. B. French, P. A. Mello, A. Pandey and S. S. M. Wong, *Rev. Mod. Phys.* **53**, 385 (1981); M. V. Berry and M. Robnik, *J. Phys. A.* **17**, 2413 (1984).

39. G. M. Zaslavskii and N. N. Filonenko, *Sov. Phys.-JETP* **38**, 317 (1974).

Figures

Figure 1. Stadium boundary for the Helmholtz equation. The boundary shape is governed by the parameter $\gamma \equiv a/R$ with the restriction that the area remain constant ($= \pi$).

Figure 2. Typical example of a single trajectory in the ($\gamma = 0$) circle. Due to conservation of angular momentum, every orbit is confined to evolve within an annulus between some minimum radius and the outer radius of the circle.

Figure 3. Typical example of a single trajectory in the $\gamma = 1$ stadium boundary.

Figure 4. Intensity distribution $|\psi_{m,n}|^2(x,y)$ in positive quadrant ($x,y > 0$) of the ($\gamma = 0$) circle. This mode is $\psi_{m,n} = \psi_{40,5} = J_{40}(k_{40,5}r)\sin 40\theta$ with eigenvalue $k_{40,5} = 65.012$.

Figure 5. Locally averaged spatial correlation function $C(\underline{x},\underline{s})$ for circular ($\gamma = 0$) mode of Fig. 4. The point $\underline{x}$ is fixed at $(r,\theta) = (0.866,0.867)$ and the correlation is plotted as a function of $|\underline{s}|$ for three angles ϕ of $\underline{s}$ relative to the x-axis. Crosses denote numerical measurements, solid line is theory based on the real part of Eq.(19). (a) $\phi = 0$. (b) $\phi = \pi/4$. (c) $\phi = \pi/2$.

Figure 6. Typical eigenfunction structure for $\gamma = 1$ stadium, again plotted in the positive quadrant (this eigenvalue is $k = 65.326$). (a) Perspective of intensity distribution. (b) Nodal curves.

Figure 7. Locally averaged spatial correlation function for $\gamma = 1$ stadium mode of Fig. 6. The reference point $\underline{x}$ is fixed at $(x,y) = (0.76,0.46)$ and $C(\underline{x},\underline{s})$ is plotted against $|\underline{s}|$ for three angles ϕ of $\underline{s}$ relative to the x-axis. Crosses denote numerical measurements, solid curve is theory based on Eq.(21). (a) $\phi = 0$. (b) $\phi = \pi/4$. (c) $\phi = \pi/2$.

Figure 8. Intensity distribution for six successive modes near $k \approx 65$ (a-f) and $k \approx 100$ (g-l). (a) $k = 65.036$. (b) $k = 65.326$. (c) $k = 65.412$. (d) $k = 65.0556$ (bouncing ball mode). (e) $k = 65.656$ (spike near boundary due to numerical error). (f) $k = 65.736$ (whispering gallery mode). (g) $k = 100.107$ (whispering gallery mode). (h) $k = 100.144$. (i) $k = 100.202$ (bouncing ball mode). (j) $k = 100.269$. (k) $k = 100.297$. (l) $k = 100.386$.

Figure 9. Probability distribution $P(\psi)$ for $\gamma = 1$ stadium mode of Fig. 6 and comparison to gaussian prediction (24). Each jagged peak in the numerical data is due to a wave "crest" or "trough" in the eigenfunction.

Figure 10. Probability distribution $P(\psi)$ for $\gamma = 1$ bouncing ball stadium mode of Fig. 8d. Large central peak is due to the large number of small values of ψ sampled in the semicircular ends of the stadium.

Figure 11. Probability distribution $P(\psi)$ for $\gamma = 0$ high angular momentum mode of Fig. 4. The peak near $\psi = 0$ represents the contribution from the large evanescent central disk region exhibited by this mode; the shift to the right of zero of this peak is due to (an unsatisfactory) binning procedure.

Figure 12. Variation of residual parameter ρ with γ. Dots at each value of γ denote separate measurements on different individual eigenfunctions; squares denote measurements on bouncing ball modes; crosses denote superposition averages.

Figure 13. (a) Intensity distribution for linear superposition of neighboring low and high angular momentum circular modes $k = 65.012, 65.067$. (b) Nodal structure of same superposition.

Figure 14. Averaged probability distribution $\bar{P}(\psi)$ for the superposition of low and high angular momentum circular modes with standard gaussian comparison.

Figure 15. Averaged probability distribution $\bar{P}(\psi)$ for $\gamma = 1$ stadium superposition ($k = 65.326, 65.412$) and gaussian comparison.

Figure 16. Averaged probability distribution of normal derivative $\bar{P}(\psi_\eta)$ for superposition of the two circular modes of Fig. 13 and gaussian comparison with same numerically determined width (= 61.87).

Figure 17. Averaged probability distribution of normal derivative $\bar{P}(\psi_\eta)$ for superposition of the two stadium modes ($k = 65.326, 65.412$) and gaussian comparison with same numerically determined width (= 61.07).

Figure 18. Evolution of six eigenvalues as γ is increased from zero. Numbers in parentheses denote angular mode number m at $\gamma = 0$. The inset schematically illustrates the possibility of an avoided eigenvalue degeneracy at the several trajectory intersections indicated in the main figure.

Figure 19. (a) Intensity distribution of $\gamma = 0$ circular mode $J_2(k_{2,20}r)\sin 2\theta$. (b) Intensity structure of the same mode at $\gamma = 0.01$. (c) $\gamma = 0.02$. (d) $\gamma = 0.03$. (e) $\gamma = 0.04$. (f) $\gamma = 0.05$. (g) $\gamma = 0.06$. (h) $\gamma = 0.07$.

Figure 20. (a) Intensity distribution of the mode at $\gamma = 0.0125$ which evolves from the circular high angular momentum mode $J_{48}(k_{48,3}r)\sin 48\theta$ at $\gamma = 0$. Note the diminished amplitude at the rim of the circle near $\theta = \pi/4$. (b) Nodal structure of the same mode.

Figure 21. Histograms measuring probability $P(\Delta E)$ of neighboring circular eigenvalue ($E = k^2$) spacings with bin size $\Delta_B E = 2$. Smooth curve is best exponential fit (37) determined by examining the cumulative distribution $N(\Delta E)$. (a) Numerically obtained eigenvalues. (b) Exact eigenvalues.

Figure 22. Cumulative distribution $N(\Delta E)$ of circular eigenvalue spacings. Solid smooth curve is best numerical fit of the form (38).

Figure 23. Histogram $P(\Delta E)$ for $\gamma = 1$ stadium eigenvalue spacings with bin size $\Delta_B E = 2$. Smooth curve is best fit of the form (39) determined by examining the cumulative distribution $N(\Delta E)$.

Figure 24. Cumulative distribution $N(\Delta E)$ of stadium eigenvalue spacings with best-fit prediction (smooth solid curve) based on the integral of Eq.(39).

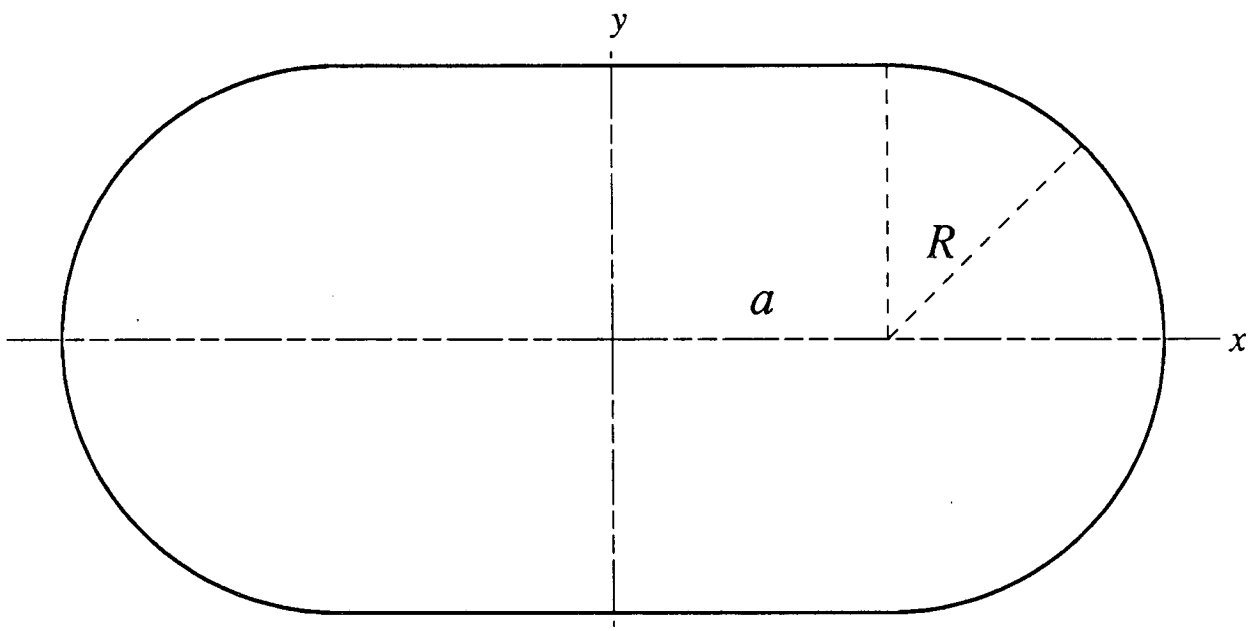

XBL 875-2444

Fig. 1

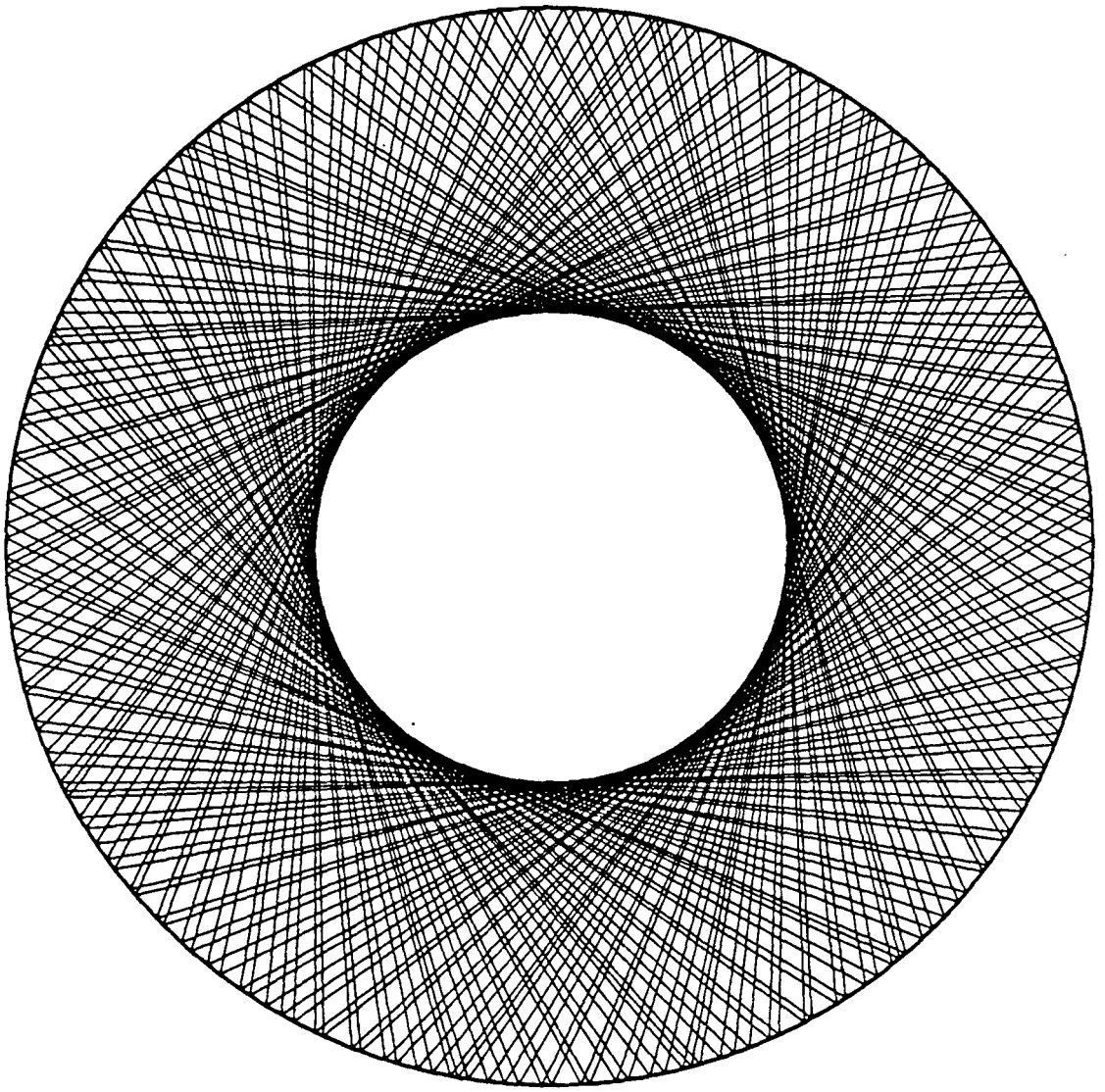

XBL 875-2445

Fig. 2

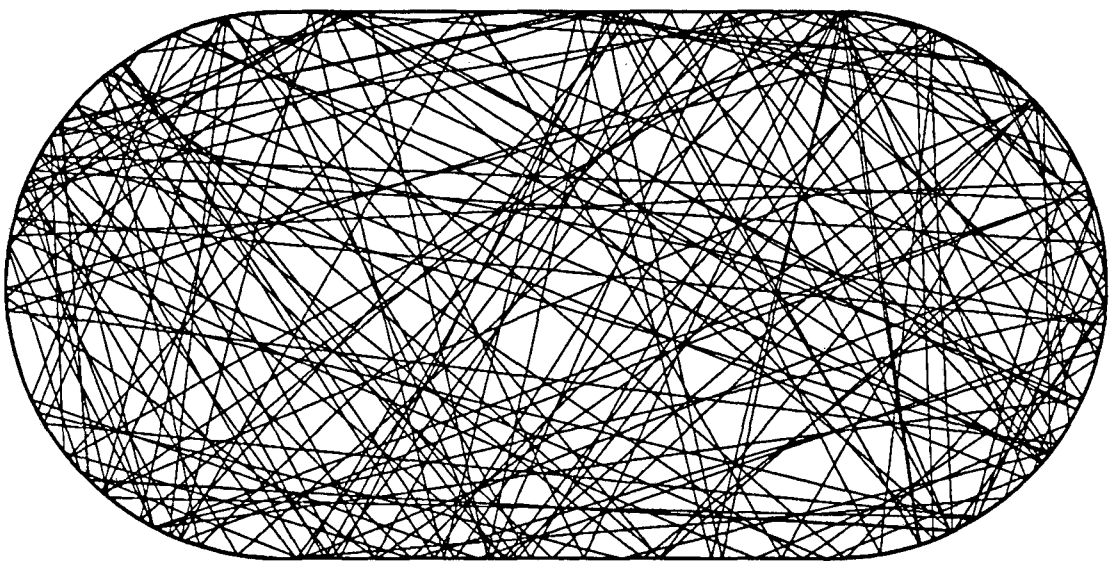

XBL 875-2446

Fig. 3

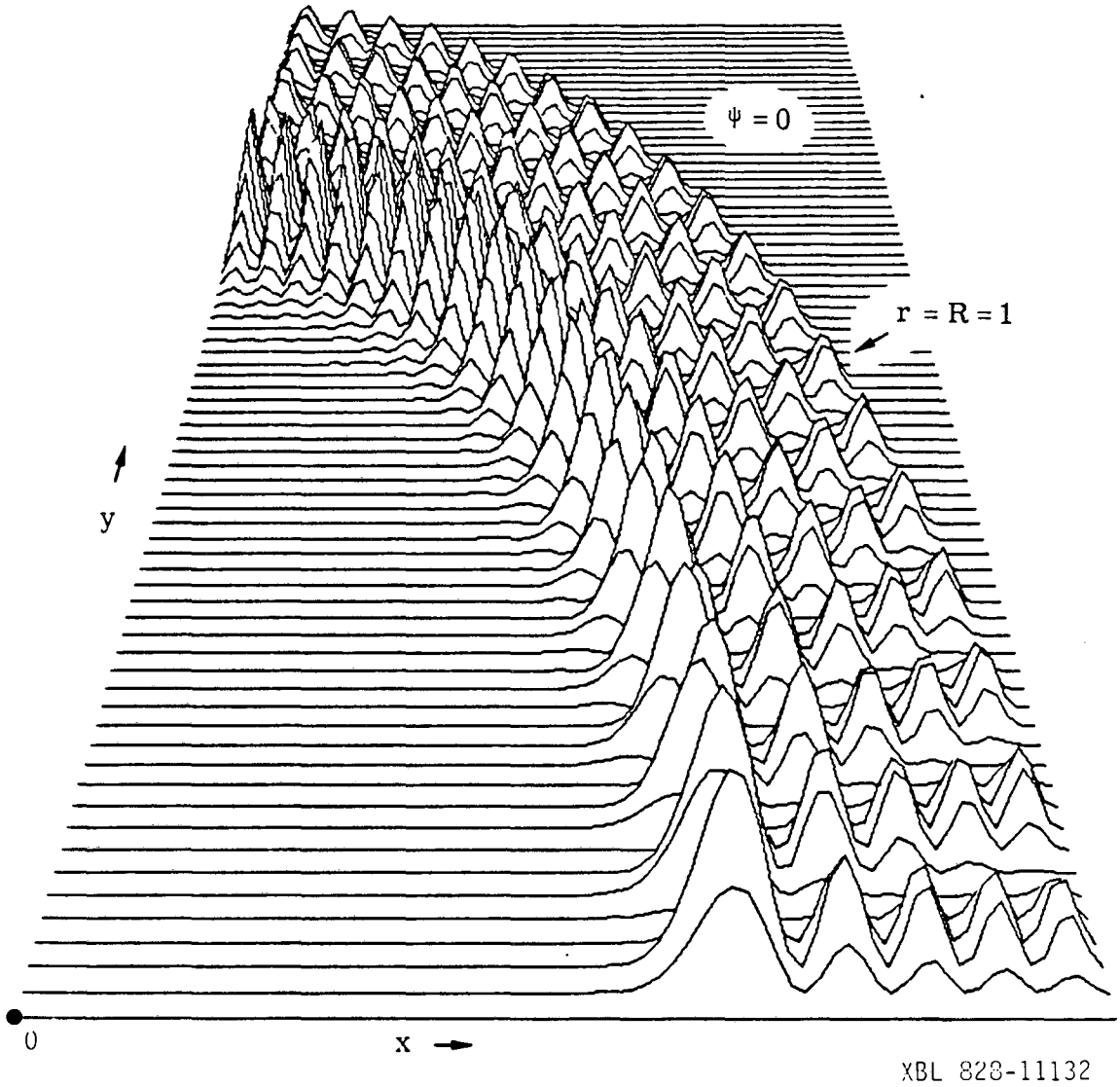

Fig. 4

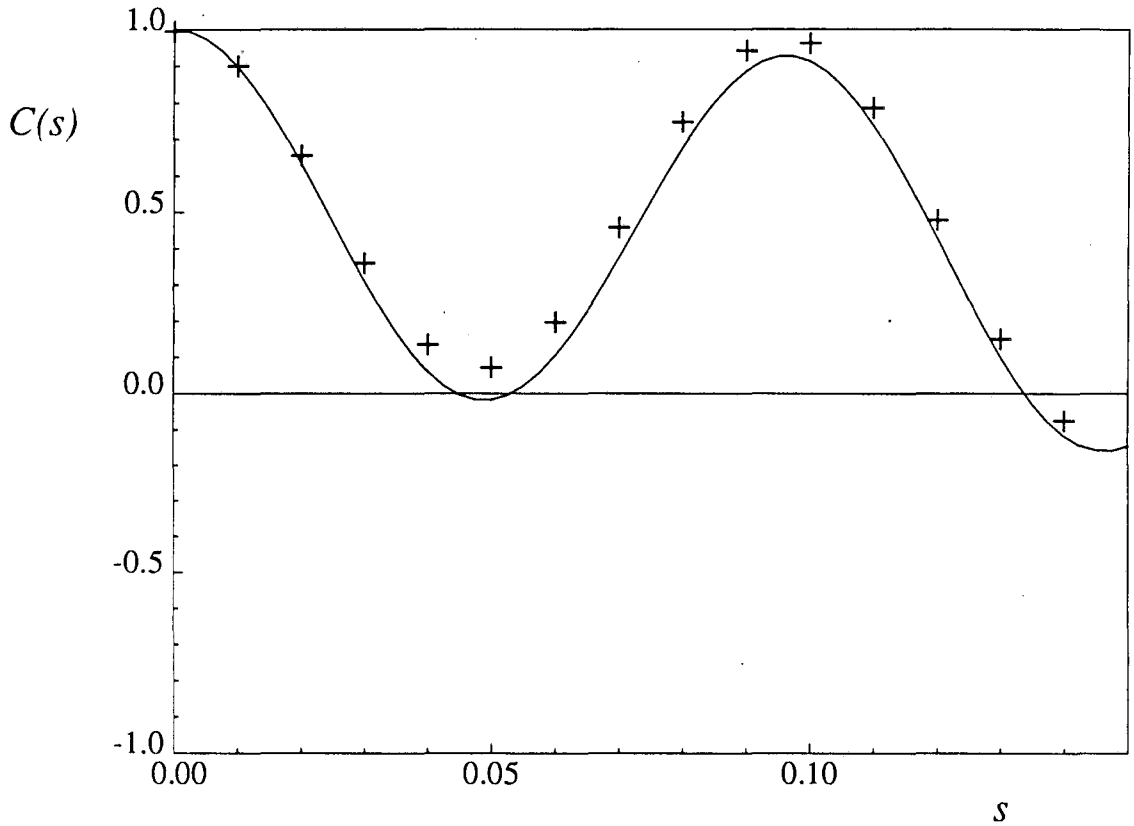

XBL 875-2447

Fig. 5a

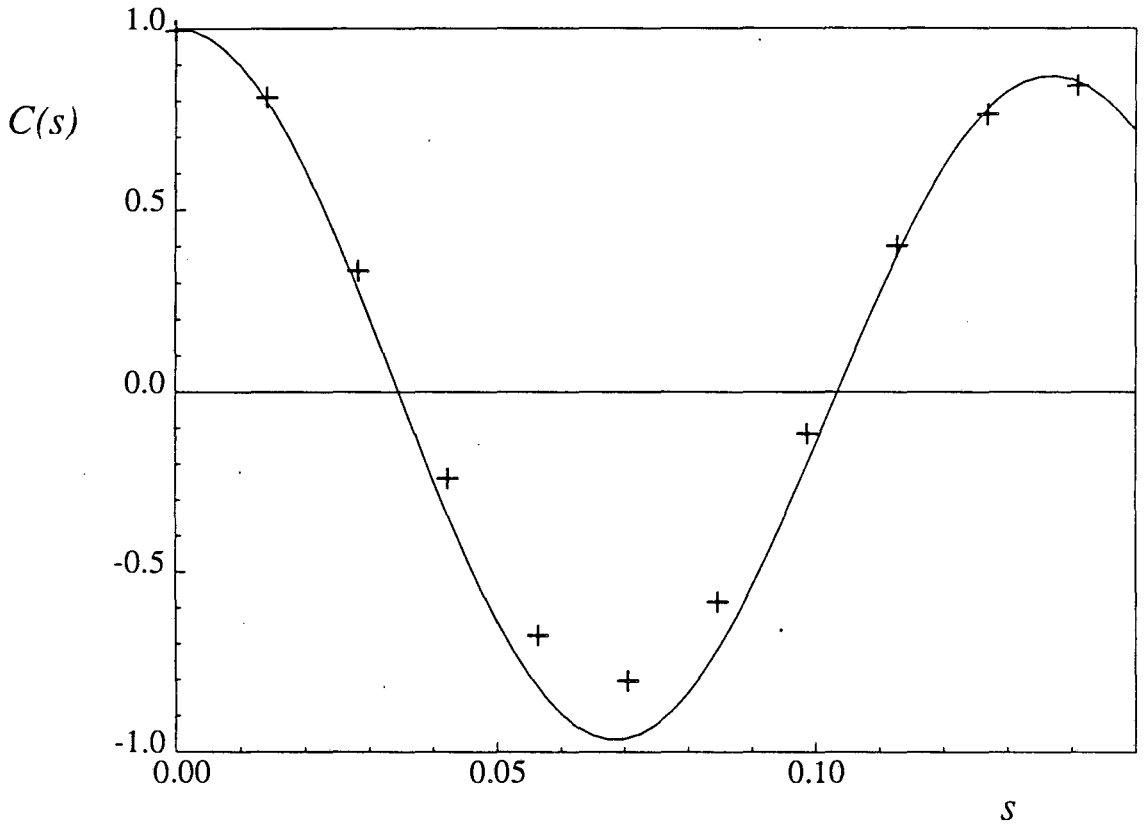

XBL 875-2448

Fig. 5b

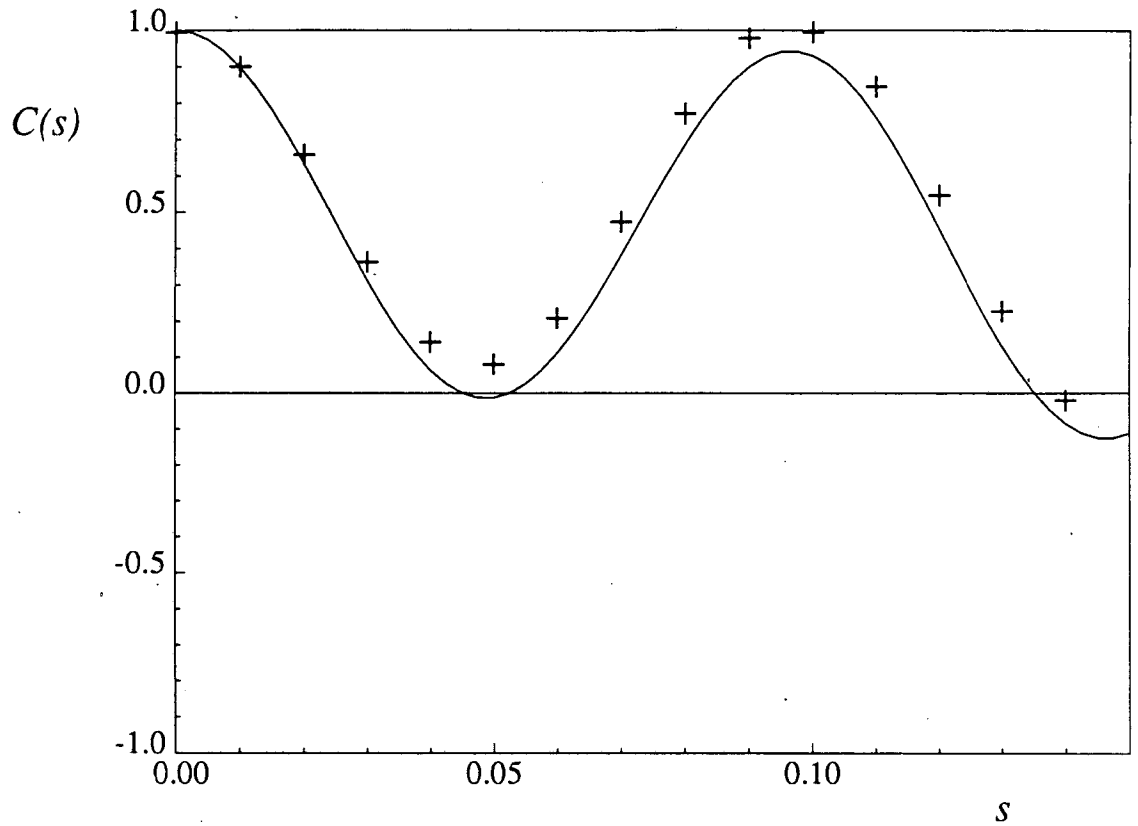

XBL 875-2449

Fig. 5c

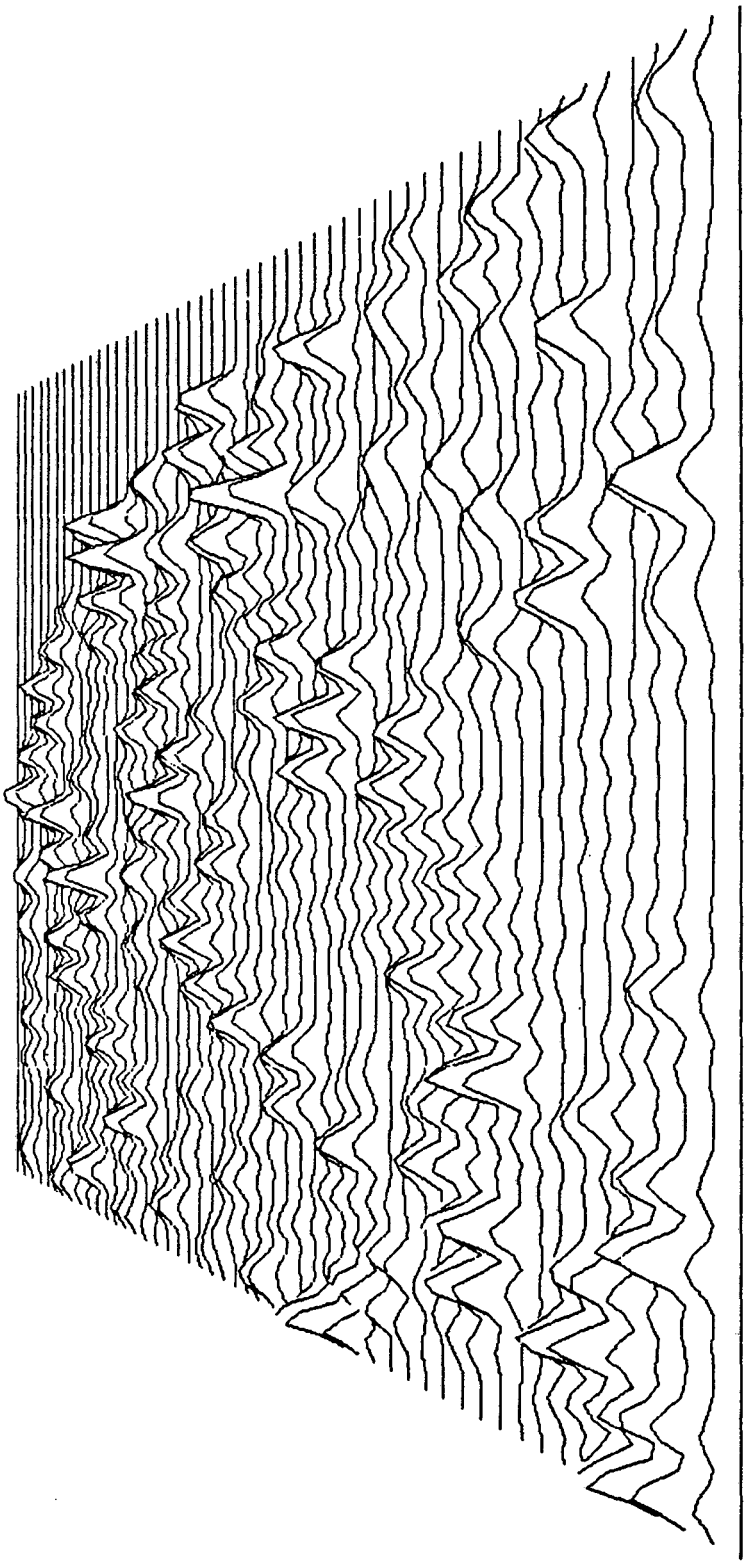

XBL 828-11128

Fig. 6a

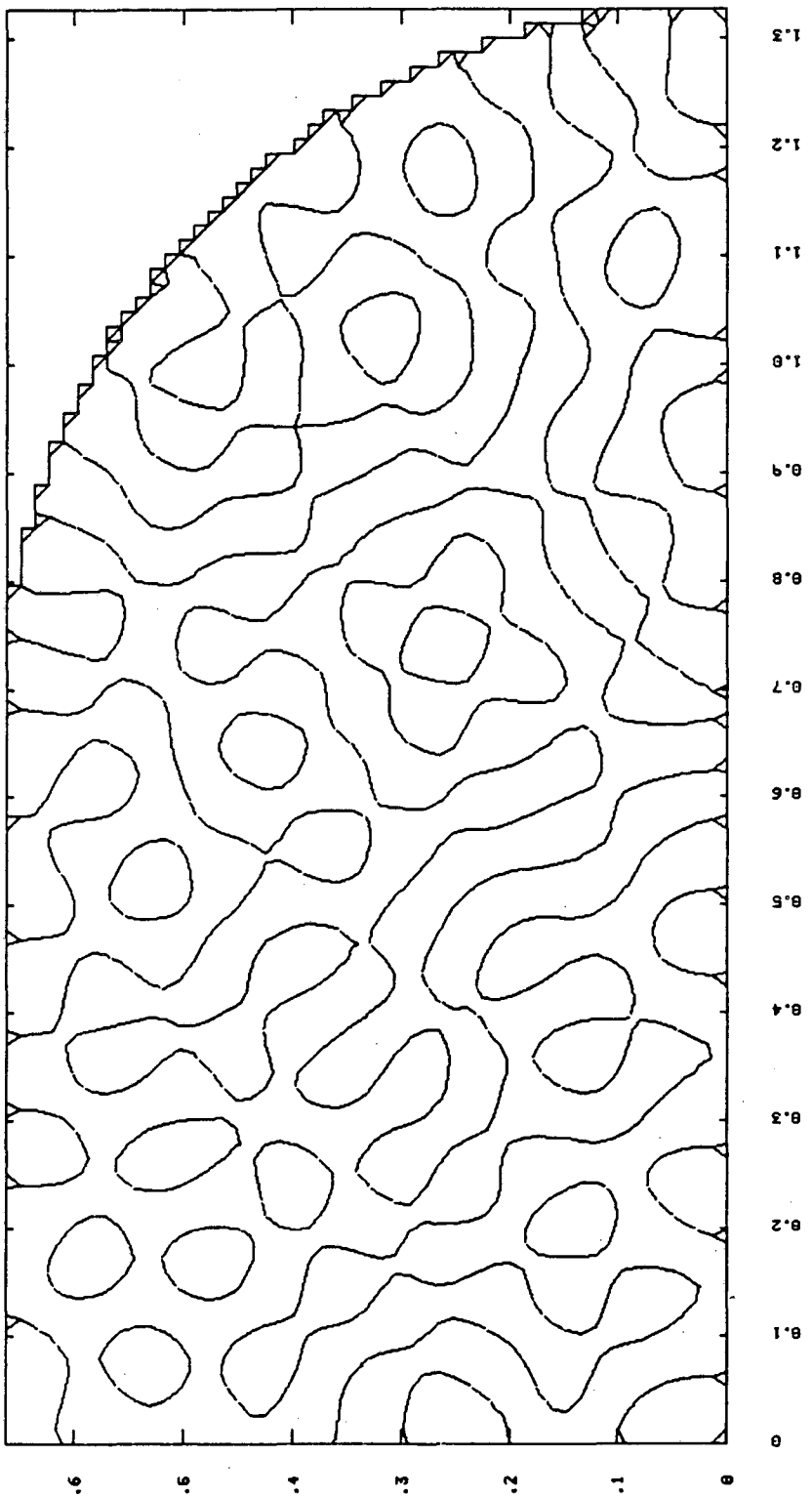

XBL 828-11129

Fig. 6b

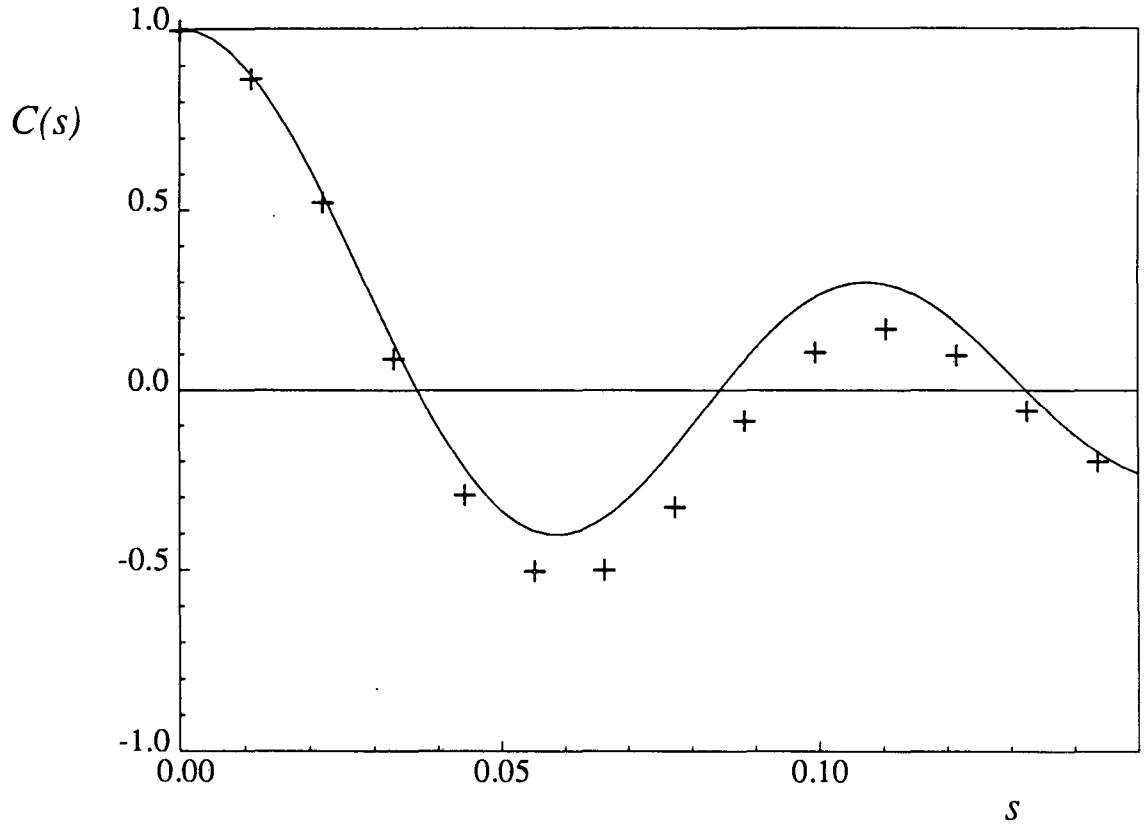

XBL 875-2450

Fig. 7a

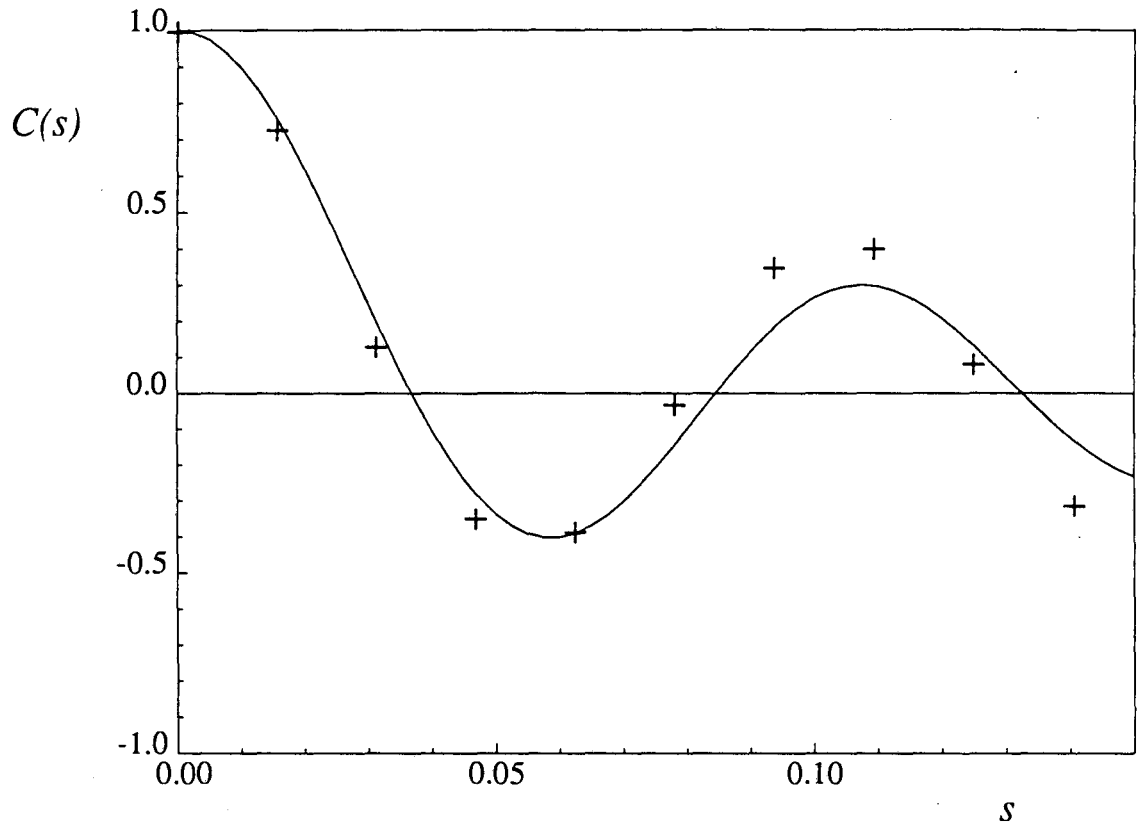

XBL 876-2451

Fig. 7b

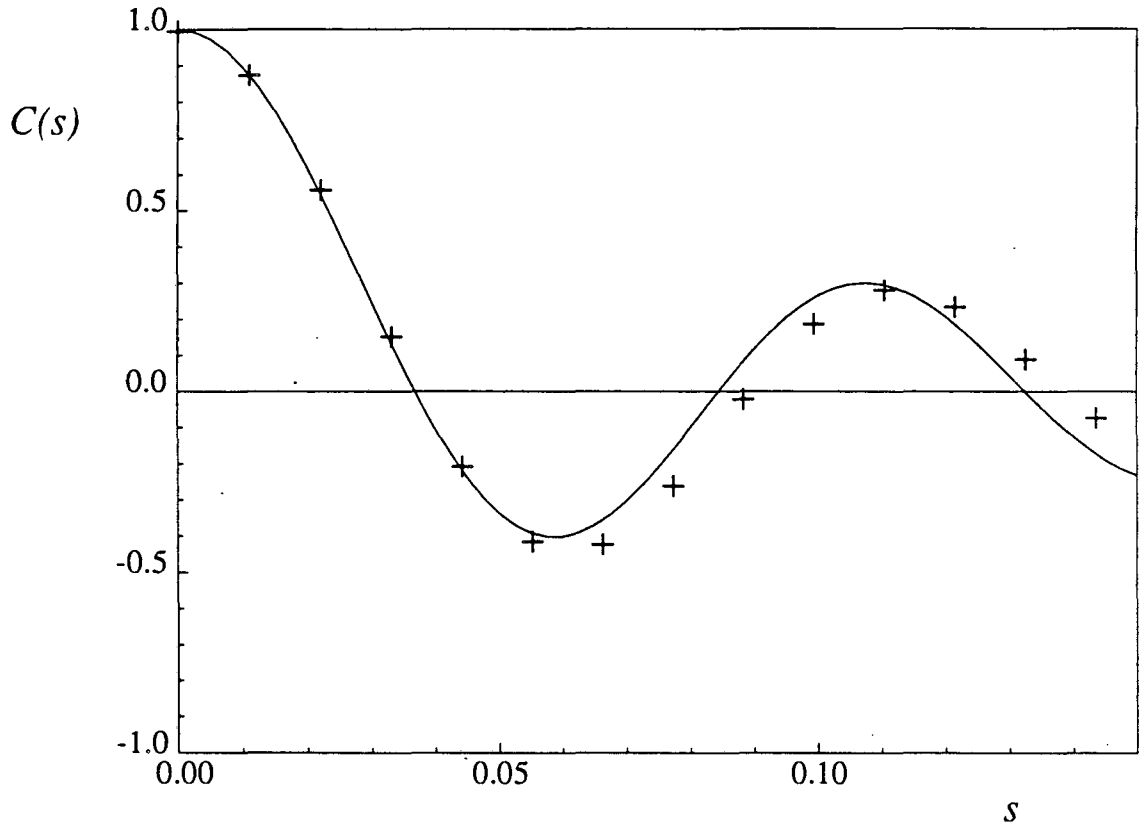

XBL 876-2452

Fig. 7c

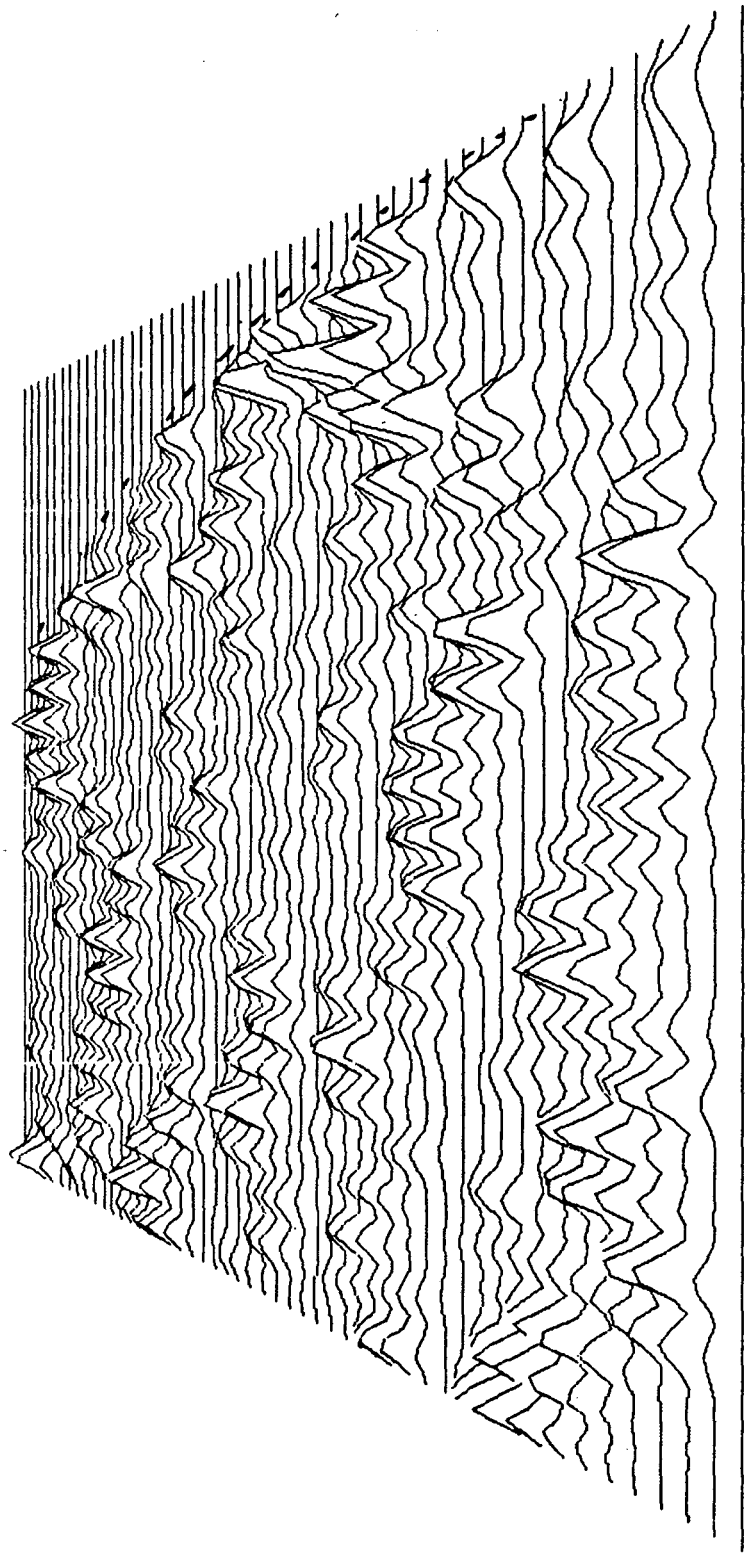

XBL 828-11123

Fig. 8a

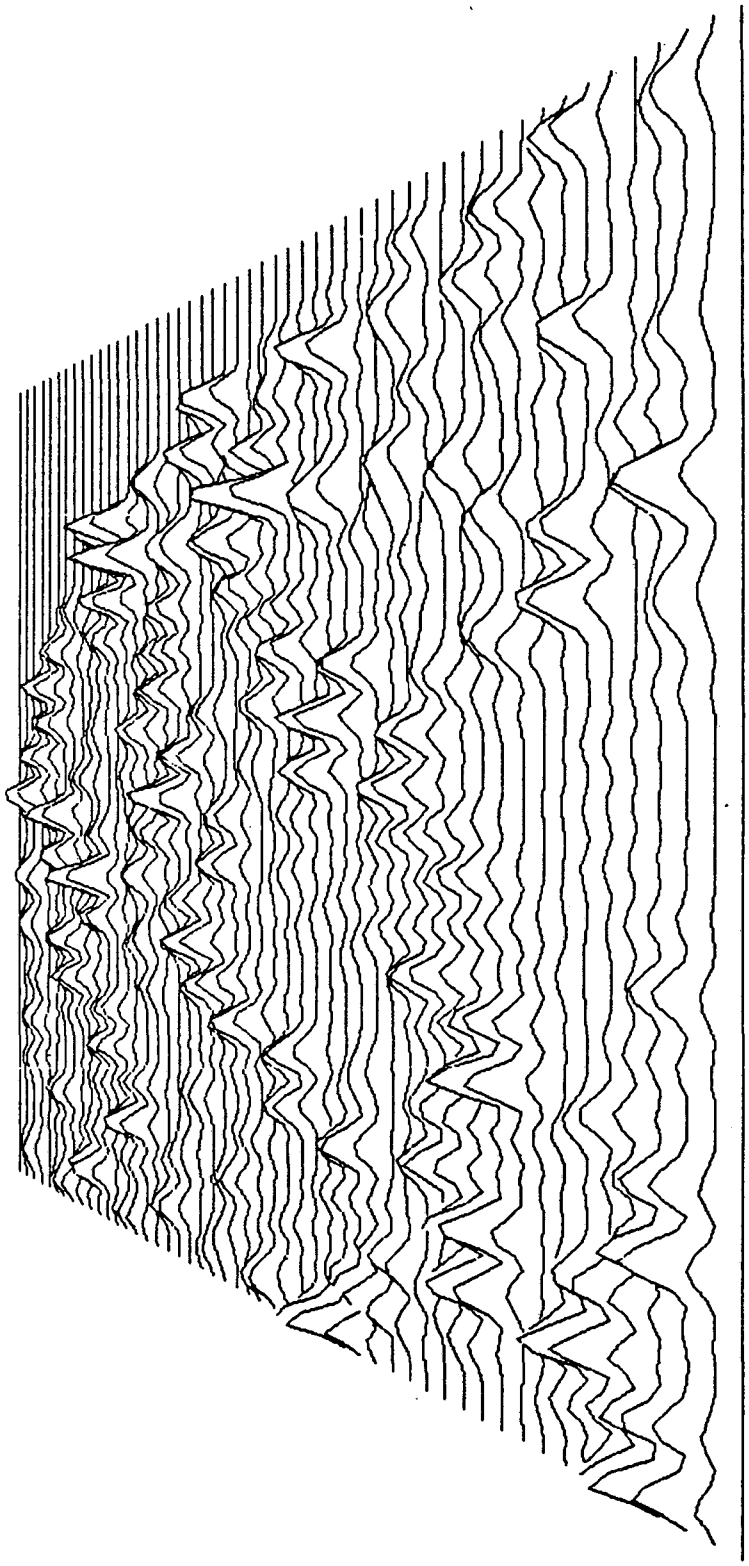

XBL 828-11128

Fig. 8b

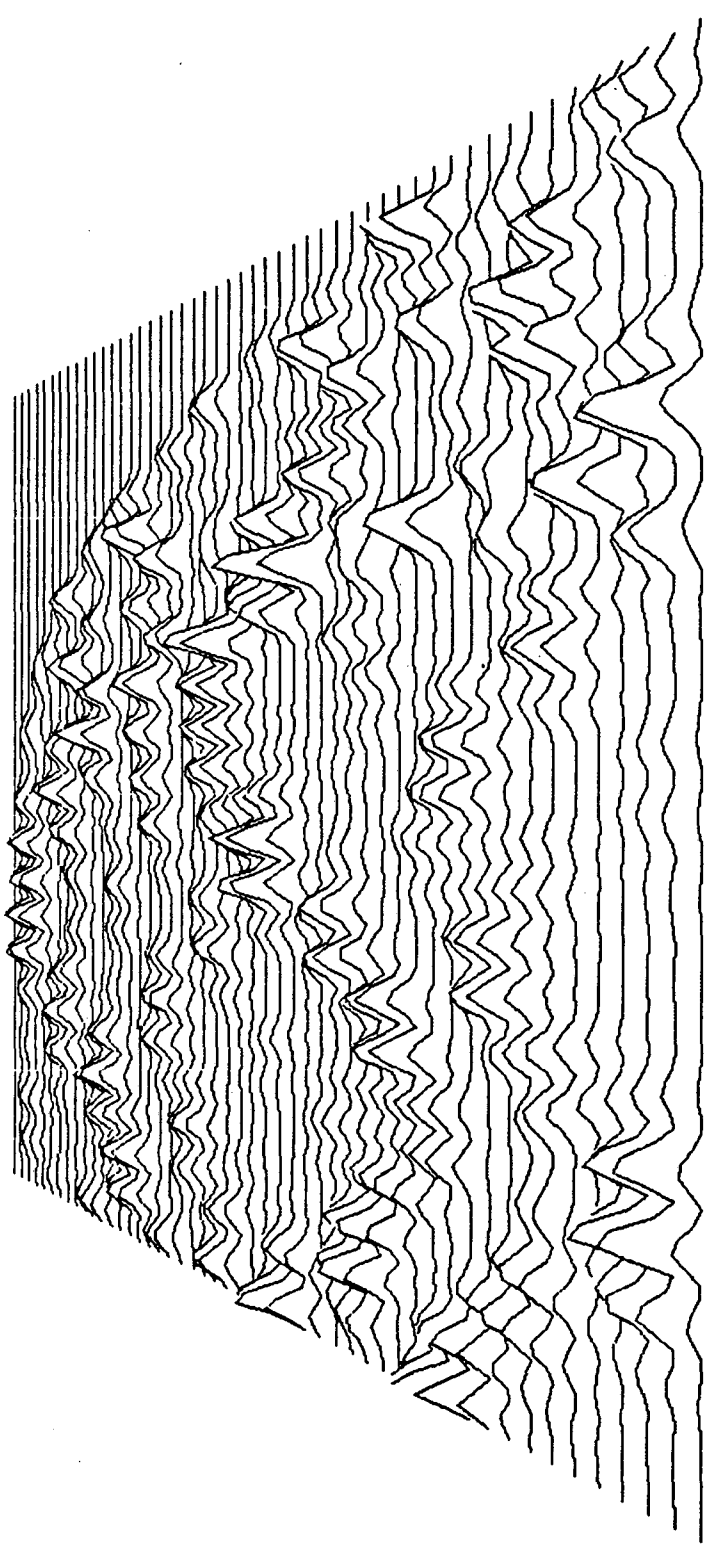

XBL 828-11122

Fig. 8c

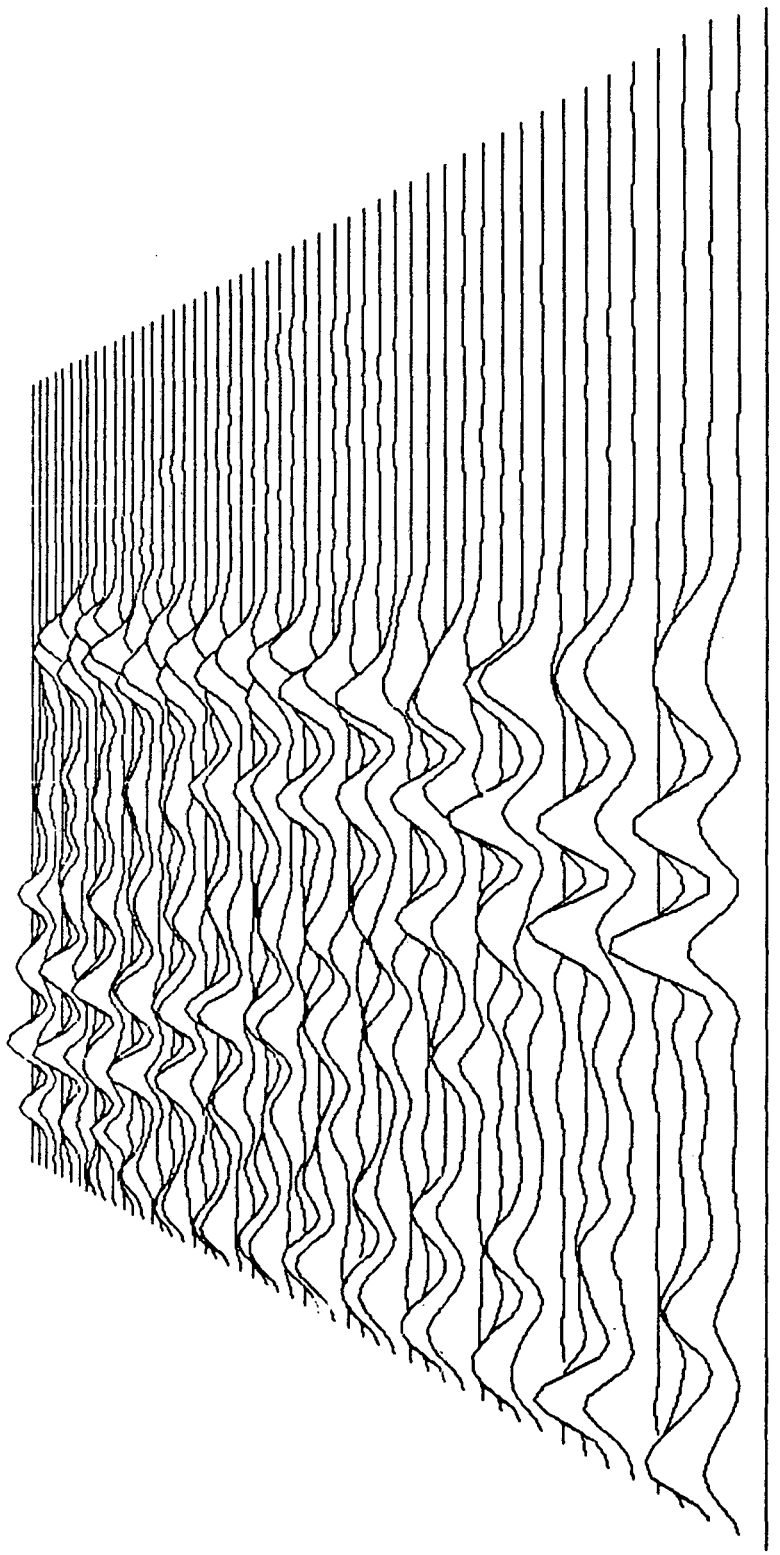

XBL 828-11121

Fig. 8d

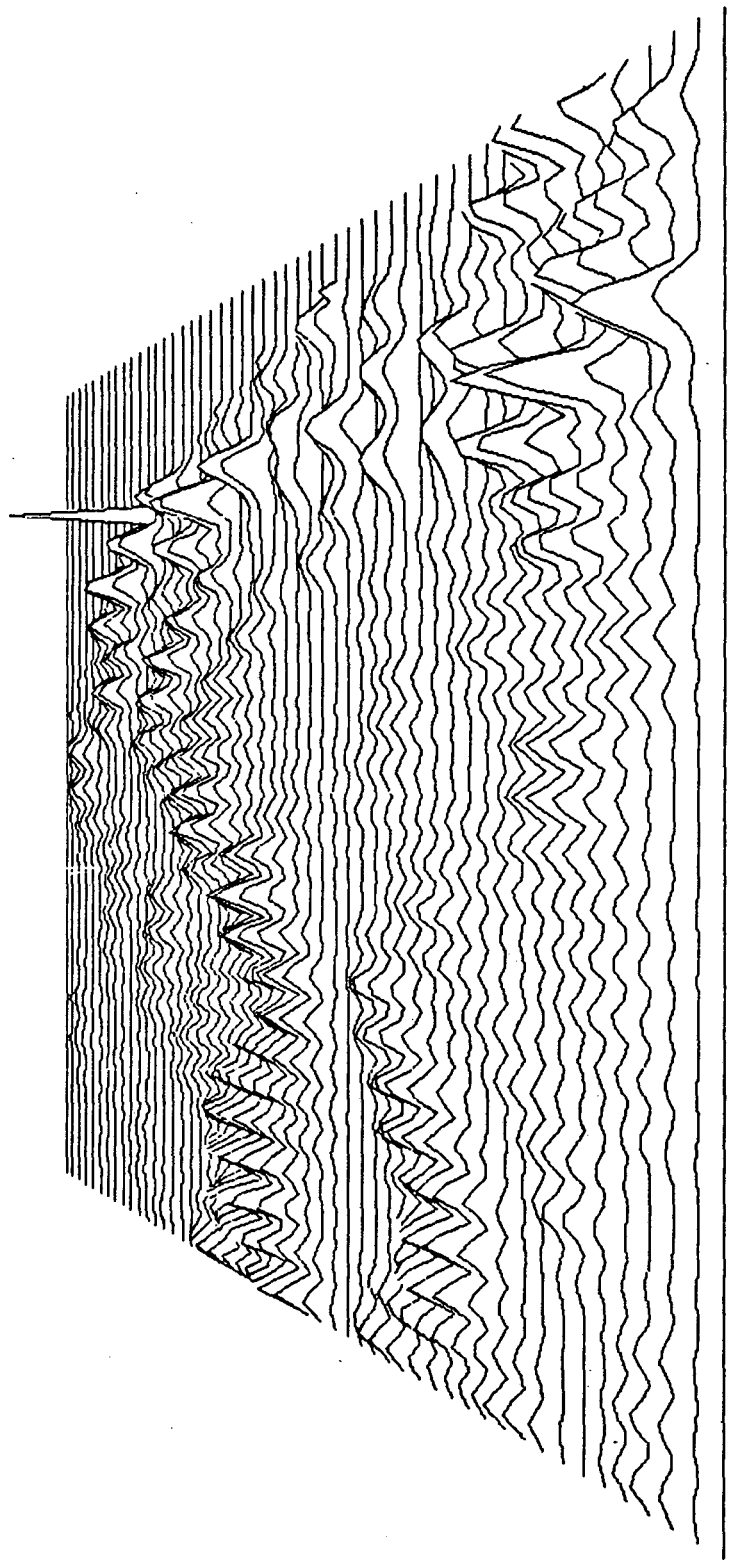

XBL 828-11120

Fig. 8e

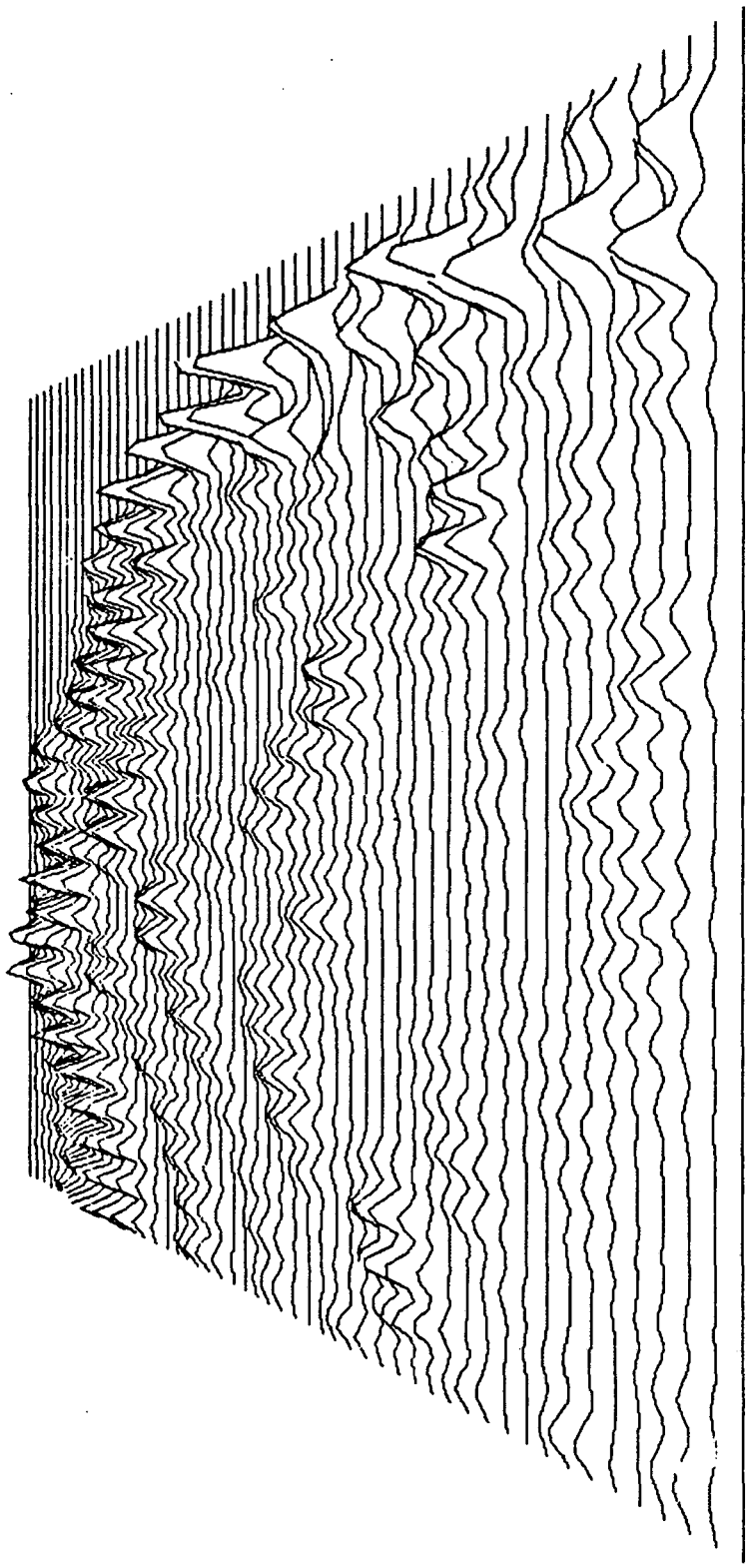

XBL 828-11119

Fig. 8f

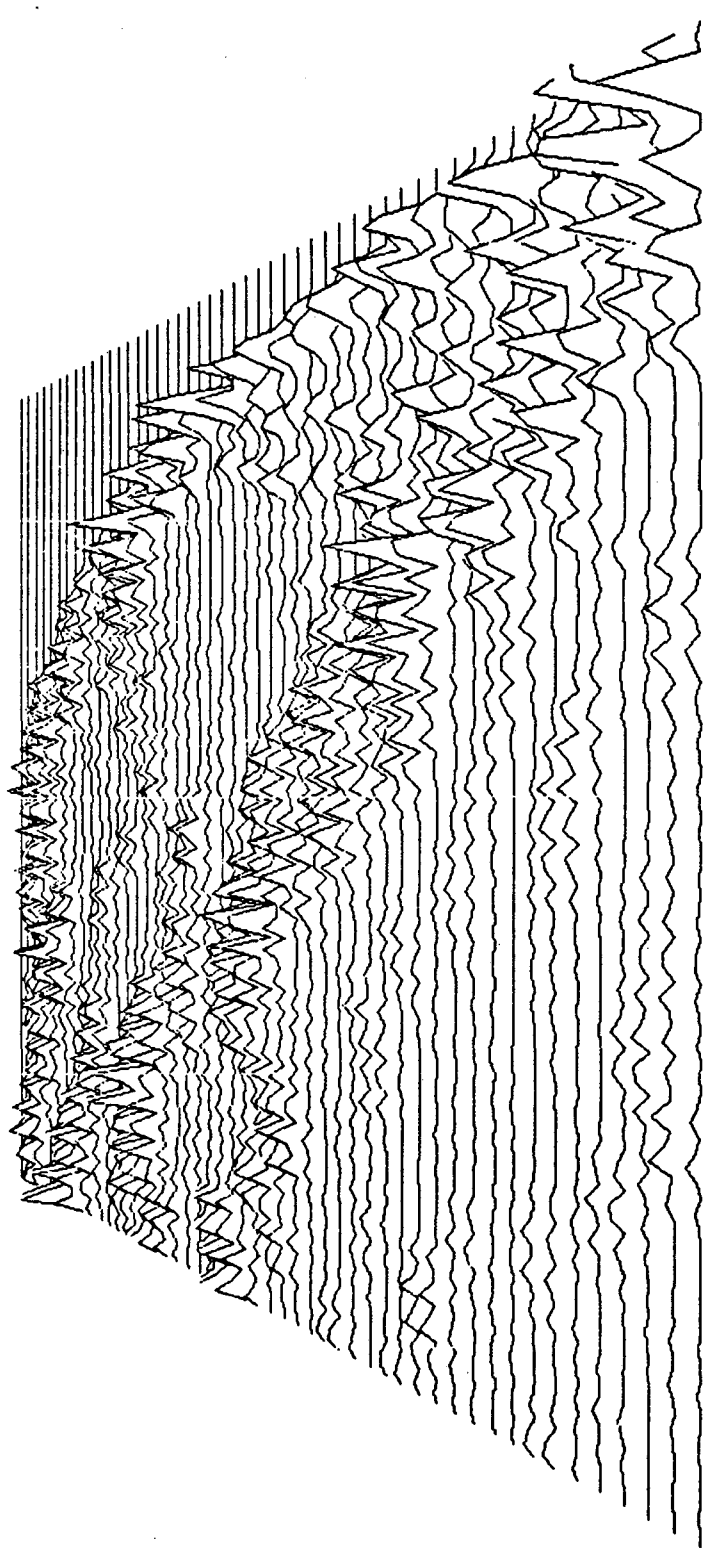

XBL 828-11118

Fig. 8g

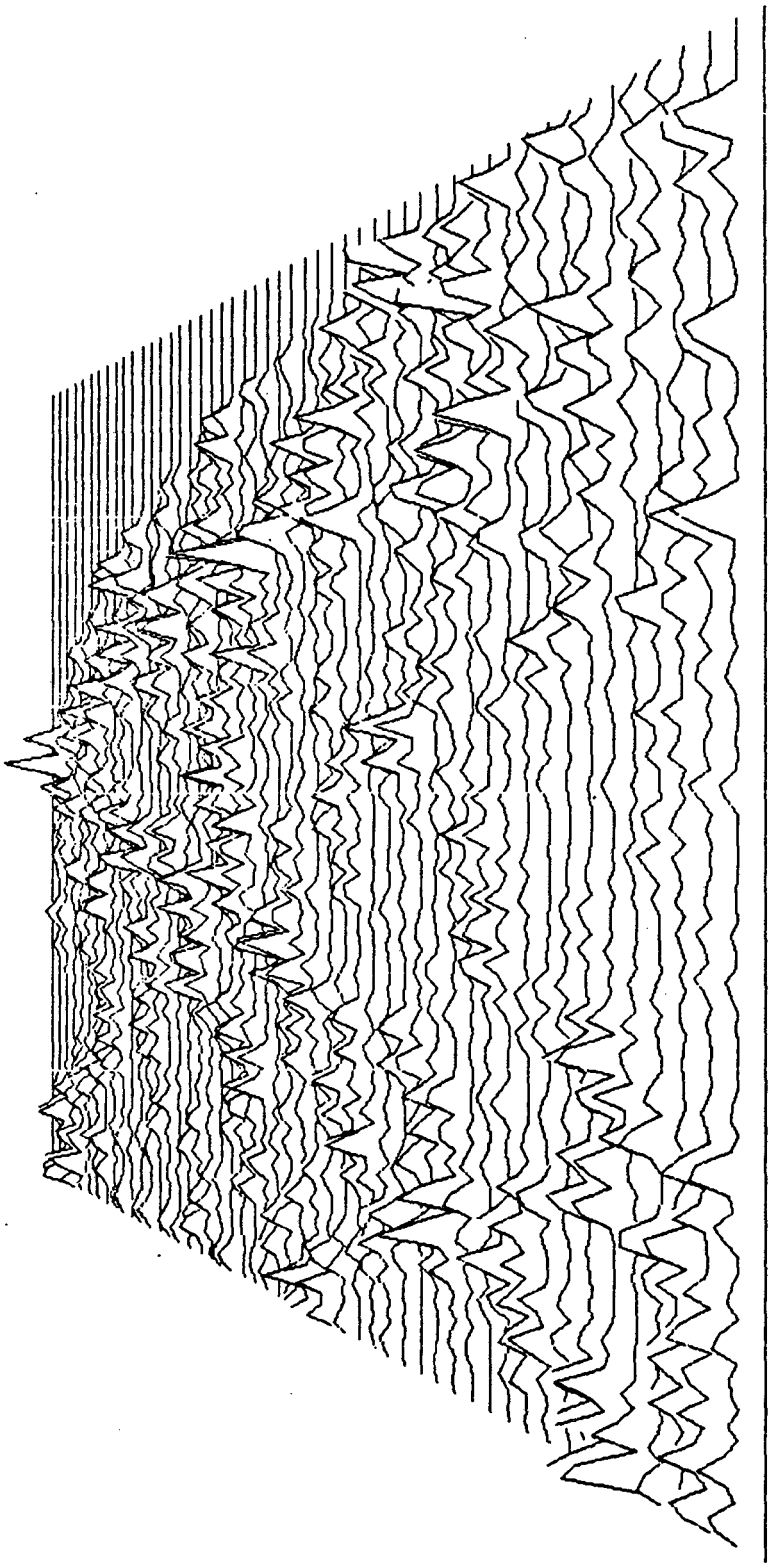

XBL 828-11117

Fig. 8h

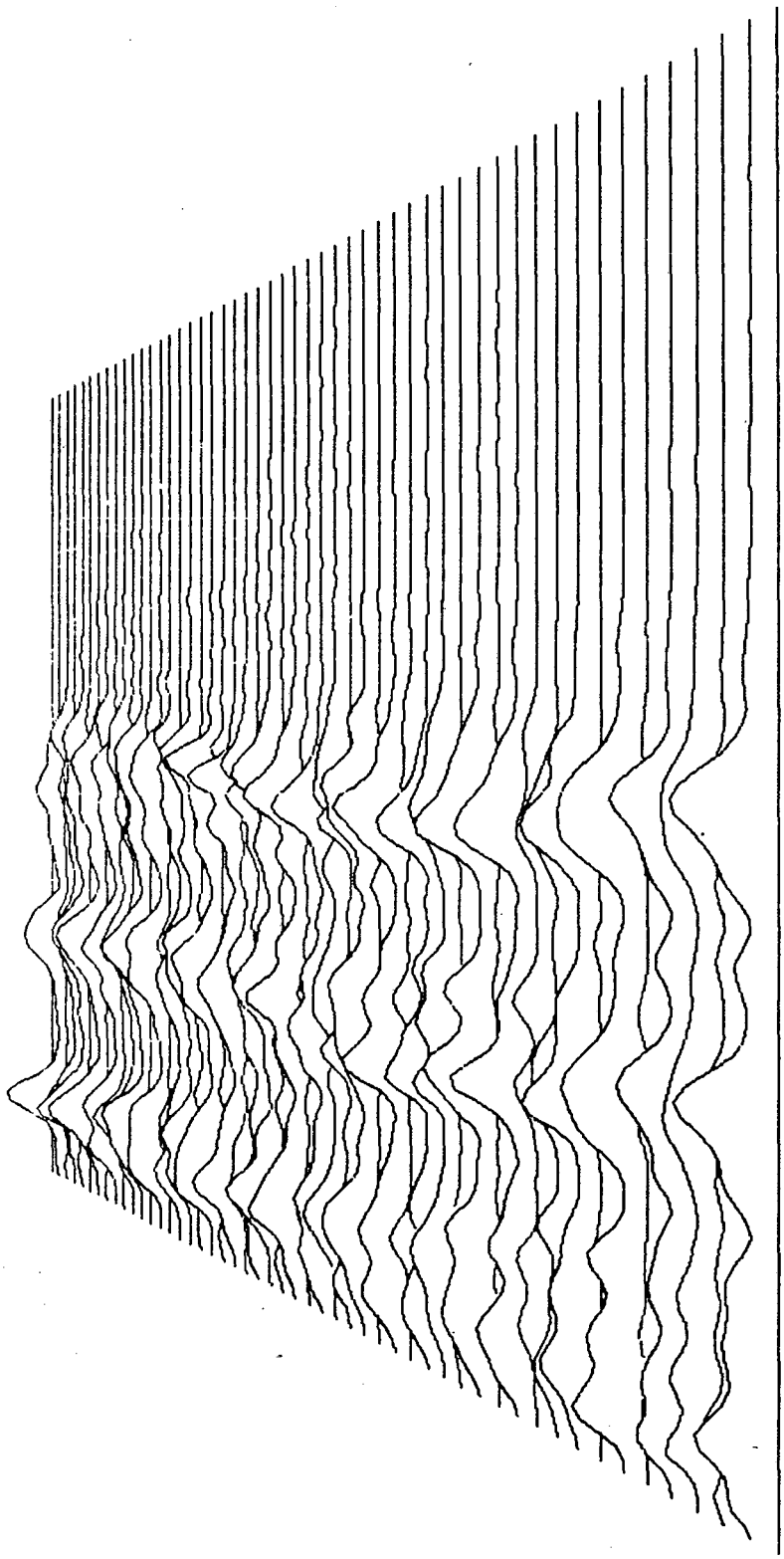

XBL 828-11116

Fig. 8i

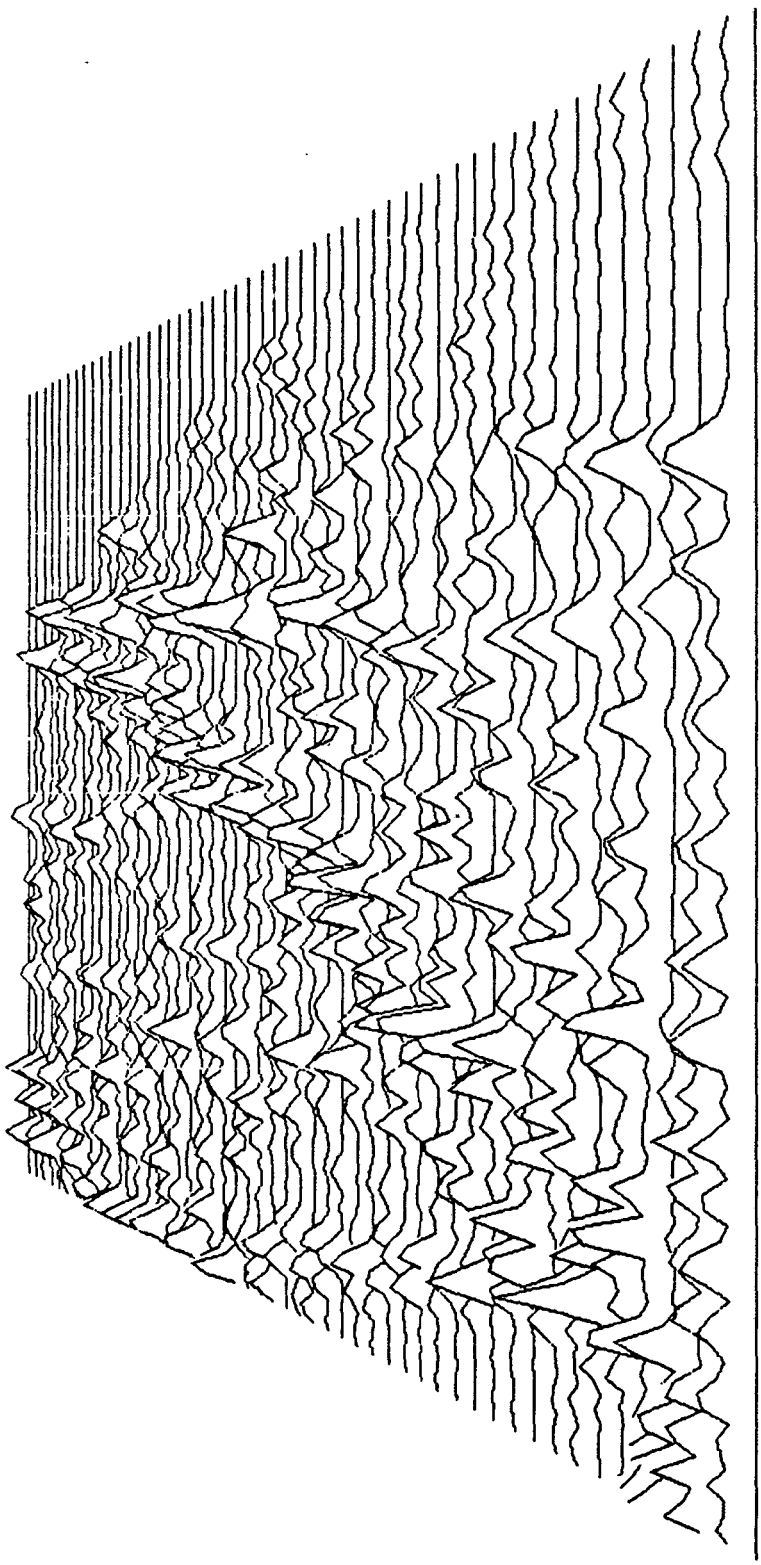

XBL 828-11115

Fig. 8j

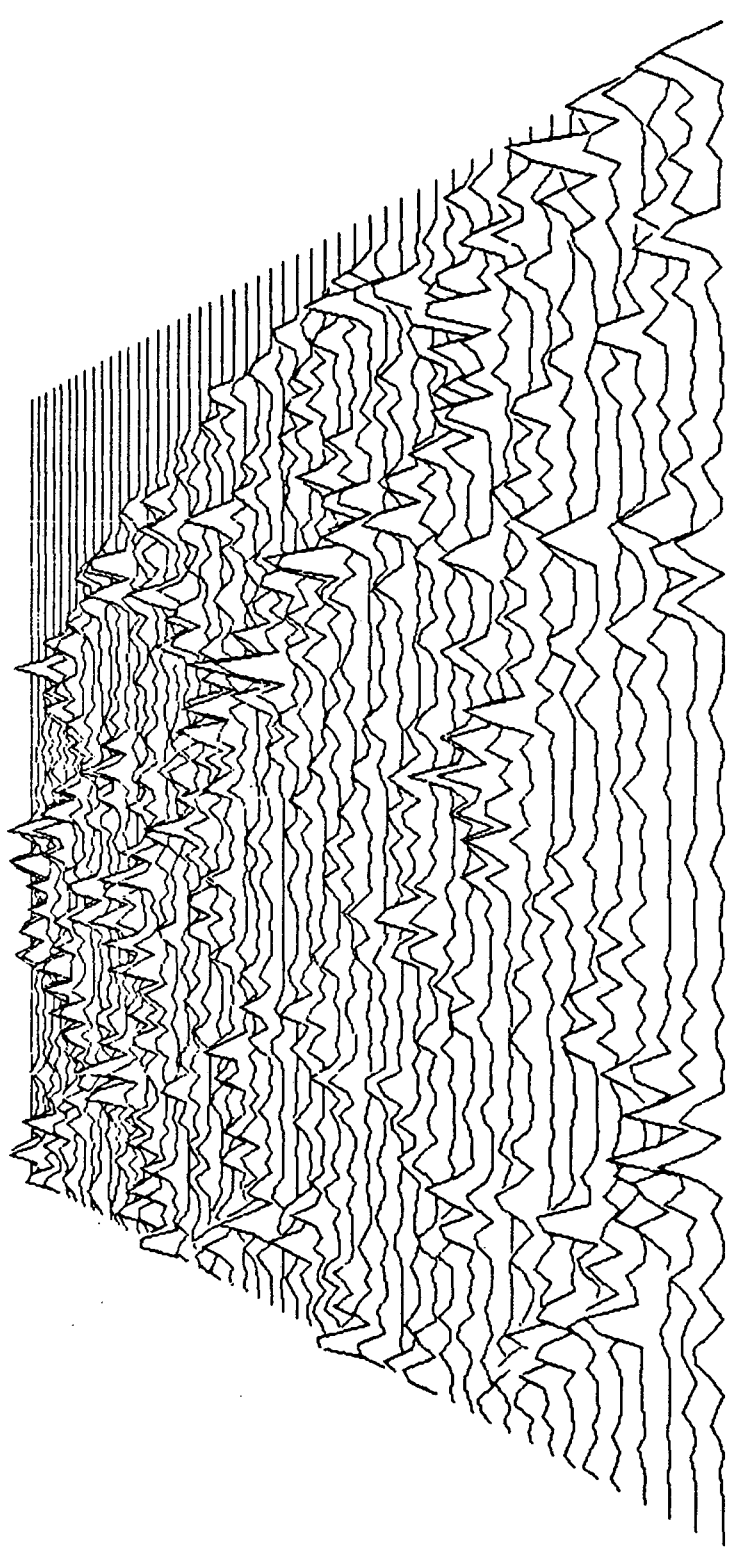

XBL 828-11114

Fig. 8k

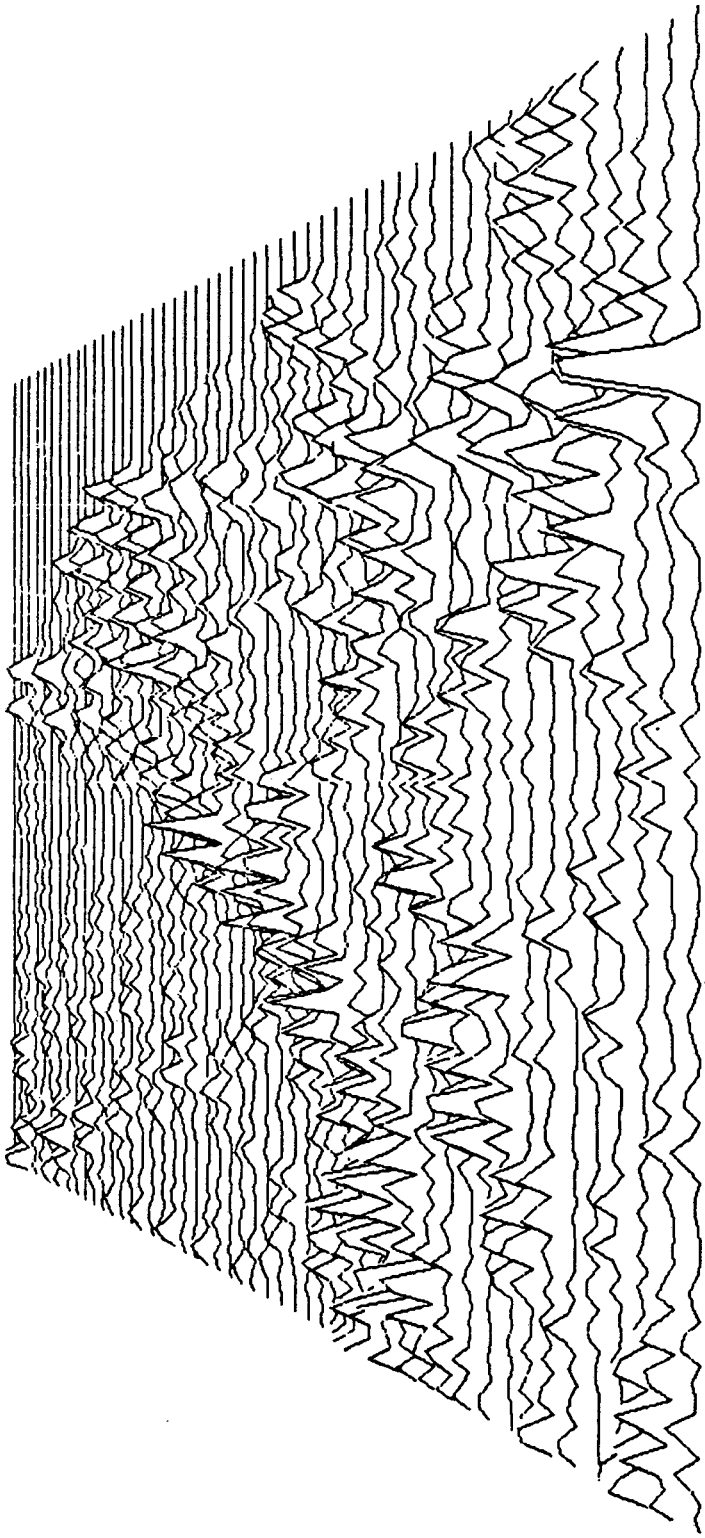

XBL 828-11113

Fig. 8L

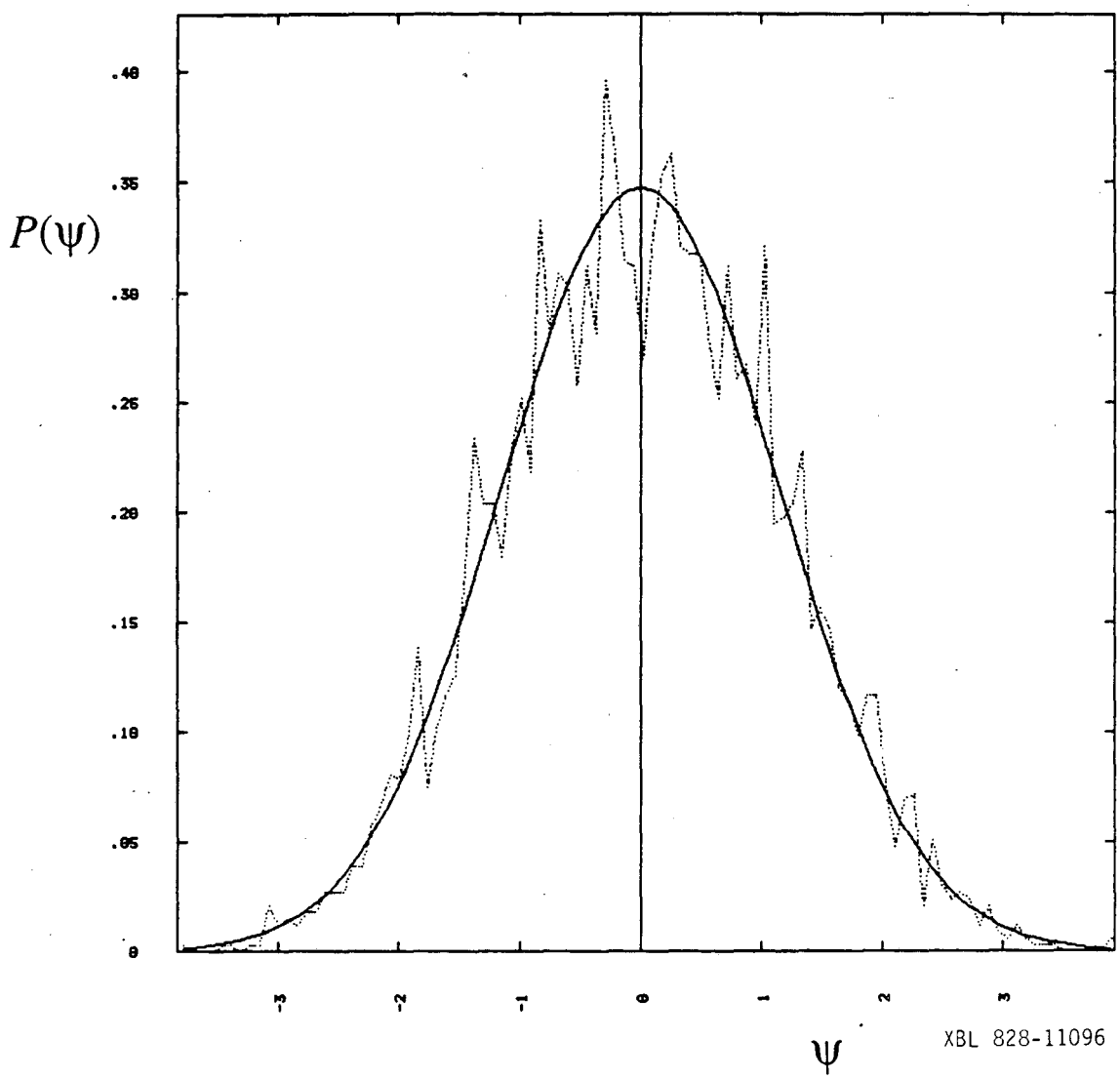

Fig. 9

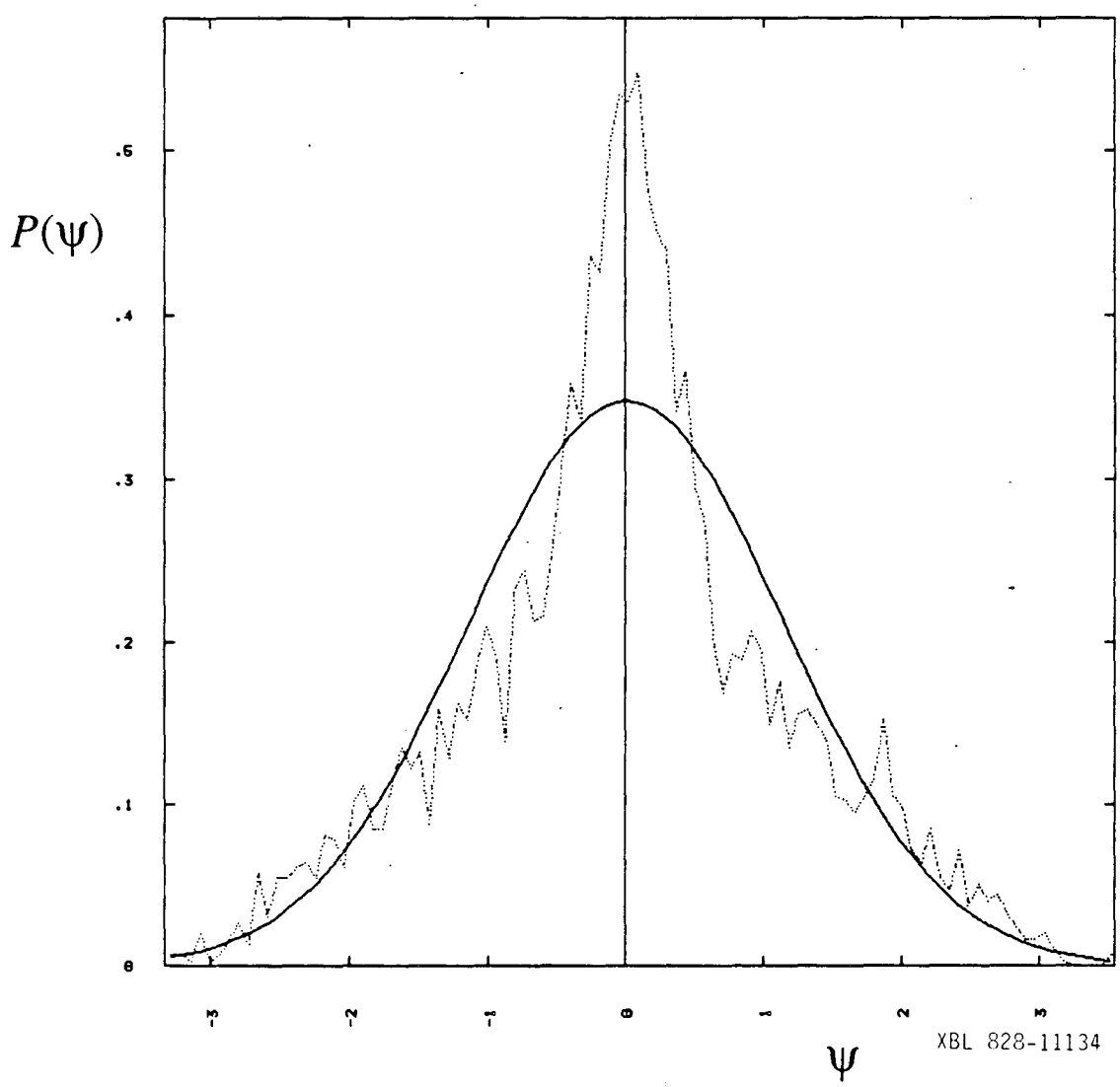

Fig. 10

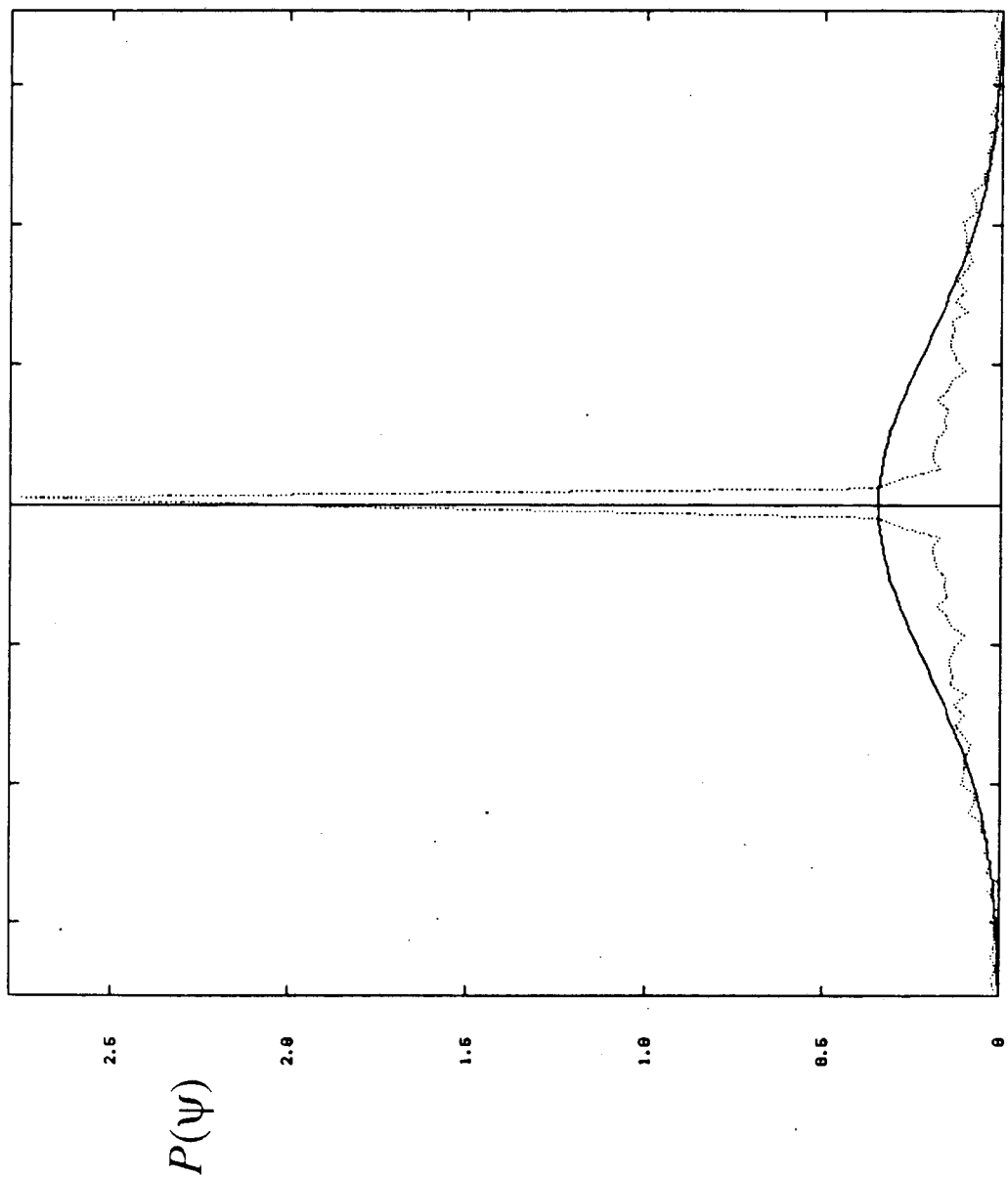

XBL 828-11103

Fig. 11

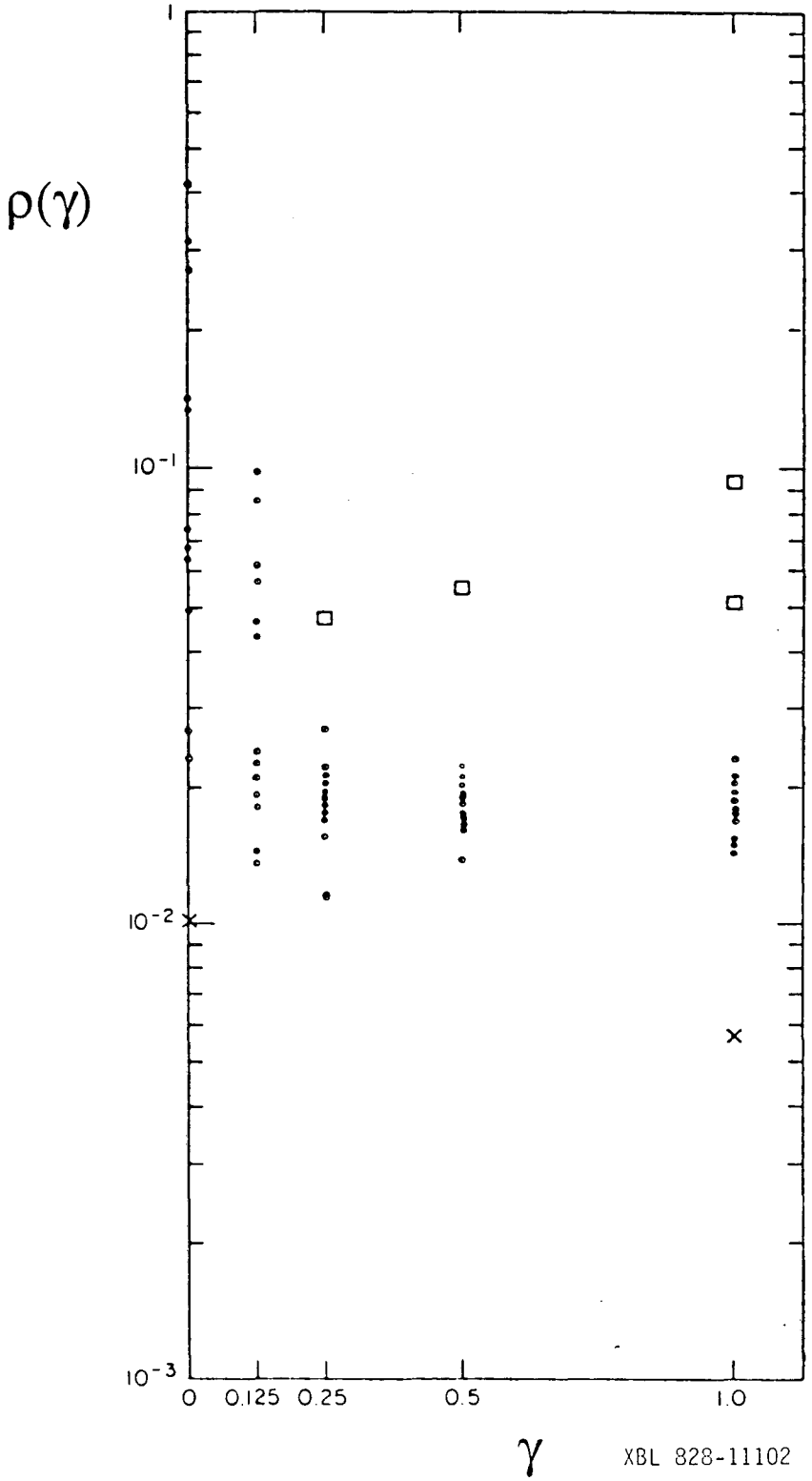

Fig. 12

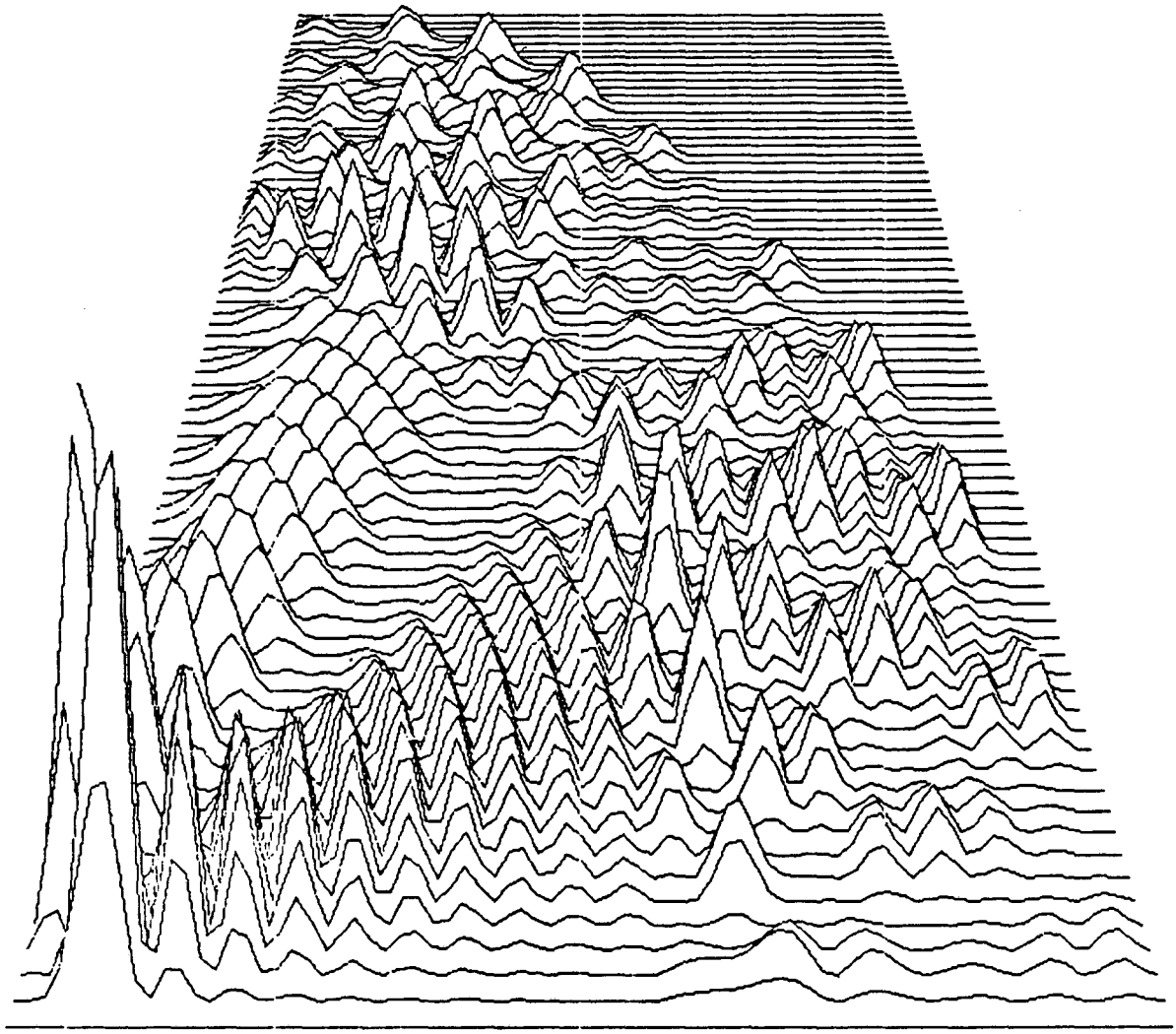

XBL 828-11125

Fig. 13a

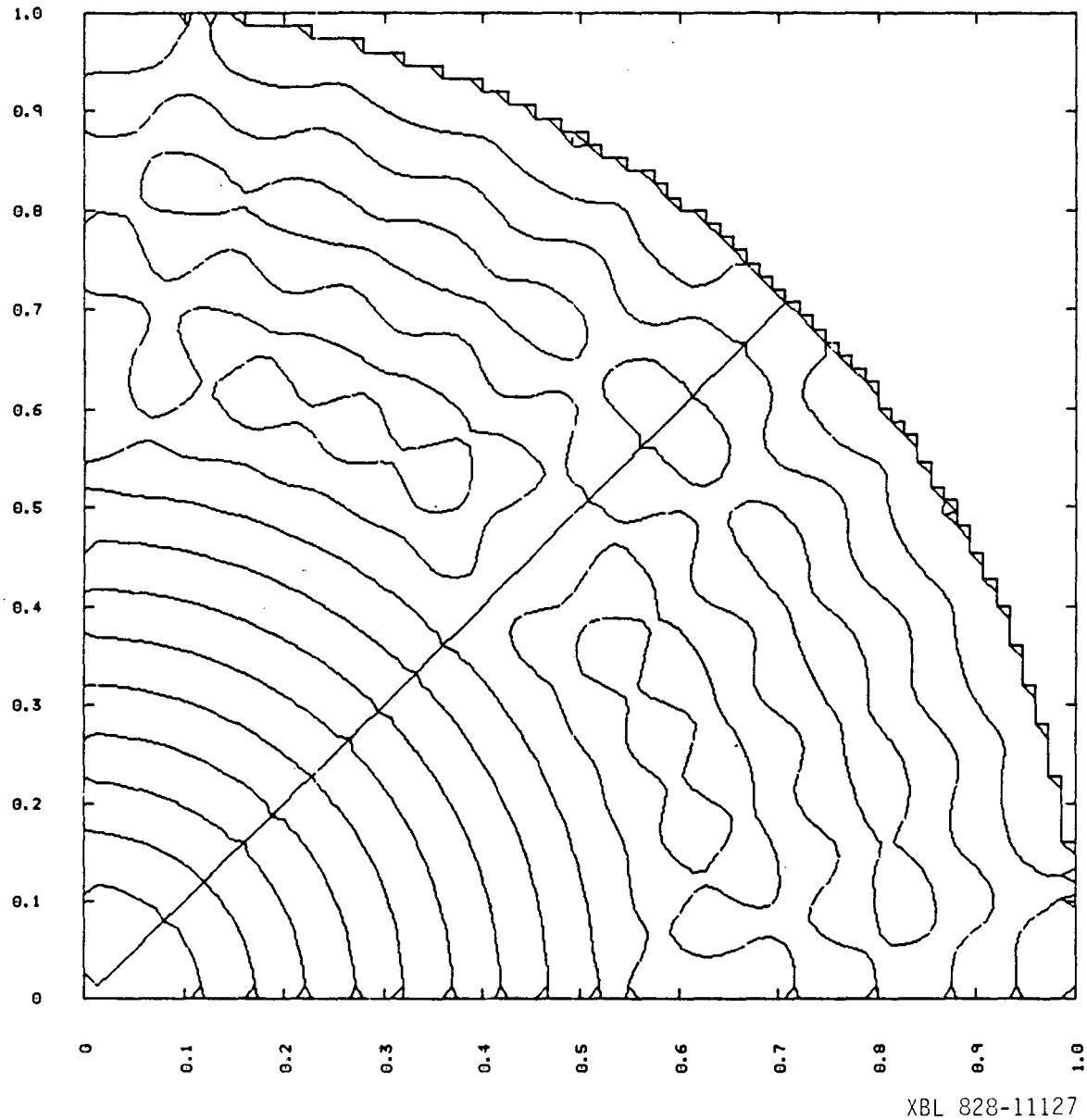
1.0
0.9
0.8
0.7
0.6
0.5
0.4
0.3
0.2
0.1
0
0
0.1
0.2
0.3
0.4
0.5
0.6
0.7
0.8
0.9
1.0
XBL 828-11127

Fig. 13b

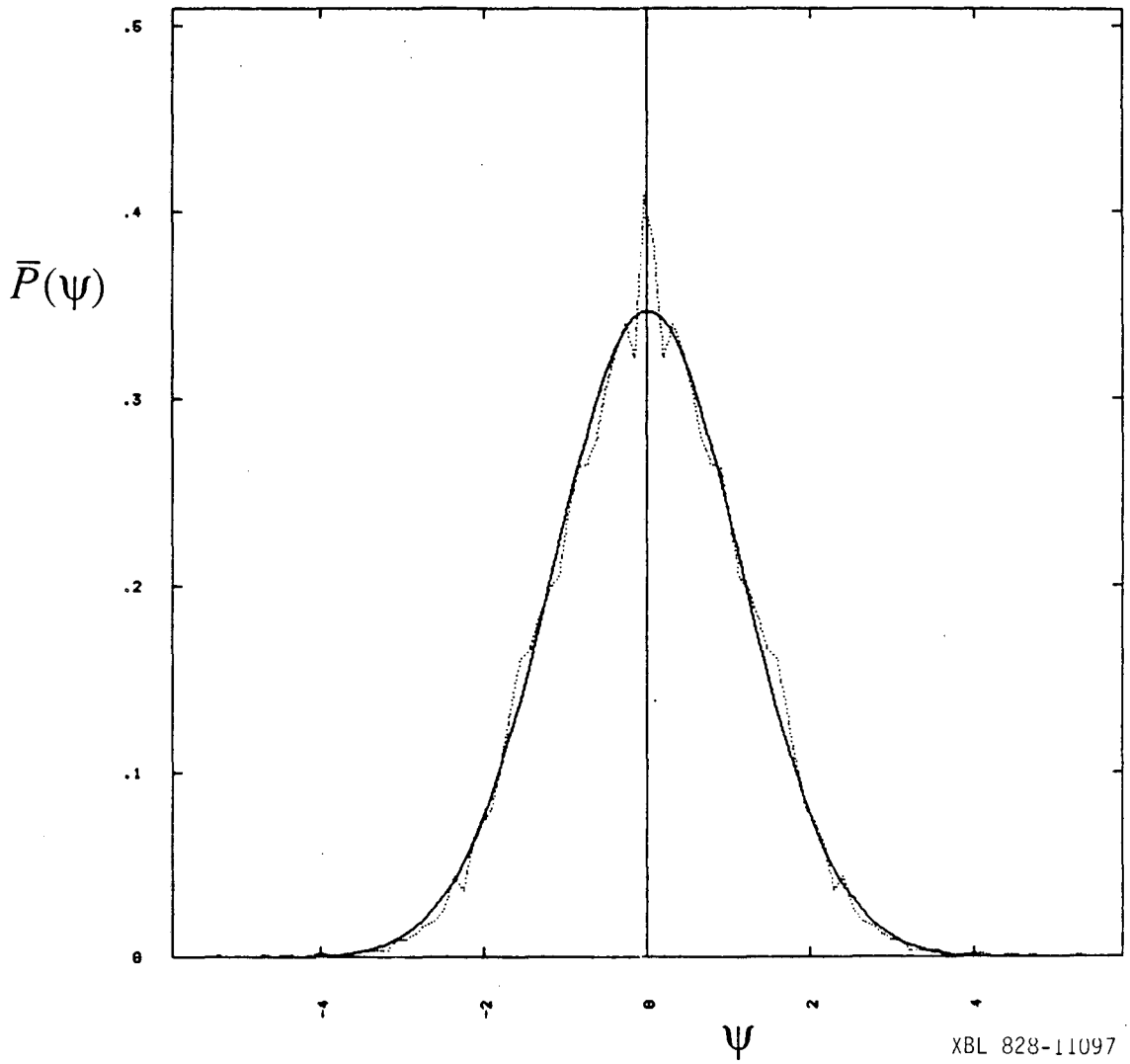

Fig. 14

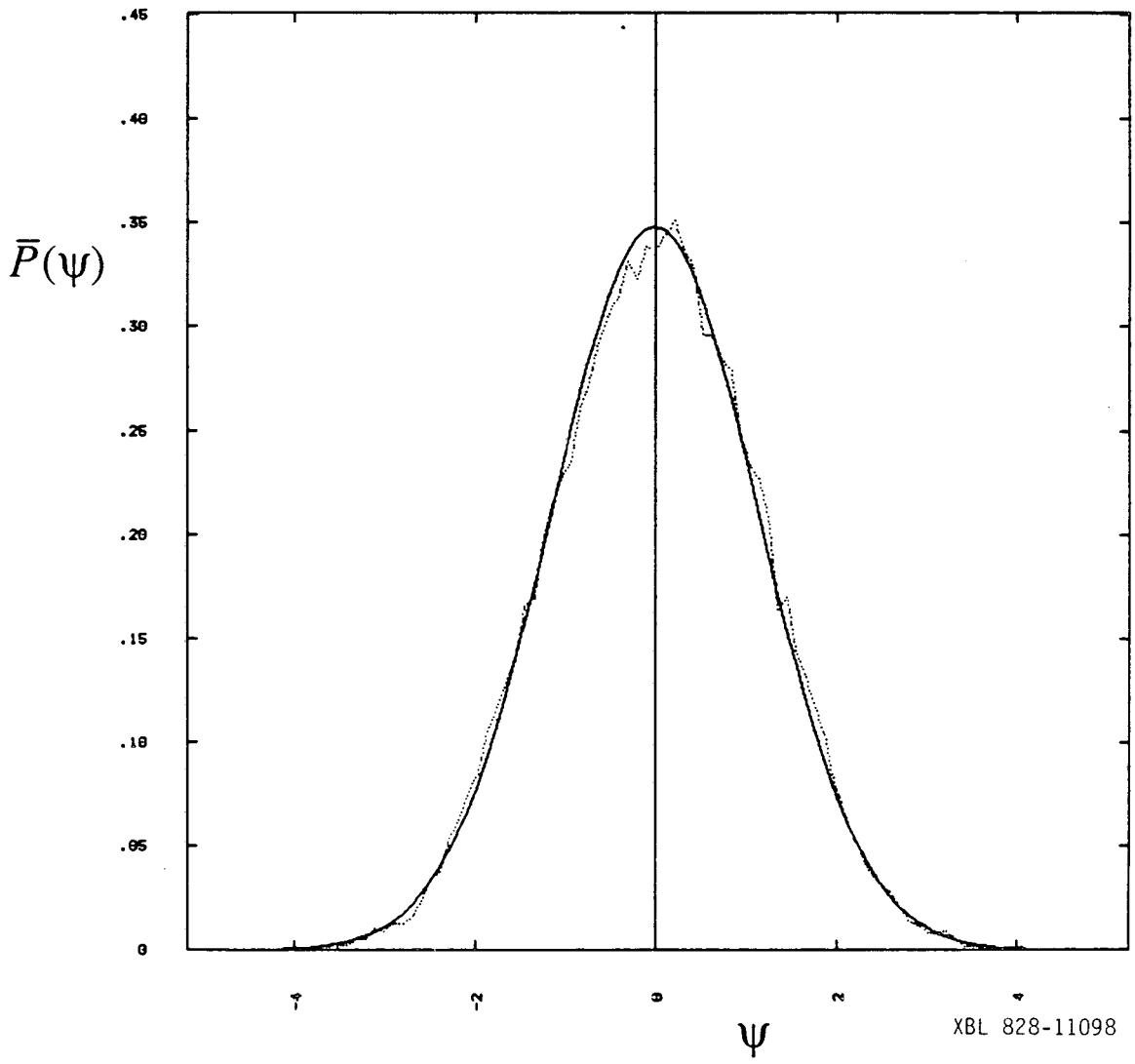

Fig. 15

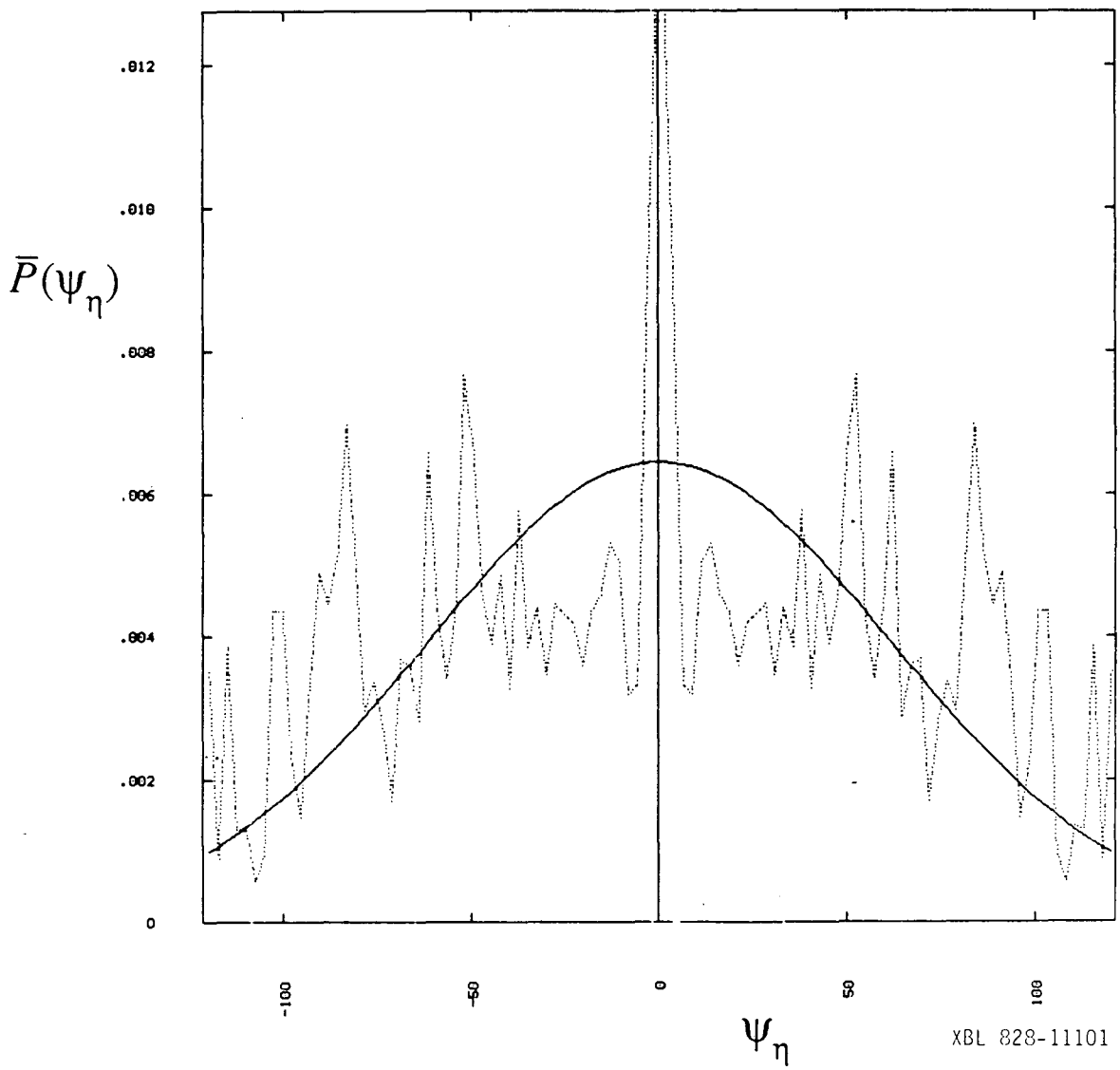
$\bar{P}(\psi_\eta)$
.012
.010
.008
.006
.004
.002
0
-100
-50
0
50
100
ψ_η
XBL 828-11101

Fig. 16

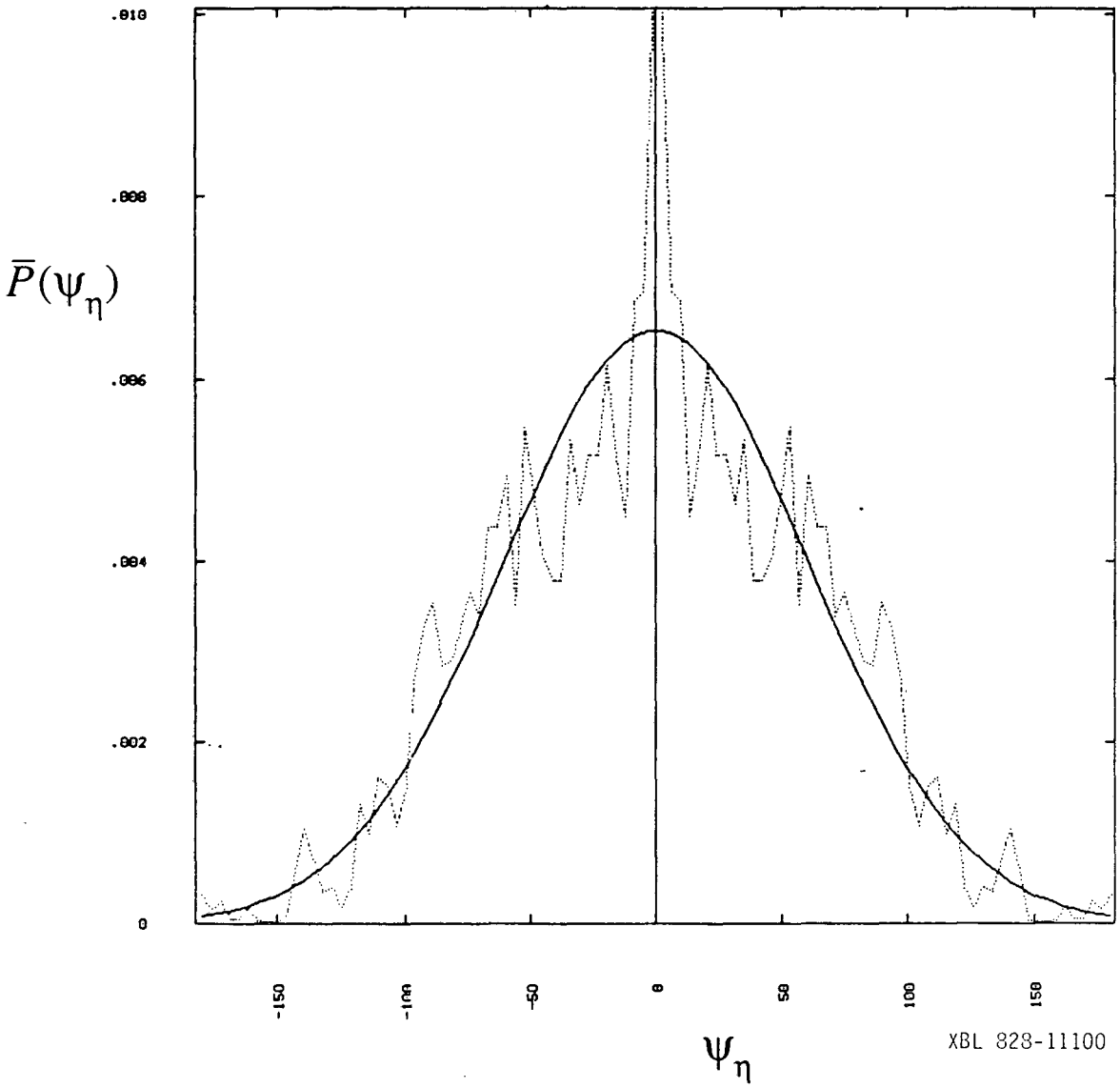
.010
.008
.006
.004
.002
0
$\bar{P}(\psi_\eta)$
-150
-100
-50
0
50
100
150
ψ_η
XBL 823-11100

Fig. 17

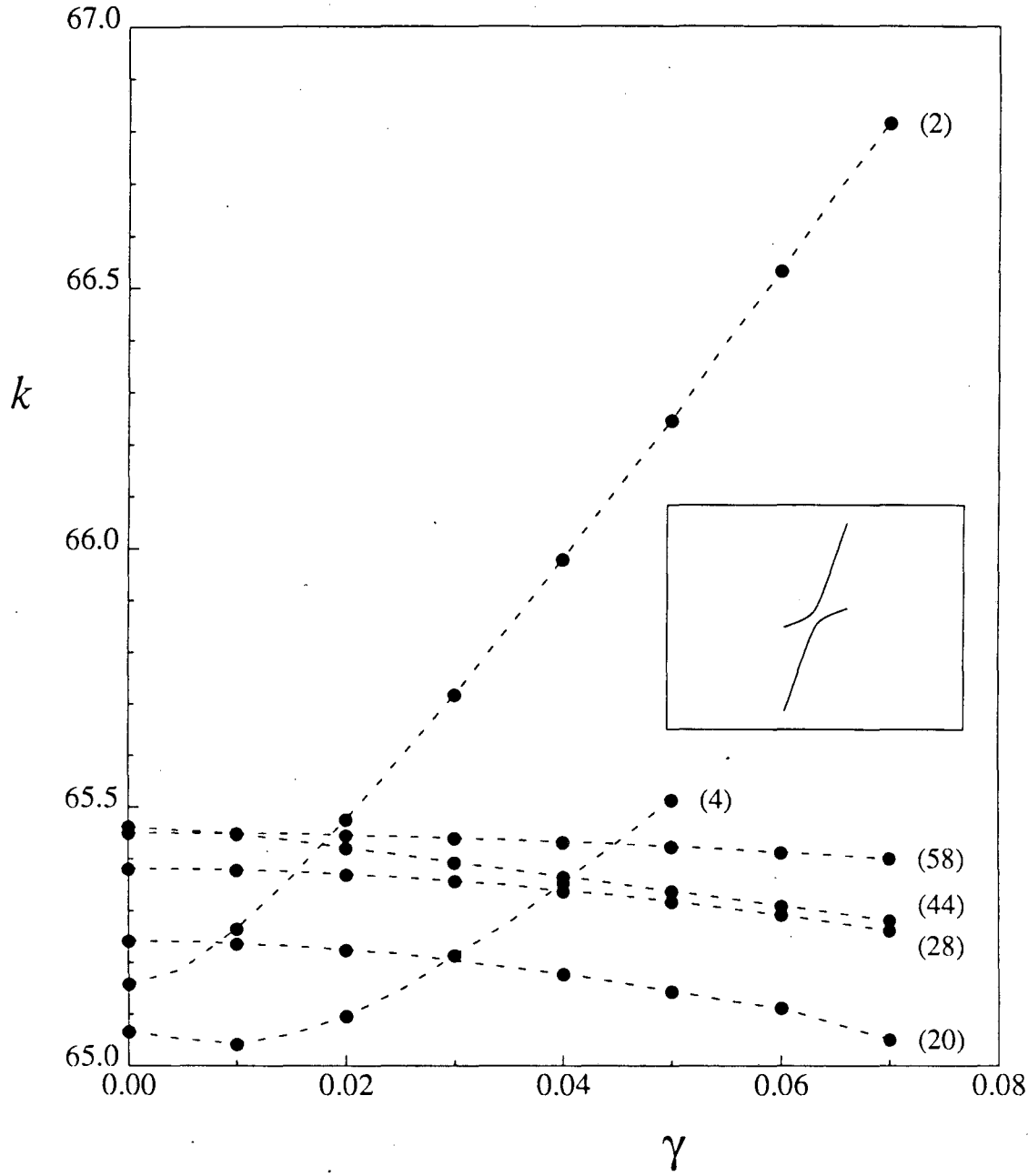

XBL 876-2453

Fig. 18

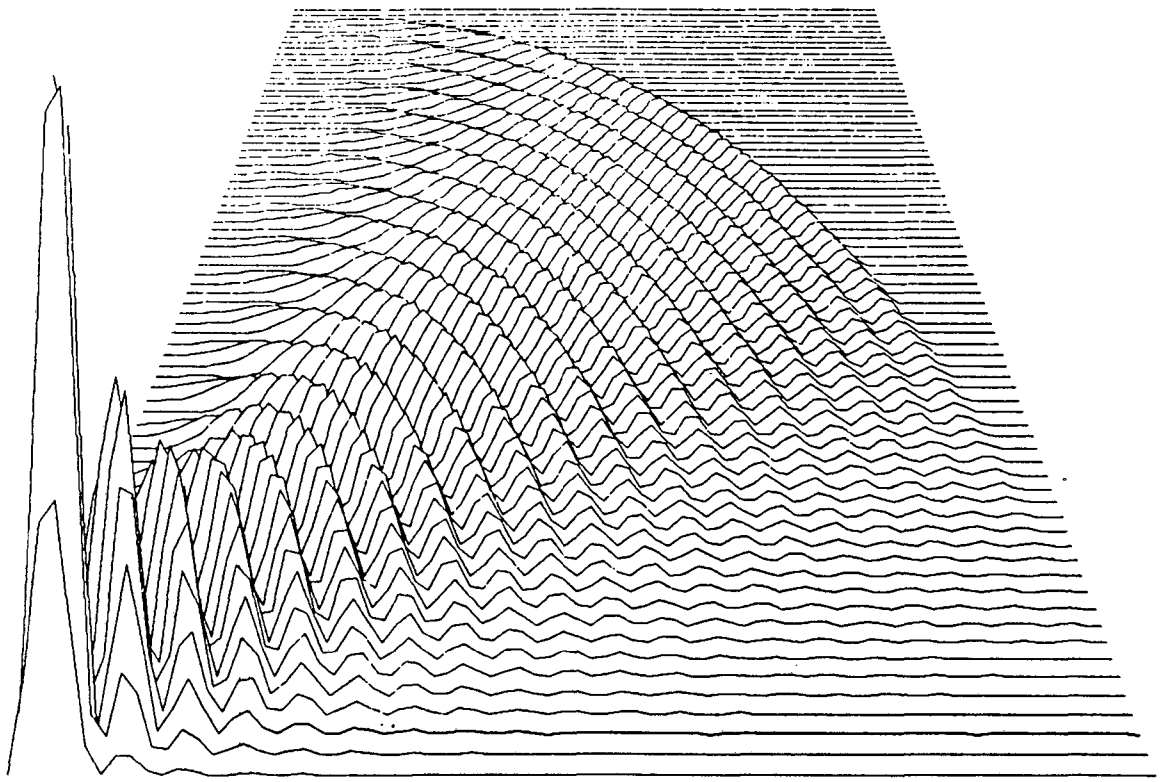

XBL 875-2226

Fig. 19a

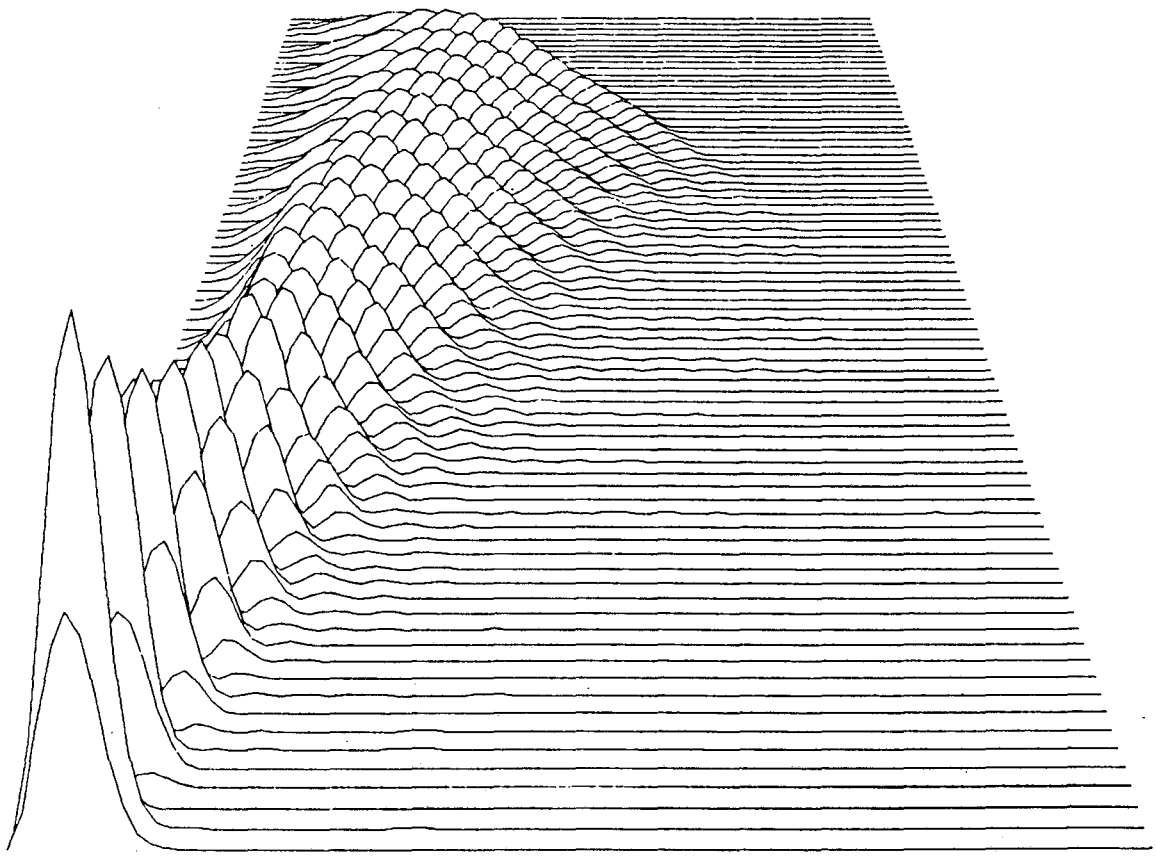

XBL 875-2227

Fig. 19b

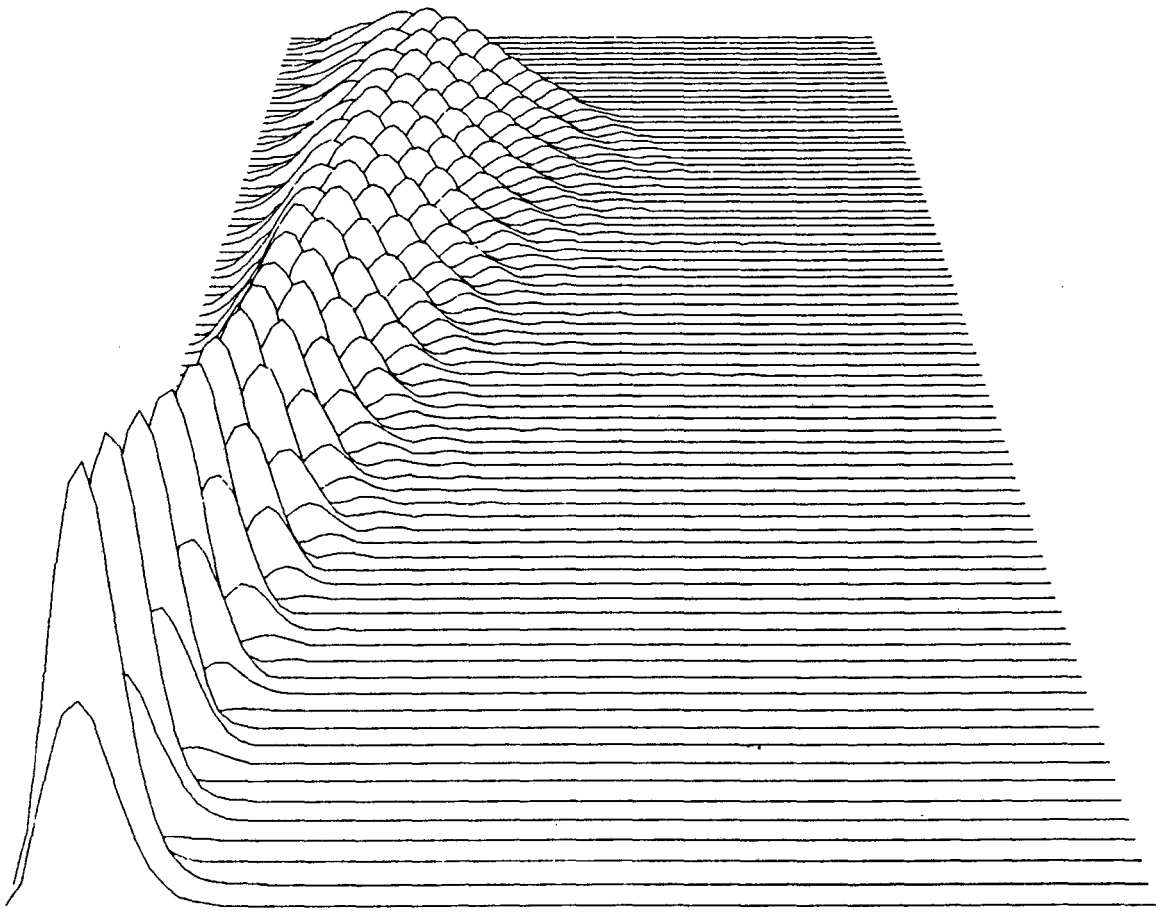

XBL 875-2228

Fig. 19c

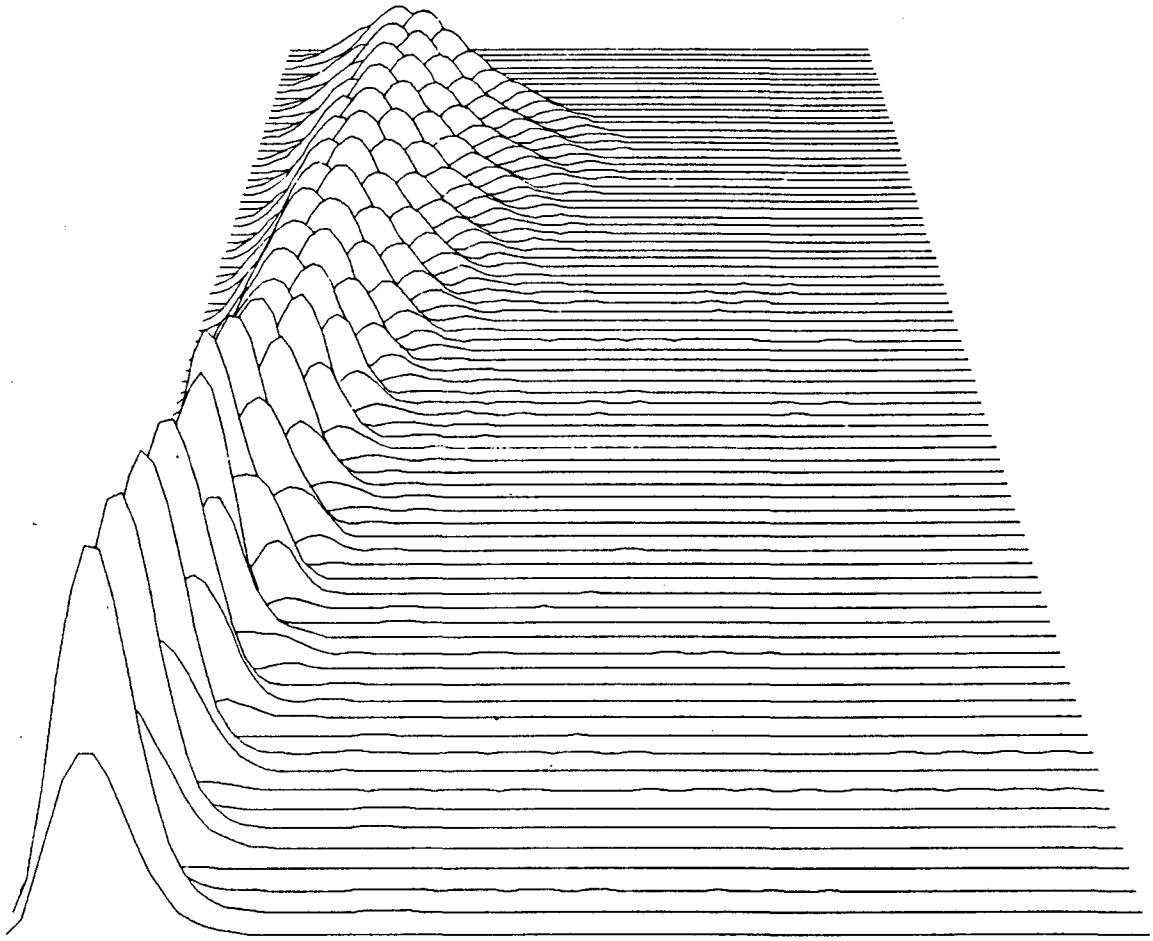

XBL 875-2229

Fig. 19d

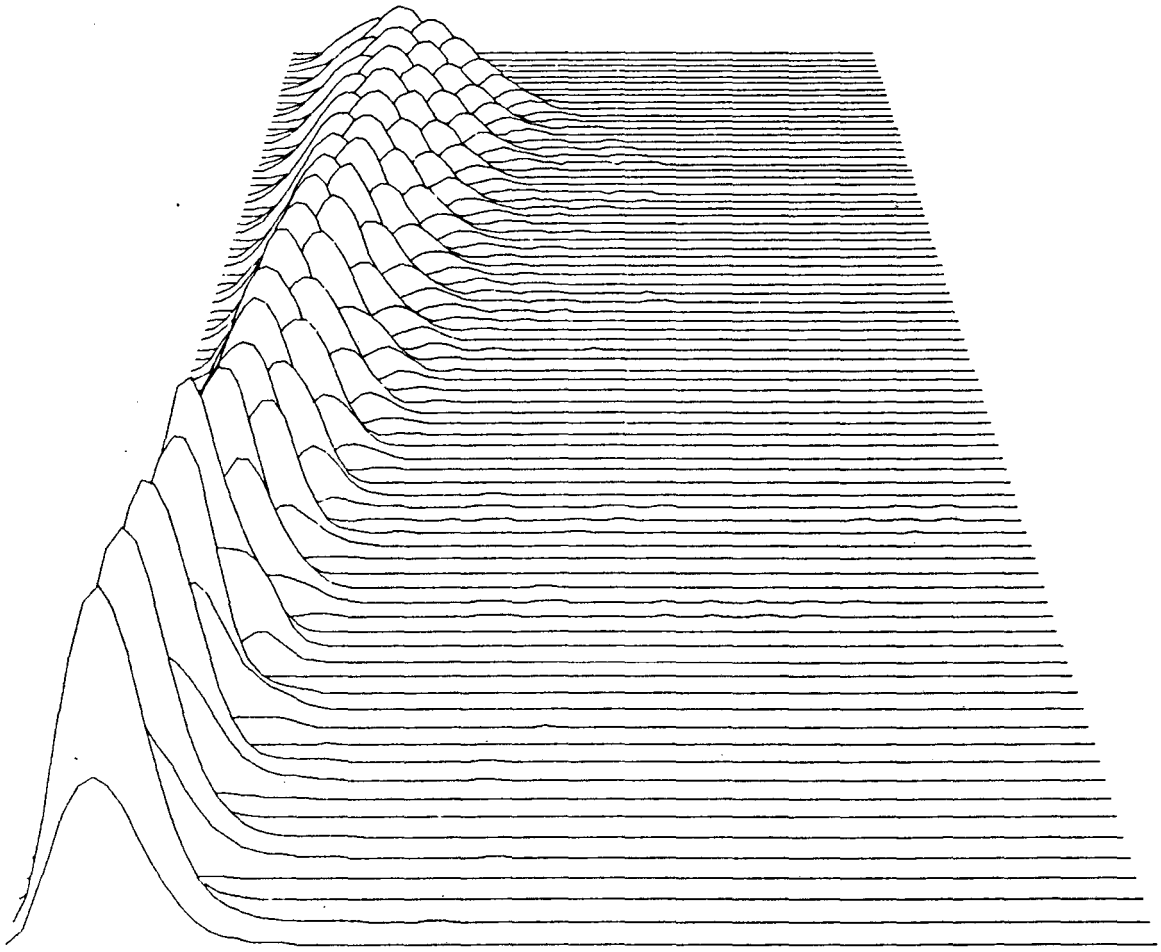

XBL 875-2230

Fig. 19e

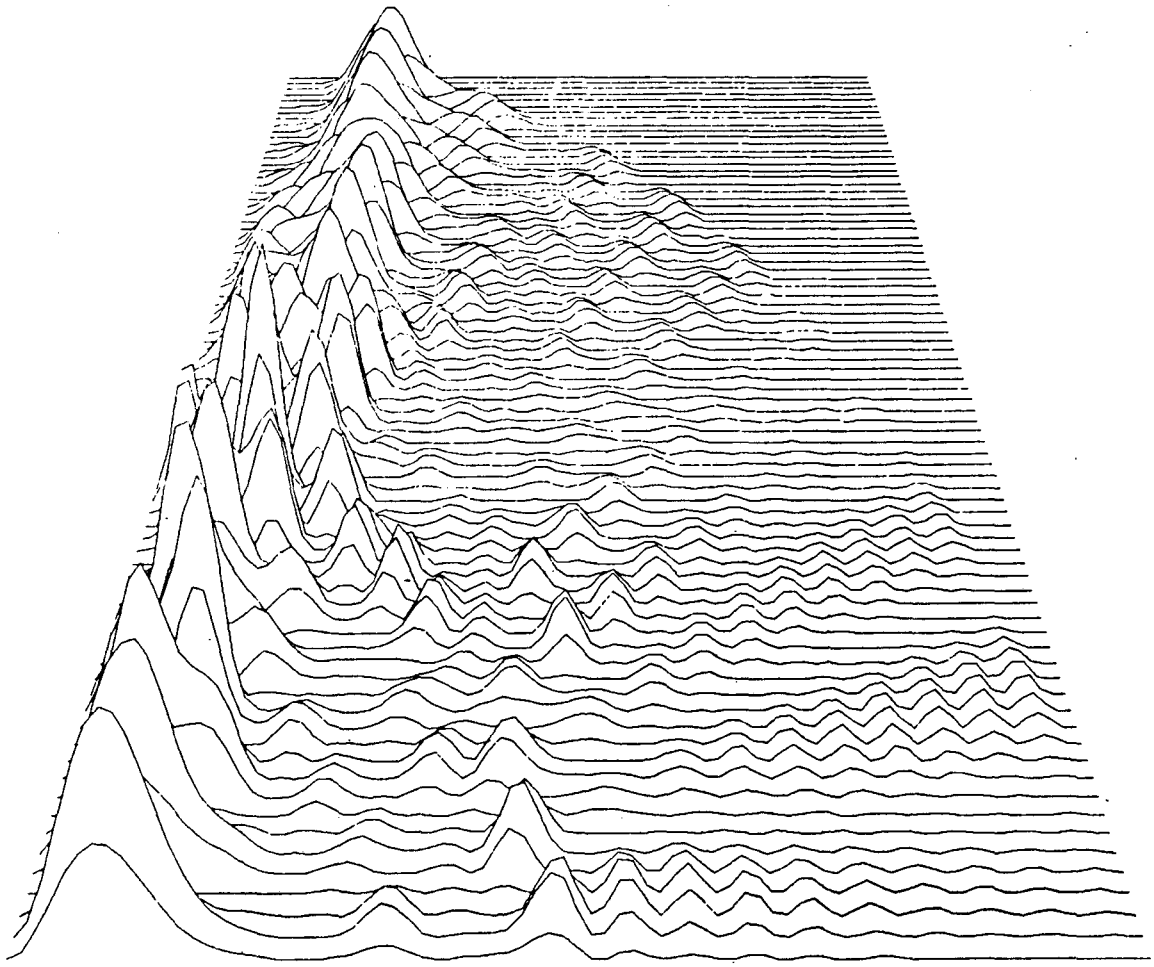

XBL 875-2231

Fig. 19f

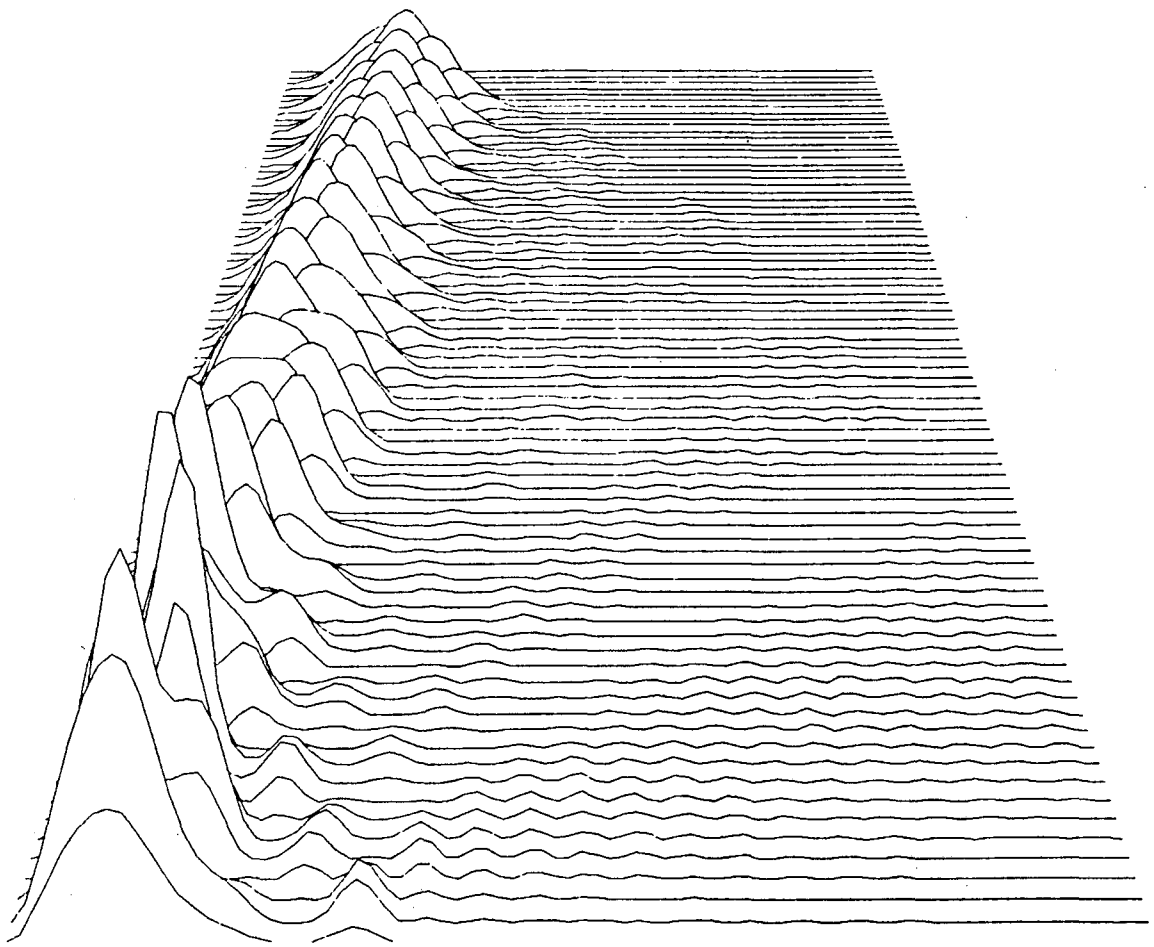

XBL 875-2232

Fig. 19g

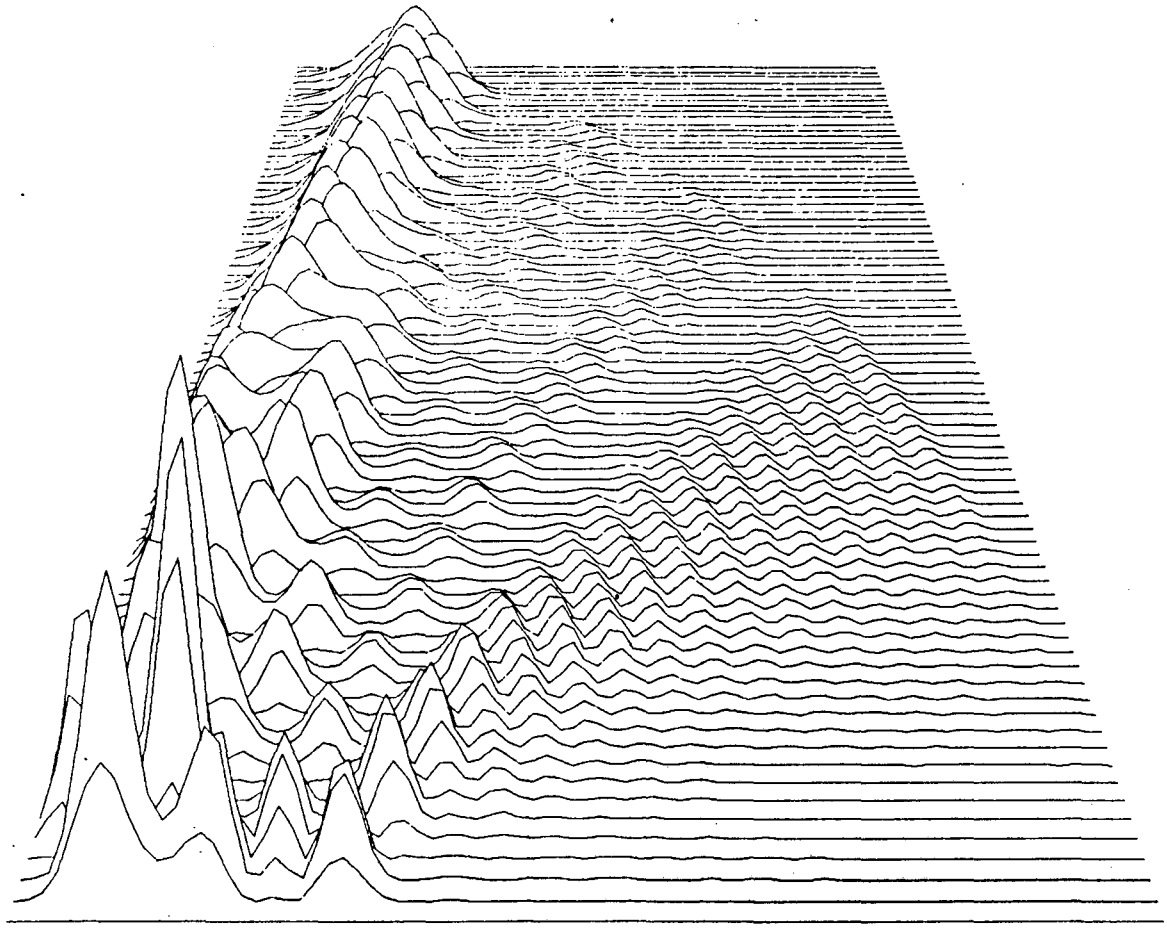

XBL 875-2233

Fig. 19h

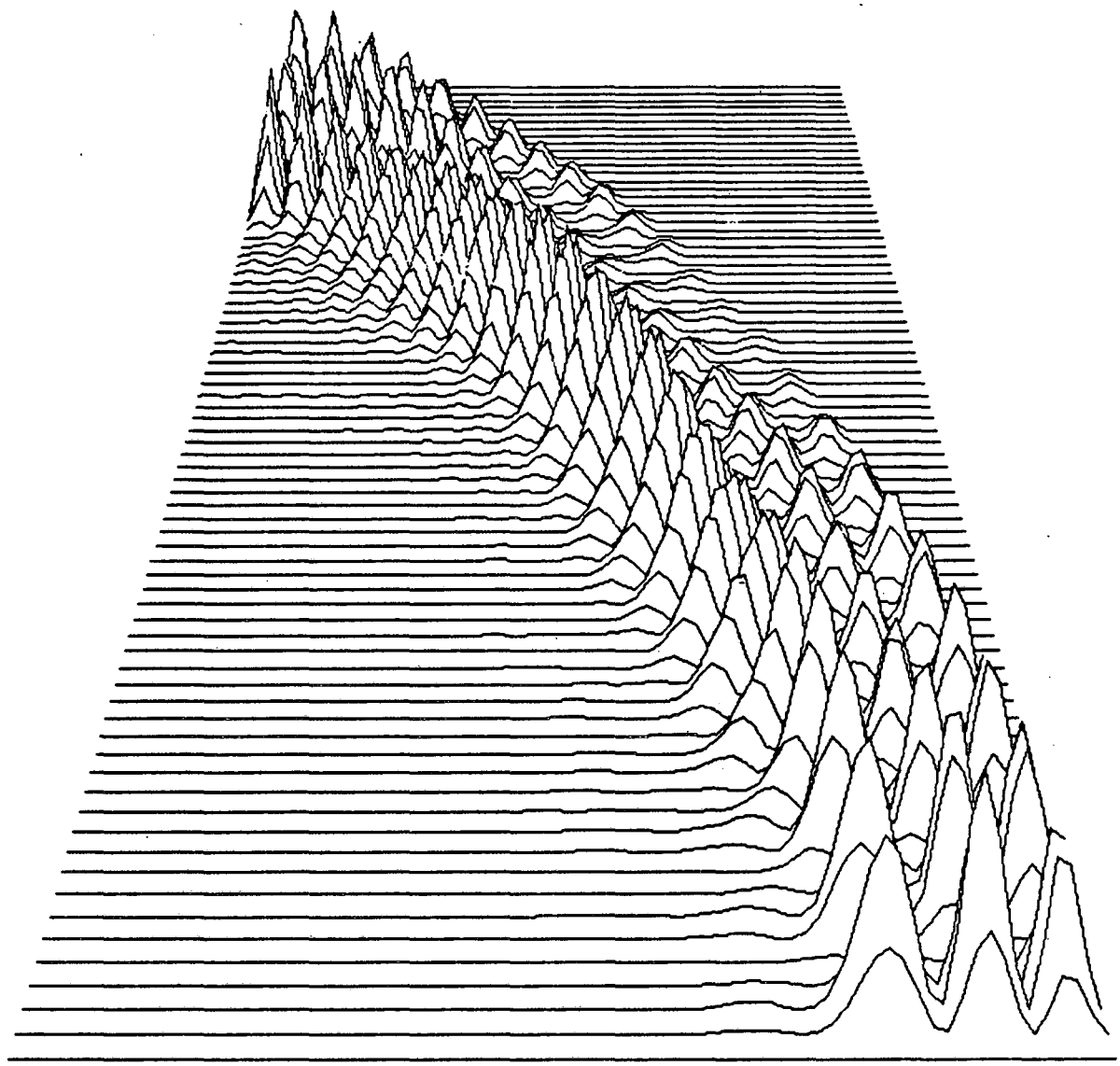

XBL 828-11111

Fig. 20a

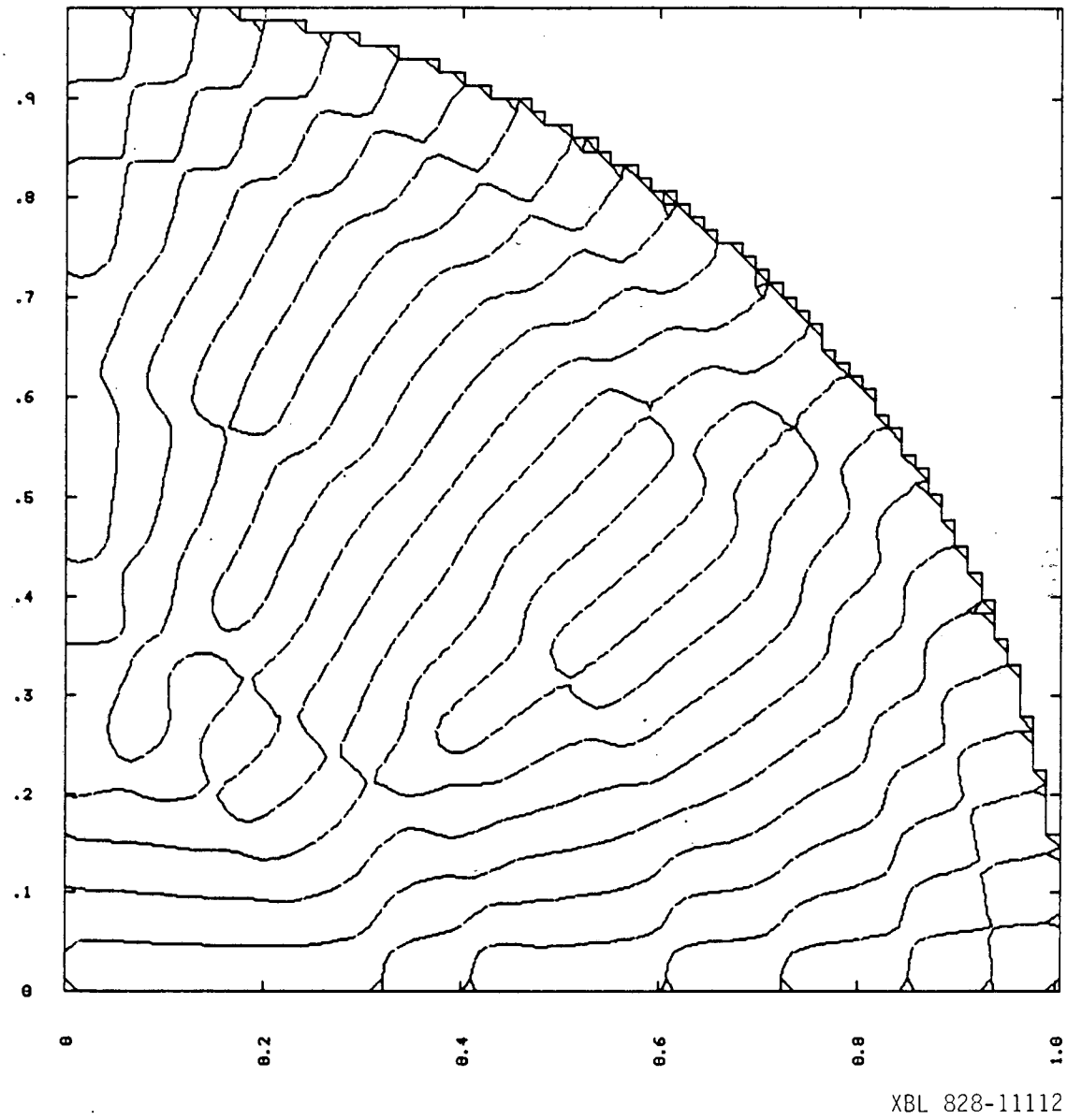

XBL 828-11112

Fig. 20b

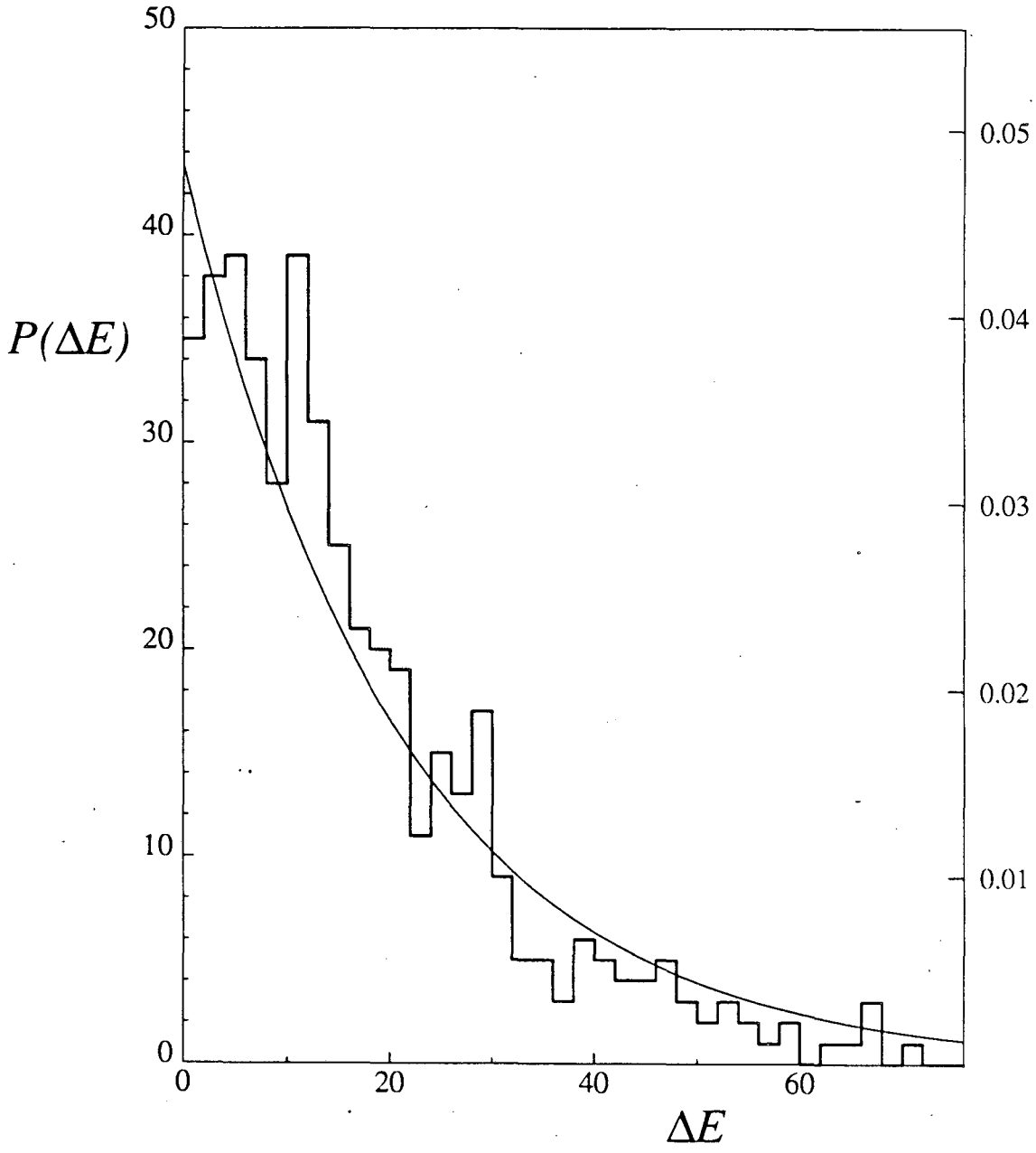

XBL 876-2454

Fig. 21a

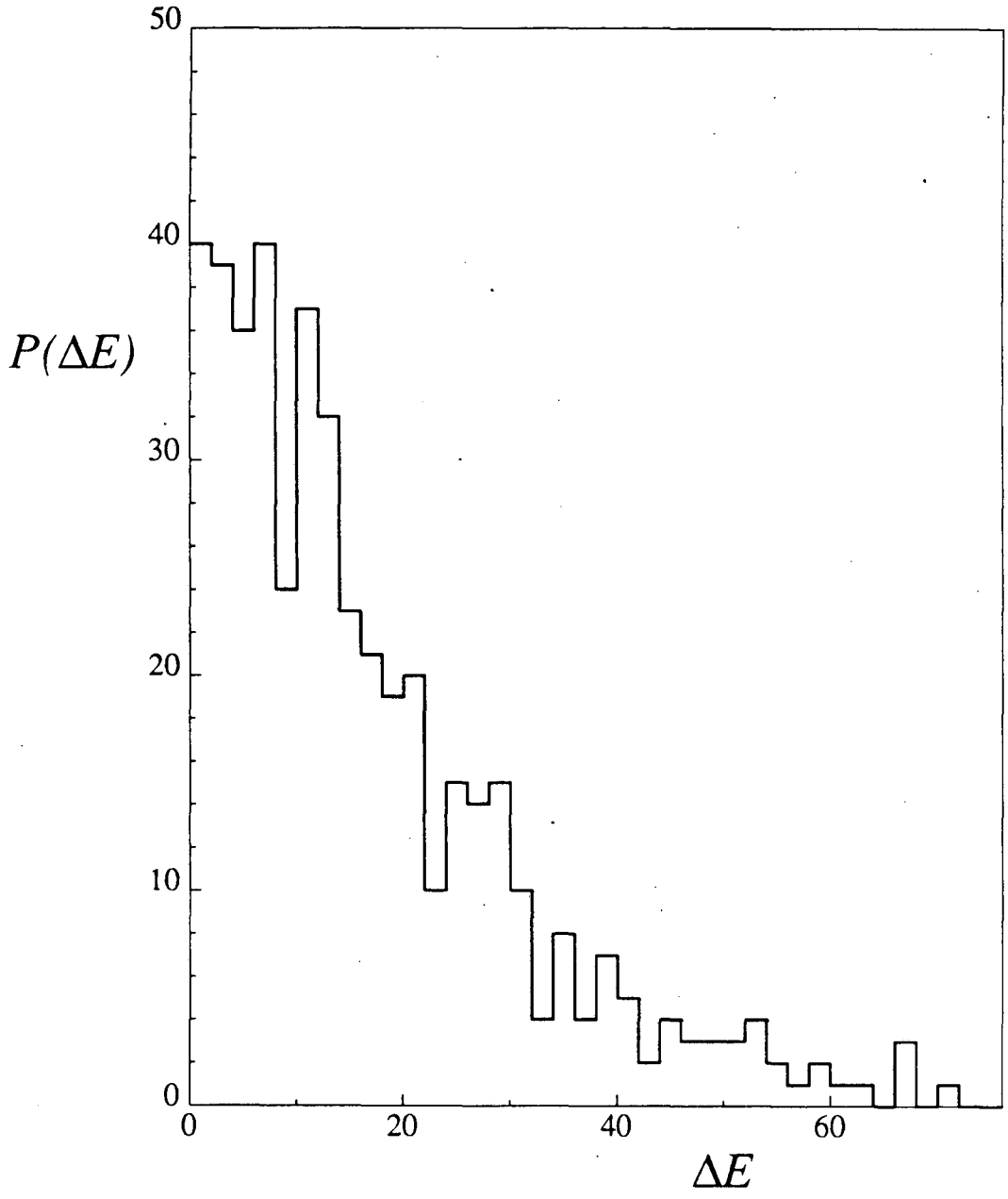

XBL 876-2455

Fig. 21b

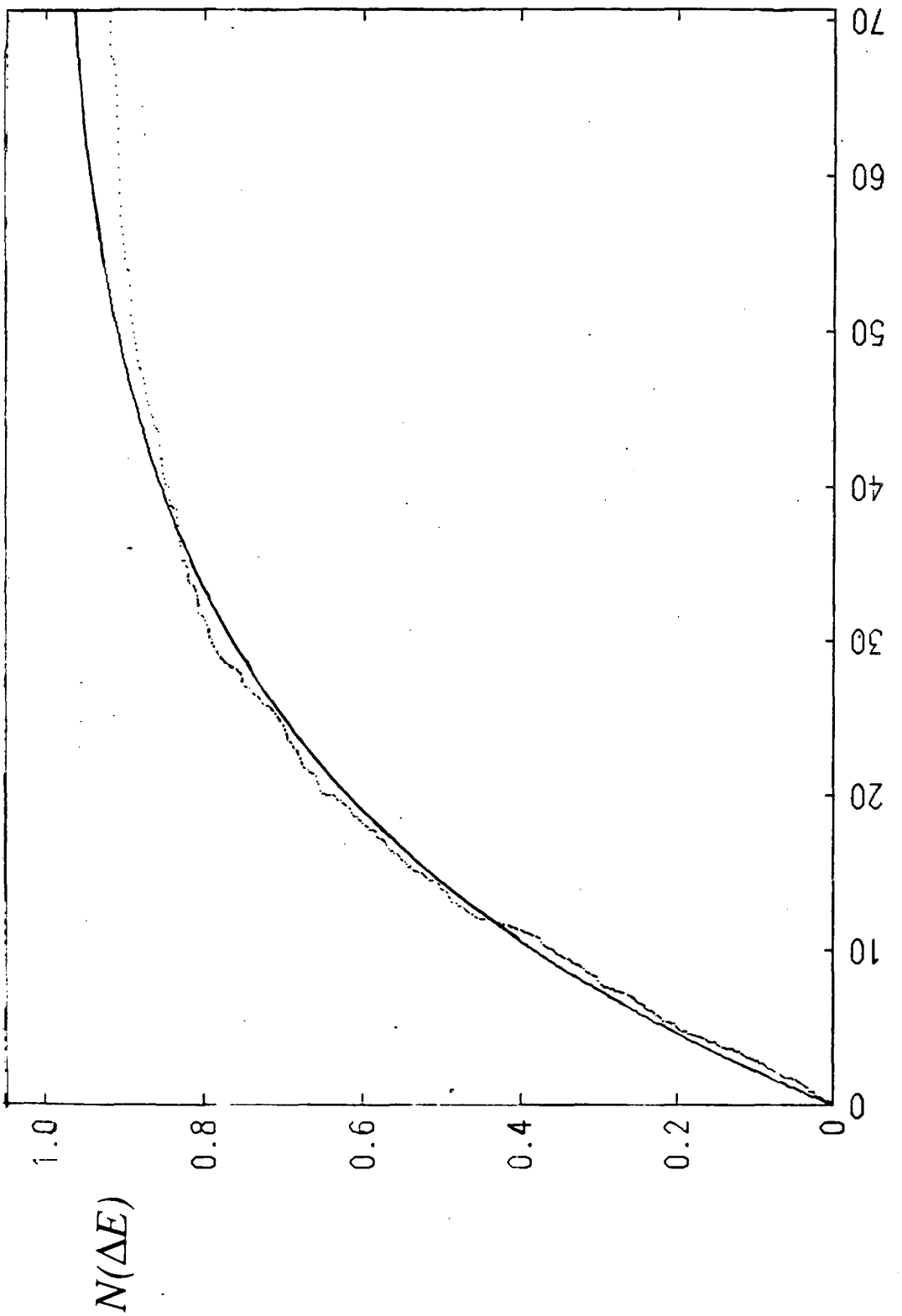

XBL 828-11136

Fig. 22

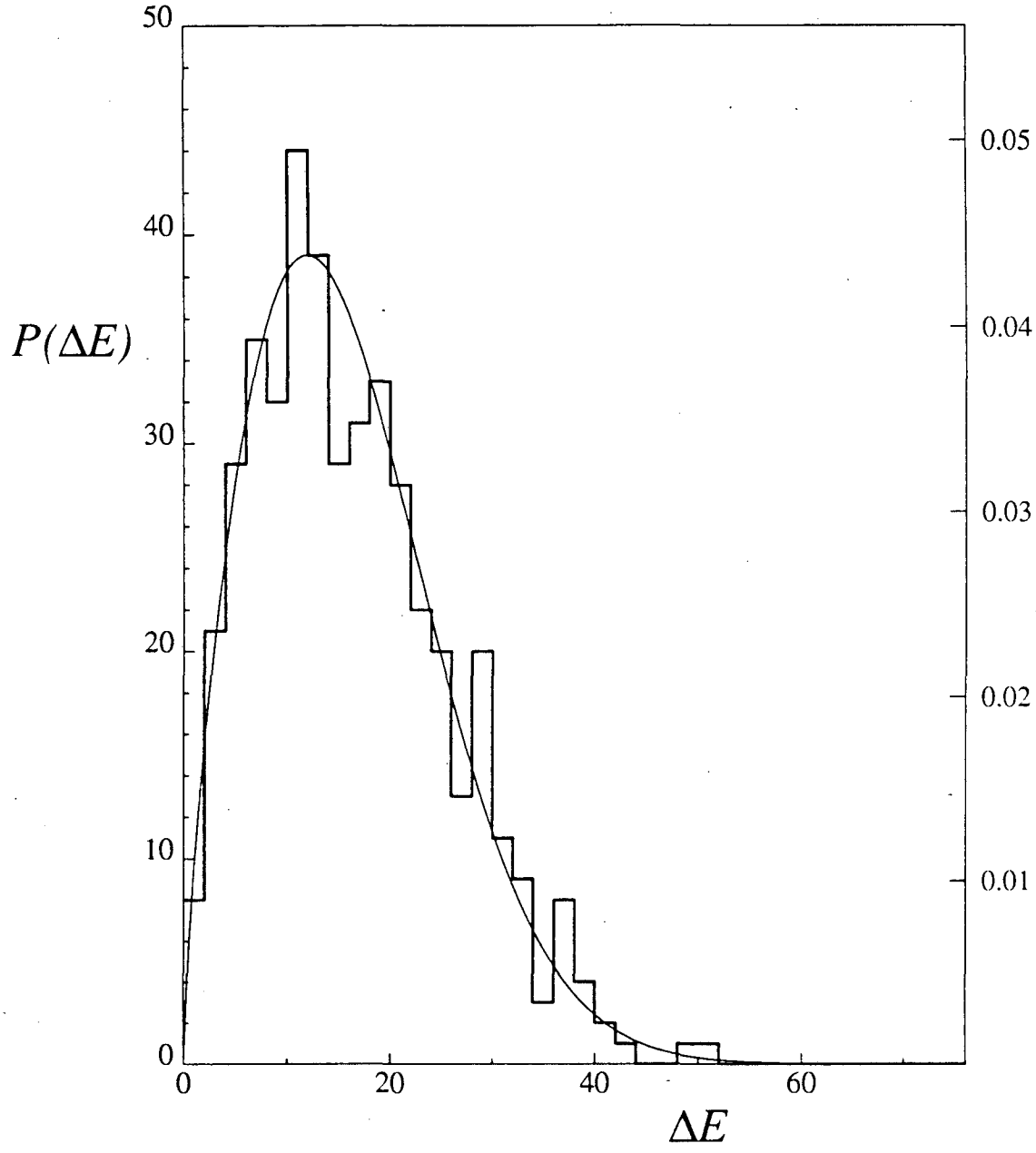

XBL 876-2456

Fig. 23

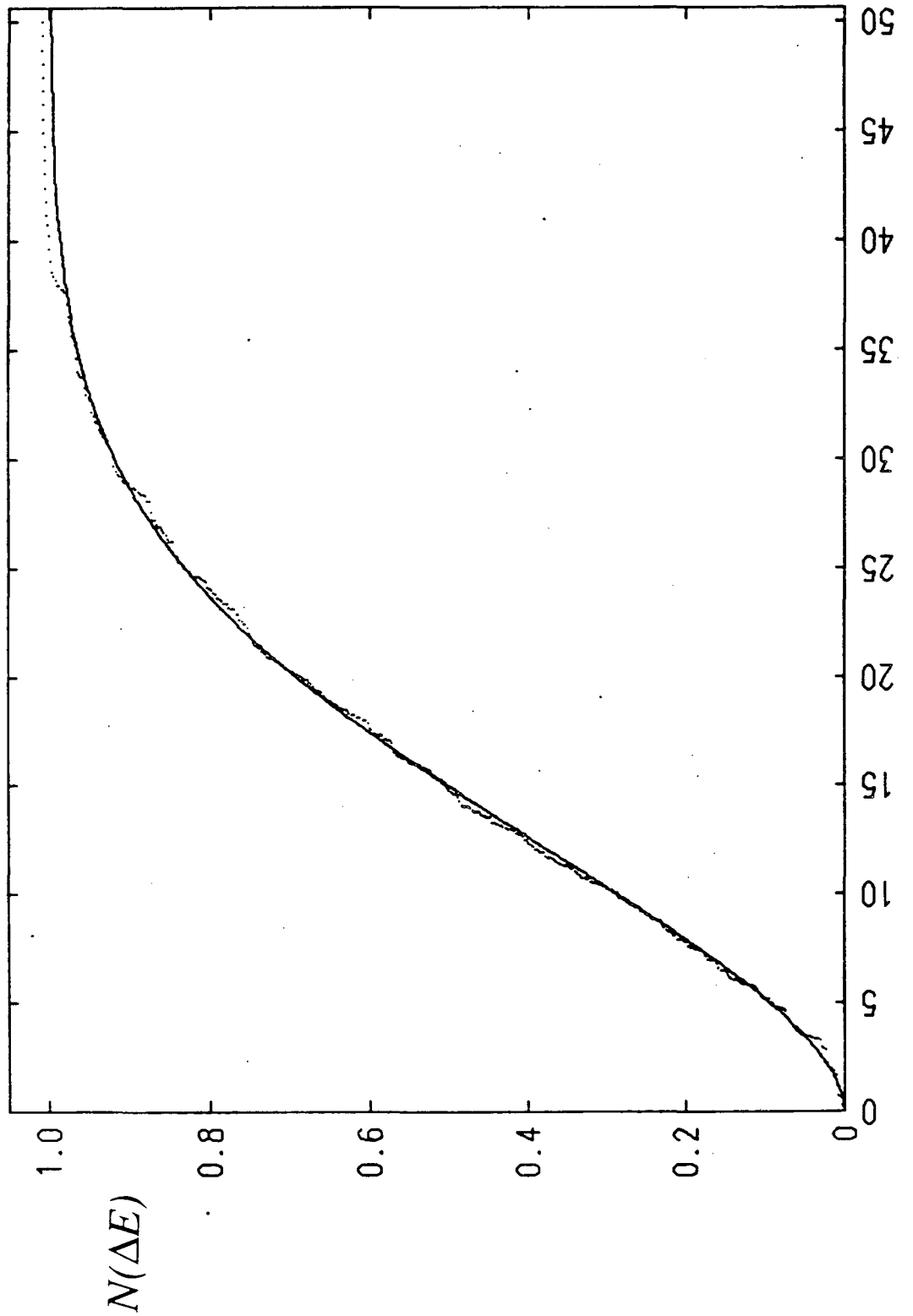

XBL 828-11135

Fig. 24

LAWRENCE BERKELEY LABORATORY
TECHNICAL INFORMATION DEPARTMENT
UNIVERSITY OF CALIFORNIA
BERKELEY, CALIFORNIA 94720